Stefan Aichinger, BSc

Determination of the Block Size and Shape Distribution in a Quarry by using Remote Sensing Techniques

Master's Thesis

Submitted in fulfilment of the requirements for the degree of

Diplom-Ingenieur

Master's programme Civil Engineering, Geotechnics and Hydraulics

at

Graz University of Technology

Supervisors

O.Univ.-Prof. Dipl.-Ing. Dr.mont. Wulf Schubert
Institute of Rock Mechanics and Tunnelling
Graz University of Technology

Andreas Anjan Buyer, M.Sc. B.Sc.
Institute of Rock Mechanics and Tunnelling
Graz University of Technology

Graz, January 2018

EIDESSTATTLICHE ERKLÄRUNG
AFFIDAVIT

Ich erkläre an Eides statt, dass ich die vorliegende Arbeit selbstständig verfasst, andere als die angegebenen Quellen/Hilfsmittel nicht benutzt, und die den benutzten Quellen wörtlich und inhaltlich entnommenen Stellen als solche kenntlich gemacht habe. Das in TUGRAZonline hochgeladene Textdokument ist mit der vorliegenden Masterarbeit identisch.

I declare that I have authored this thesis independently, that I have not used other than the declared sources/resources, and that I have explicitly marked all material which has been quoted either literally or by content from the used sources. The text document uploaded to TUGRAZonline is identical to the present master's thesis.

Datum / Date	Unterschrift / Signature

Principle of equality

Due to reasons of legibility, this work does not include gender-specific formulations. However, the used male expressions stand for both genders.

Acknowledgements

At this point, I would like to thank all the people, who supported me during my studies and the work at this master's thesis and therefore contributed to my successful graduation.
Especially, I would like to point out the cooperation with Mr. Dipl.-Ing. Stefan Fehleisen, who kindly enabled the field studies in the quarry in Gallmannsegg.
I want to thank my supervisors O.Univ.-Prof. Dipl.-Ing. Dr.mont. Wulf Schubert and Andreas Anjan Buyer, M.Sc., B.Sc. for their engagement and their great interest in my work.
Finally, I want to express my parents Anna and Erwin my greatest gratitude, since they enabled my studies through their incessant support.

Danksagung

An dieser Stelle möchte ich all jenen danken, die mich während meines Studiums und dem Schreiben dieser Arbeit unterstützt haben und somit zum erfolgreichen Abschluss meines Studiums beigetragen haben.
Besonders hervorheben möchte ich die Zusammenarbeit mit Herrn Dipl.-Ing. Stefan Fehleisen, der die grundlegende Feldstudie im Steinbruch Gallmannsegg durch sein Entgegenkommen problemlos ermöglichte.
Meinen Betreuern O.Univ.-Prof. Dipl.-Ing. Dr.mont. Wulf Schubert und Andreas Anjan Buyer, M.Sc., B.Sc. möchte ich für ihr Engagement und dem großen Interesse an meiner Arbeit danken.
Zuletzt möchte ich meinen Eltern Anna und Erwin meinen größten Dank aussprechen, da sie mir mein Studium erst durch ihre unablässige Unterstützung ermöglicht haben.

Abstract

Rock engineering in blocky rock masses demands a sound knowledge about the joint network, since the discontinuities represent the planes of weakness along which blocks will detach and/or which reduce the global rock mass strength and stiffness. Hence, the effort in collecting characteristic data should be as high as possible. However, this data collection is very time consuming and thus seldom as detailed as necessary, besides the strong dependency of the quality and experience of the mapping geologist. Additionally, the characterisation is reduced to the identification of the main joint sets along with their orientation and an estimation of the joint set spacing. Other parameters, like the block shape and the block volume distribution or the main orientation of the blocks are seldom collected or determined.

With the development and increasing application of digital surface mapping techniques in rock mass characterisation, the time needed on site can be reduced and the degree of detail in the mapping of discontinuities is improved. However, the full potential of this development is still not reached and for example the block size and shape distribution are still not determined in the standard process.

The work presented in this study displays a continuous work flow from the data collection in the field to the determination of the block size and shape distribution, generated by the intersection of joint sets. For the process, a marble quarry in Styria (Austria) was digitally mapped using photogrammetry. The joint sets are semi-automatically identified with the Discontinuity Set Extractor whose results are transferred into the software ShapeMetriX^{3D}, where the joint set spacing along with its standard deviations is determined. These parameters are used to generate numerical block models using 3DEC and determine the block sizes, block shapes and main orientation of the blocks in a row of simulations.

Kurzfassung

Geotechnische Erkundungen und Analysen erfordern grundlegende Kenntnisse über die Zerklüftung des Gebirges oder eines Aufschlusses. Klüfte und andere Trennflächen stellen Schwachstellen im Gefüge des Gesteins dar, an denen Blockversagen auftreten kann und/oder die Gebirgsfestigkeit und -steifigkeit verringert wird. Daher sollte der Aufwand für eine entsprechende Charakterisierung bzw. Vorauserkundung so umfassend als möglich betrieben werden. Allerdings ist diese Datenerhebung besonders zeitaufwändig und wird daher selten im benötigten Detaillierungsgrad ausgeführt. Außerdem besteht ein nicht unbedeutender Zusammenhang zwischen der Qualität der Datenerfassung und der Erfahrung des eingesetzten Geologen. Weiters wird die Gebirgscharakterisierung zumeist auf die Feststellung der wichtigsten Trennflächenorientierungen und den dazugehörigen Trennflächenabständen reduziert. Andere Daten, wie die Blockformen, die Blockgrößenverteilung sowie die Blockorientierungen, werden nur sporadisch und durch subjektive Beschreibungen bestimmt. Mit dem zunehmenden Einsatz von Fernerkundungsmethoden bei der Feldarbeit kann die benötigte Zeit vor Ort erheblich reduziert und der Detaillierungsgrad der Datenerhebung erhöht werden. Jedoch wird das volle Potenzial dieser Entwicklungen bisher nicht ausgeschöpft und die Blockgrößen- und Blockformverteilungen sind bis dato nicht Teil von standardisierten Charakterisierungsprozessen.

Diese Studie veranschaulicht einen kontinuierlichen Arbeitsablauf von der Datenerhebung mittels Fernerkundung bis zur Bestimmung der Blockgrößen- und Blockformverteilungen, die sich aus den vorhandenen Trennflächenscharen ergeben. Für diesen Prozess wurde ein Marmorsteinbruch in der Steiermark (Österreich) mittels Fotogrammmetrie aufgenommen. Die Trennflächen werden halbautomatisch anhand des Discontinuity Set Extractors identifiziert und dessen Ergebnisse in die Software ShapeMetrix^{3D} übertragen. Darauffolgend werden die Trennflächenabstände einschließlich der dazugehörigen Standardabweichungen bestimmt. Diese Parameter werden eingesetzt, um unter der Verwendung von 3DEC numerische Modelle zu erstellen und aus ebendiesen die Blockgrößen-, Blockformverteilung und die Hauptorientierungen der Blöcke in mehreren Simulationsreihen zu ermitteln.

Table of contents

1 Introduction 1

2 State of Research 3

2.1 In situ block size distribution ... 3

2.2 In situ block shape distribution ... 8

3 Methodology 11

3.1 Data acquisition ... 11

3.2 Generation of the DSM ... 12

3.3 Discontinuity network characterisation ... 14

3.3.1 Discontinuity identification ... 15

3.3.2 Joint normal spacing ... 19

3.4 Modelling of the IBSD and BSD ... 19

3.4.1 Determination of the model size and model composition ... 19

3.4.2 Persistence study ... 21

3.4.3 Distribution of the block shapes and orientations ... 24

4 Results 26

4.1 Discontinuity network characterisation ... 26

4.1.1 Discontinuity identification ... 26

4.1.2 Joint normal spacing ... 28

4.2 Modelling of the IBSD ... 29

4.2.1 Persistence study ... 29

4.2.2 Distribution of the block shapes and orientations ... 38

5 Interpretation and Discussion 42

5.1 Discontinuity network characterisation ... 42

5.2 IBSD compared to analytical approaches ... 42

5.2.1 Analytical approach after Palmström ... 43

5.2.1 Analytical approach after Cai et al. ... 45

5.2.2 Analytical approach after Kluckner et al. ... 47

5.3 Block shape distributions ... 49

6 Conclusion and Outlook 52

7 Bibliography 54

List of figures

Figure 1.1: Importance of the block size for stability investigations in tunnelling (Palmström, 2000). 1

Figure 1.2: Visualisation of an example for the applied numeric models with eliminated boundary blocks, the single blocks are coloured differently. 2

Figure 2.1: Modified quantification of GSI chart, based on V_b and J_C (Cai et al., 2004). 5

Figure 2.2: Blocks, delimited through joint sets (Cai et al., 2004). 6

Figure 2.3: Block shape examples (Palmström, 2005). 9

Figure 2.4: Block shape diagram showing zones that encompass basic shapes and simple sample blocks (Kalenchuk et al., 2006). 9

Figure 3.1: Flowchart for the data gathering and processing. 11

Figure 3.2: (a) Location of the marble quarry in Gallmannsegg, (b) location of Gallmannsegg on a map with Graz, marked with red arrows (Bundesamt für Eich- und Vermessungswesen (BEV), 2005). 12

Figure 3.3: Section of the layout map of the quarry, including the investigated outcrops: The main outcrop wall, marked with a red ellipse and referred as Outcrop I (OC I) and the left edge of the main outcrop wall, marked with a blue ellipse and referred as Outcrop II (OC II) (Schuscha, 2016). 13

Figure 3.4: 3D point cloud model of the (a) outcrop I for the SMX analysis and of the (b) OC II for the DSE analysis, visualised in CloudCompare. 14

Figure 3.5: Overview of Outcrop II (compass direction: west-south-west), which was used for the DSE analysis. 17

Figure 3.6: DSE evaluation No. 9 with three assigned discontinuity sets. 18

Figure 3.7: Quarry outcrop used for the manual SMX investigation. 18

Figure 3.8: Diagram for the rating of the used outcrop area of the numeric model compared to its mean block surface area (Kluckner et al., 2015). 20

Figure 3.9: Trace lengths of (a) joint set 1, (b) joint set 2 and (c) joint set 3. 23

Figure 3.10: (a) Replication 14 and (b) replication 43 of the model 110 as exemplary block shape distributions. 25

Figure 4.1: (a) Point cloud of the side wall of the outcrop and (b) the stereographic projection with the appropriate plane poles. Joint set 1 is marked in blue, joint set 2 in green and joint

set 3 in yellow 3D points in (a) and principal poles in (b). 27

Figure 4.2: Stereographic projection of the through the SMX analysis evaluated and assigned plane poles. Joint set 1 is marked with blue, joint set 2 with red and joint set 3 with green plane poles. The black plane poles were not assigned. 28

Figure 4.3: Result for block volumes of test series 1. 30

Figure 4.4: Results for cumulative distribution function of test series 1 including (a) model 110, (b) model 102 and (c) model 103. 31

Figure 4.5: Result for block volumes of test series 2. 32

Figure 4.6: Results for cumulative distribution function of test series 2 including (a) model 404, (b) model 405 and (c) model 409. 33

Figure 4.7: Result for block volumes of test series 3. 34

Figure 4.8: Results for cumulative distribution function of test series 3 including (a) model 406, (b) model 414 and (c) model 910. 35

Figure 4.9: Result for block volumes of test series 4. 36

Figure 4.10: Results for cumulative distribution function of test series 4 including (a) model 903, (b) model 902 and (c) model 901. 37

Figure 4.11: (a) Density plot of the block shape distribution and (b) density plot of the orientations of the main axes of the blocks of model 110, test series 1. 39

Figure 4.12: (a) Density plot of the block shape distribution and (b) density plot of the orientations of the main axes of the blocks of model 102, test series 1. 40

Figure 4.13: (a) Density plot of the block shape distribution and (b) density plot of the orientations of the main axes of the blocks of model 103, test series 1. 41

Figure 5.1: Mean values and quantile values of the IBSD of all test series including three model replications each, compared to the analytical approach of Palmström (2005)..... 44

Figure 5.2: Mean values and quantile values of the IBSD of all test series including three model replications each, compared to the analytical approach of Cai et al. (2004). 46

Figure 5.3: Mean values and quantile values of the IBSD of all test series including three model replications each, compared to the analytical approach of Kluckner et al. (2015). . 48

Figure 5.4: Peak values of the density distribution based on the total number of blocks in relation to the persistence of the investigated test series with exponential tend lines. 50

Figure 5.5: Main block shape types with various vertex to vertex distances of the same length and different orientations (red lines), modified from Palmström (1995). 51

Figure 6.1: Trace map for the evaluation of the joint normal spacing for discontinuity set 1 (a), discontinuity set 2 (b) and discontinuity set 3 (c), obtained by ShapeMetrix^{3D}. 61

Figure 6.2: (a) Density plot of the block shape distribution and (b) density plot of the orientations of the main axes of the blocks of model 404, test series 2. 62

Figure 6.3: (a) Density plot of the block shape distribution and (b) density plot of the orientations of the main axes of the blocks of model 405, test series 2. 63

Figure 6.4: (a) Density plot of the block shape distribution and (b) density plot of the orientations of the main axes of the blocks of model 409, test series 2. 64

Figure 6.5: (a) Density plot of the block shape distribution and (b) density plot of the orientations of the main axes of the blocks of model 406, test series 3. 65

Figure 6.6: (a) Density plot of the block shape distribution and (b) density plot of the orientations of the main axes of the blocks of model 414, test series 3. 66

Figure 6.7: (a) Density plot of the block shape distribution and (b) density plot of the orientations of the main axes of the blocks of model 910, test series 3. 67

Figure 6.8: (a) Density plot of the block shape distribution and (b) density plot of the orientations of the main axes of the blocks of model 903, test series 4. 68

Figure 6.9: (a) Density plot of the block shape distribution and (b) density plot of the orientations of the main axes of the blocks of model 902, test series 4. 69

Figure 6.10: (a) Density plot of the block shape distribution and (b) density plot of the orientations of the main axes of the blocks of model 901, test series 4. 70

List of tables

Table 3.1: Description of the input parameters of the DSE analysis (Riquelme et al., 2014; 2015). 16

Table 3.2: Input parameters for the DSE parameter study. 17

Table 3.3: 3DEC input parameters for the foliation and the two major discontinuity sets. .19

Table 3.4: Determination of the ratio of the block surface area to the model face. 21

Table 3.5: Persistence values of test series, with three model simulations each. 23

Table 4.1: Combined input values for numeric modelling with three joint sets. 26

Table 4.2: Results for the orientation of the joints in quarry face “Outcrop II” obtained from the DSE. 26

Table 4.3: Results, obtained from manual SMX analyses of the two DSM with various membership angles. 27

Table 4.4: Spacing parameters for three joint sets, obtained through SMX. 29

Table 4.5: Spacing parameters evaluated from the DSE generated structure map. 29

Table 4.6: Results of test series 1 for block volumes with corresponding standard deviations. 30

Table 4.7: Results of test series 2 for block volumes with corresponding standard deviations. 32

Table 4.8: Results of test series 3 for block volumes with corresponding standard deviations. 34

Table 4.9: Results of test series 4 for block volumes with corresponding standard deviations. 36

Table 5.1: Joint normal spacing without standard deviation and angles between joint sets for the analytical approaches. 43

Table 5.2: Block volumes resulting from the analytical approach of Cai et al. (2004). 45

Table 5.3: Quantile values resulting from the analytical approach of Kluckner et al. (2015). 47

Table 6.1: Quality of the generated DSM. 58

Table 6.2: DSE results of the parameter study to evaluate optimised input values to assign a maximum number of 3d points to the discontinuity sets. 59

Abbreviations

3DEC .....three-dimensional distinct element code
BSCM .....block shape characterisation method
BSD .....block shape distribution
BSD .....block size distribution
GSI .....geological strength index
D.....dip angle
DD .....dip direction
DS .....discontinuity set
DSE .....discontinuity set extractor
DSM .....digital surface model
DFN .....discrete fracture network
F .....joint frequency
IBSD .....in-situ block size distribution
KDE .....kernel density estimation
n .....number of measured joints
Q.....rock mass quality
RQD .....rock quality designation
RMR .....rock mass rating
SMX.....ShapeMetriX^{3D}
s .....joint normal spacing

1 Introduction

The characterisation of rock masses is an important subject to specify strength properties and consequently the rock mass stability. Current methods of rock mass characterisation (ÖNORM, RMR, Q, GSI, etc.) propose miscellaneous assumptions and simplifications like the in situ block size and shape distribution.

For example, in the latest approved Austrian standard, the estimation of the IBSD (in situ block size distribution) is prescribed with literal descriptions for defined block size ranges. However, these values are seldom determined. The same accounts for the block shape distribution, whereby the suggested block forms are subjective and mathematically not clearly describable (ÖNORM EN ISO 14689-1). With regard to the increasing degree of digitalization, this is not state-of-the-art.

The results of a sound classification of the IBSD can be used to approximate the rock mass strength or to investigate the stability and other specifications, like bolt length or shotcrete linings (Palmström, 2005). As an illustration, an example is depicted in Figure 1.1. Furthermore, a IBSD with a certain safety factor can be applied for the design of rock fall nets instead of a measured maximum value. Moreover, the optimization of the explosive consumption or the blasting design is in interest for tunnel advances or quarry excavations.

Figure 1.1: Importance of the block size for stability investigations in tunnelling (Palmström, 2000).

To address the above-mentioned issues, the following methods are expected to prove the available possibilities of a digital outcrop characterisation and give a more detailed and comprehensive outcrop description. Therefore, the focus of this work is set on the determination of the in-situ block size distribution (IBSD) as well as the block shape distribution (BSD) combined with the corresponding dominant block orientations.

The first step of the study was the data collection by using photogrammetry.

Photogrammetry is a reliable technique for the generation of a digital surface model, which can be used to determine the following significant input parameters for the required joint set investigations (Gaich et al., 2017):

- Joint orientation (dip and dip direction)
- Joint spacing
- Number of measured joints

To estimate the orientation of the joint sets, a study which offers a semi-automatic method to identify and analyse surfaces of rock outcrops is used. The approach is packed into the MATLAB® application Discontinuity Set Exctractor (DSE) according to Riquelme et al. (2014). Furthermore, the joint normal spacing of the joint sets is estimated by using the software ShapeMetriX^{3D} (3GSM GmbH, 2017).

The obtained data is used for the determination of the in situ block size distribution, using the 3-Dimensional Distinct Element Code - 3DEC (Itasca Consulting Group, 2017). As there is examined proven method to obtain the block size distribution (Kluckner et al., 2015), this work also concentrates on the validation and comparison of this method to a modelled quarry. This approach applies the block shape characterisation method after Kalenchuk et al. (2006), which provides a mathematical solution by using the coordinates of the block vertices. Figure 1.2 shows an example for an investigated cubic shaped model.

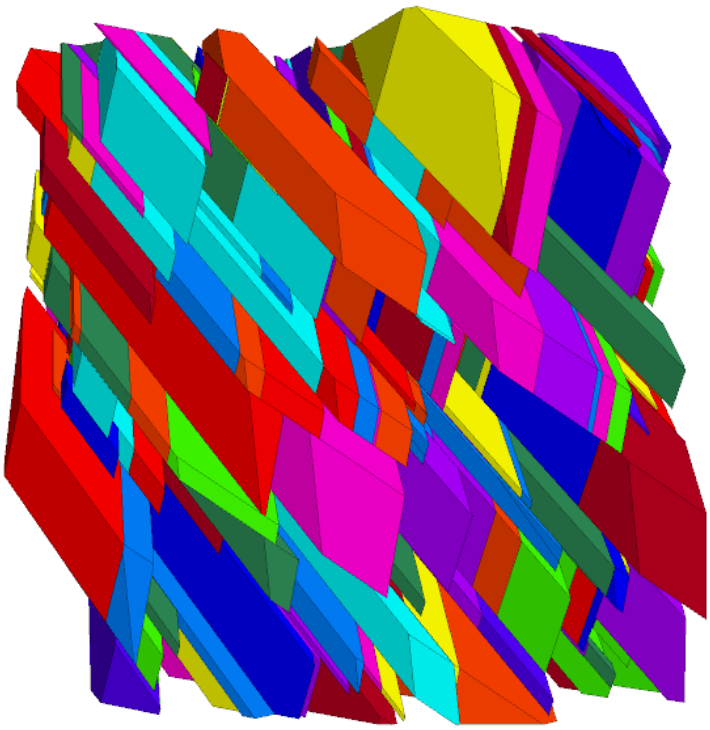

Figure 1.2: Visualisation of an example for the applied numeric models with eliminated boundary blocks, the single blocks are coloured differently.

2 State of Research

2.1 In situ block size distribution

Since the IBSD has always been seen as a relevant factor for the design of rock engineering projects, this chapter gives an overview and improvement of the current methods of the determination of the IBSD and the BSD, along with a description of the relevant procedures which were used in this work.

An early method including block sizes of a jointed rock mass was to combine the Rock Quality Designation index (RQD) with the number of joint sets J_n. This quotient, used in equation (2.1) to determine the rock mass quality Q, describes the relative block size of the rock mass (Barton et al., 1974).

$$Q = \frac{RQD}{J_n} \cdot \frac{J_r}{J_a} \cdot \frac{J_w}{SRF} \tag{2.1}$$

The Rock Mass Rating system (RMR) offers another way to meet a certain statement concerning the block size of rock masses, by combining the RQD with the joint spacing parameter amongst others (Bieniawski, 1989).

The introduction of the Geological Strength Index (GSI) gave a possibility to calculate the GSI from the RMR_{89} or after Barton et al. (1974), shown in equation (2.2) and (2.3) (Hoek et al., 1998a).

$$GSI = RMR_{89}{}' - 5 \tag{2.2}$$

$$GSI = 9 \log_e \left(\frac{RQD}{J_n} \cdot \frac{J_r}{J_a} \right) + 44 \tag{2.3}$$

Palmström (1995) investigated various methods for the determination of the block volume. For instance, the influence of different block types (block shapes) combined with the volumetric joint count J_V was considered. Moreover, the publication of Palmström (2000) summarises the relevant main methods for the measurement of the block size, considering the degree of jointing or the joint density. The block volume can be determined with the average joint spacing of three present major joint sets. The block volume can be calculated by equation (2.4), where s_1, s_2, s_3 are the average joint normal spacing and γ_1, γ_2 and γ_3 the

angles between the joint sets. As the complete block size distribution is unknown in most of the practical scenarios, the quotation of the average values $V_{b,50\%}$, $V_{b,25\%}$ and $V_{b,75\%}$ holds for a significant block size distribution. Within a later approach, the correlation between RQD and some other measurement methods for block size were investigated. It was concluded, that there is a poor correlation and the application of the RQD classification system can cause some inaccuracies at the block size characterisation (Palmström, 2005).

$$V_B = \frac{s_1 \cdot s_2 \cdot s_3}{\sin\gamma_1 \sin\gamma_2 \cdot \sin\gamma_3}. \tag{2.4}$$

The discussion on modelling parameters of a research for a mining project has shown, that the influence of the two main parameters discontinuity density and the persistence factor of the examined discontinuities are key values for determining the block size and shapes of a rock mass. In the course of this study, the application MAKEBLOCK was developed to estimate the block size distributions of ore deposits (Wang et al., 2003).
A quantitative approach by Cai et al. (2004) presents the usage of the GSI system, connected to quantitative input parameters. It uses the block volume and a descriptive joint condition factor as quantitative characterisation factors instead of the description of structure and block surface conditions from Hoek et al. (1998b). For discontinuous joint sets, equation (2.5) is provided to calculate the appropriate block volume.

$$V_B = \frac{s_1 \cdot s_2 \cdot s_3}{\sqrt[3]{p_1 \cdot p_2 \cdot p_3} \cdot \sin\gamma_1 \sin\gamma_2 \cdot \sin\gamma_3} \tag{2.5}$$

The block volume (V_B) is calculated through s_i, which stands for the average joint spacing of the DS, p_i for the equivalent persistence values and γ_i for the angles between the joint sets. Furthermore, the formula was applied to a hydro-power project in Kannagawa and was confirmed through a back calculation from the measured values. Figure 2.1 contains the modified GSI chart with the block volume V_B at the ordinate and the joint condition factor J_C at the abscissa (Cai et al., 2004).

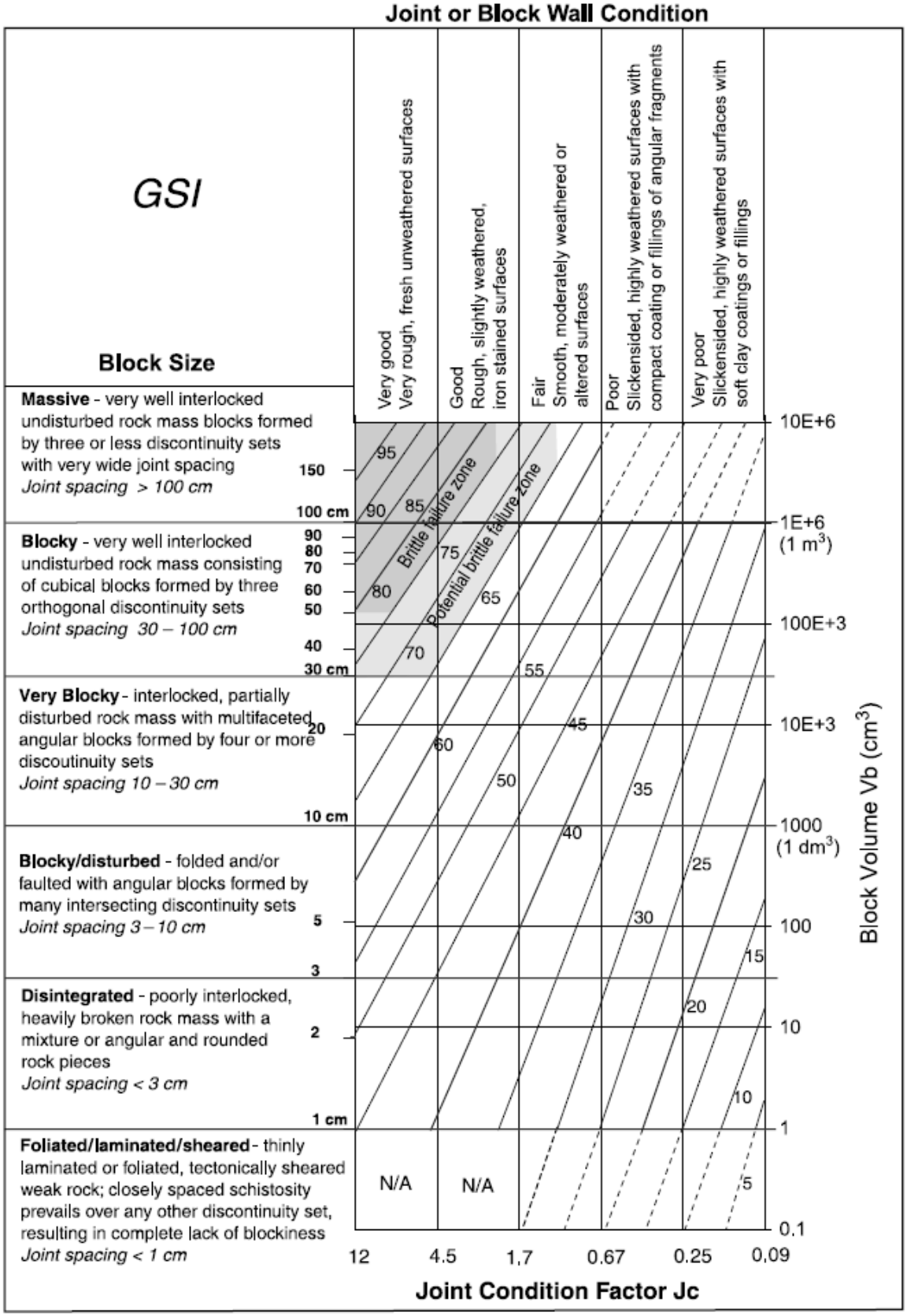

Figure 2.1: Modified quantification of GSI chart, based on V_b and J_C (Cai et al., 2004).

To improve the approach for a quantitative application of the GSI system for rock mass classification, Cai et al. (2007) proposed a method (cf. equation (2.5) and Figure 2.2) to

describe the relation between the joint persistence and the block volume distribution. Equation (2.6) describes the mathematical correlation between the block volume V_B and the joint condition factor J_C.

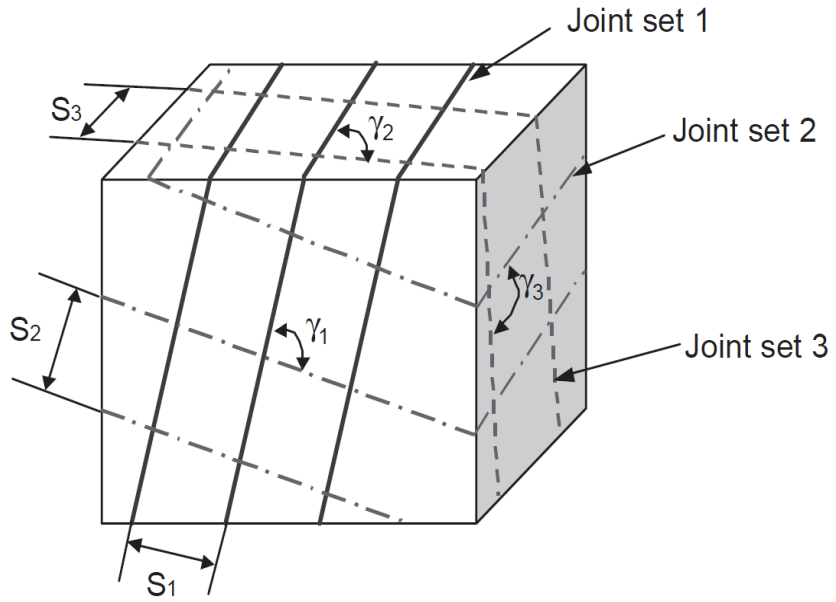

Figure 2.2: Blocks, delimited through joint sets (Cai et al., 2004).

$$GSI(V_B, J_C) = \frac{26.5 + 8.79 \ln J_C + 0.9 \ln V_B}{1 + 0.0151 \ln J_C - 0.0253 \ln V_B} \tag{2.6}$$

The possibility of varying the persistence allowed a statistical analysis regarding the influence of the geometric joint parameters on the block size distribution. The application of the distinct element code entails to the limitation of assuming minimum one fully persistent joint set (Kim et al., 2006).

However, following to the accumulation of uncertain applications of the original GSI system as well as the reduction of the rock strength solely on block sizes and the joint surfaces, a quantification of the GSI utilizing the RQD index and the joint condition ratio $JCond_{89}$ was provided by Hoek et al. (2013).

Another method for the estimation of the IBSD is based on Monte Carlo simulations. It includes a realistic discrete fracture network (DFN) generator with polyhedral modelling. User-specified statistical distributions for discontinuity relevant input parameters are considered. The approach improves the limitations of previous scientific publications regarding the amount of discontinuity sets, finite persistence percentages and polyhedral properties of fractures (Elmouttie & Poropat, 2012).

Lambert et al. (2012) evaluate the in-situ block size distribution by combining the DFN generation of Elmouttie and Poropat with digital photogrammetry for the geological mapping, which corresponds to this approach.

Stavropoulou (2013) presented a method to determine the block volume distribution from drill core investigations, but only by consideration of parallel and persistent joints. This research was also conducted by Kern (2017).

By the adaptation of the Floodfill algorithm, Chen et al. (2017) propose a new method to obtain the block size distribution. In the process, potential block edges are identified in a 3D point cloud and investigated by following defined block forming conditions.

Summarizing, the evaluation of the IBSD by using 3DEC is described as a standard technique to effectively analyse cumulative volume distribution curves.

The current procedure of creating a numeric model needs the geometrical parameters of the rock fracturing joint sets. Therefore, the orientation, dip angle, spacing and continuity enter the desired model. The mentioned parameters are varied with a statistical approach, supported by 3DEC.

With these parameters known, it is feasible to generate a cubic numeric model in 3DEC, which includes the estimated joint sets with statistical deviations. To figure out the IBSD, a realistic representation of the investigated outcrop surface is not obligatorily needed, wherefore a cubic assignment of the model is chosen. Since the determination of the IBSD and BSD is purely controlled by the rock mass geometry, no information about other rock mass properties is necessary. Moreover, the issue of the distinction between convex and concave blocks, which is discussed by Pötsch (2011) is excluded in this study.

In Addition to the previous methods to obtain the IBSD, Kluckner et al. (2015) and Söllner (2014) propose a modified formula (cf. equation (2.7)) for the block volume evaluation with the introduced transformation factor T.

$$V_{b,\{mean,25\%,50\%,75\%\}} = \frac{s_1 \cdot s_2 \cdot s_3}{\sin\gamma_1 \cdot \sin\gamma_2 \cdot \sin\gamma_3} \cdot T_{\{mean,25\%,50\%,75\%\}} \tag{2.7}$$

The equation indicates that the IBSD is represented by its quantile values, which are defined by the following empirical equations (cf. equation (2.8) to (2.11)), whereby the appropriate transformation factors are comprised. (Söllner, 2014)

$$V_{b,mean} = \frac{s_1 \cdot s_2 \cdot s_3}{\sin\gamma_1 \cdot \sin\gamma_2 \cdot \sin\gamma_3} \cdot T_{mean} = \frac{s_1 \cdot s_2 \cdot s_3}{\sin\gamma_1 \cdot \sin\gamma_2 \cdot \sin\gamma_3} \cdot 1.01 \cdot \left(\frac{p_1 + p_2 + p_3}{3}\right)^{-2.86} \tag{2.8}$$

$$V_{b,75\%} = \frac{s_1 \cdot s_2 \cdot s_3}{\sin\gamma_1 \cdot \sin\gamma_2 \cdot \sin\gamma_3} \cdot T_{75\%} = \frac{s_1 \cdot s_2 \cdot s_3}{\sin\gamma_1 \cdot \sin\gamma_2 \cdot \sin\gamma_3} \cdot 1.11 \cdot \left(\frac{p_1 + p_2 + p_3}{3}\right)^{-2.87} \quad (2.9)$$

$$V_{b,50\%} = \frac{s_1 \cdot s_2 \cdot s_3}{\sin\gamma_1 \cdot \sin\gamma_2 \cdot \sin\gamma_3} \cdot T_{50\%} = \frac{s_1 \cdot s_2 \cdot s_3}{\sin\gamma_1 \cdot \sin\gamma_2 \cdot \sin\gamma_3} \cdot 0.76 \cdot \left(\frac{p_1 + p_2 + p_3}{3}\right)^{-2.39} \quad (2.10)$$

$$V_{b,25\%} = \frac{s_1 \cdot s_2 \cdot s_3}{\sin\gamma_1 \cdot \sin\gamma_2 \cdot \sin\gamma_3} \cdot T_{25\%} = \frac{s_1 \cdot s_2 \cdot s_3}{\sin\gamma_1 \cdot \sin\gamma_2 \cdot \sin\gamma_3} \cdot 0.69 \cdot \left(\frac{p_1 + p_2 + p_3}{3}\right)^{-1.71} \quad (2.11)$$

As this approach was only verified with orthogonal joint set orientations, this work concentrates on further investigations and validation of the suggested formulas by using real values of the joint network in the investigated quarry.

The latest approved Austrian standard only prescribes the determination of the thickness of a foliation and the joint normal spacing with corresponding relativizing designations for defined ranges. Furthermore, the same practice is valid for block dimensions and block shapes, which are described with generalised geometric terms (ÖNORM EN ISO 14689-1).

2.2 In situ block shape distribution

Another important factor to describe a rock mass geometry is the block shape distribution. The block shape on one hand controls the rock mass stability in terms of instable and kinematical free blocks and on the other hand the rock mass strength in terms of stress distributions (Gottsbacher, 2017). And again, several different approaches like the Austrian standard (ÖNORM EN ISO 14689-1) and the suggestion of the International Society for Rock Mechanics (1978) exist, but are mostly subjective, which is, regarding the mentioned influences not state-of-the-art. Figure 2.3 shows the different block shape types, which are used for the block shape classification in the mentioned approaches.

The recommendations are missing a method for accurate measurements of block volumes and the classification of the shapes, but contain descriptive and mathematically complex describable suggestions for the rock mass characterisation.

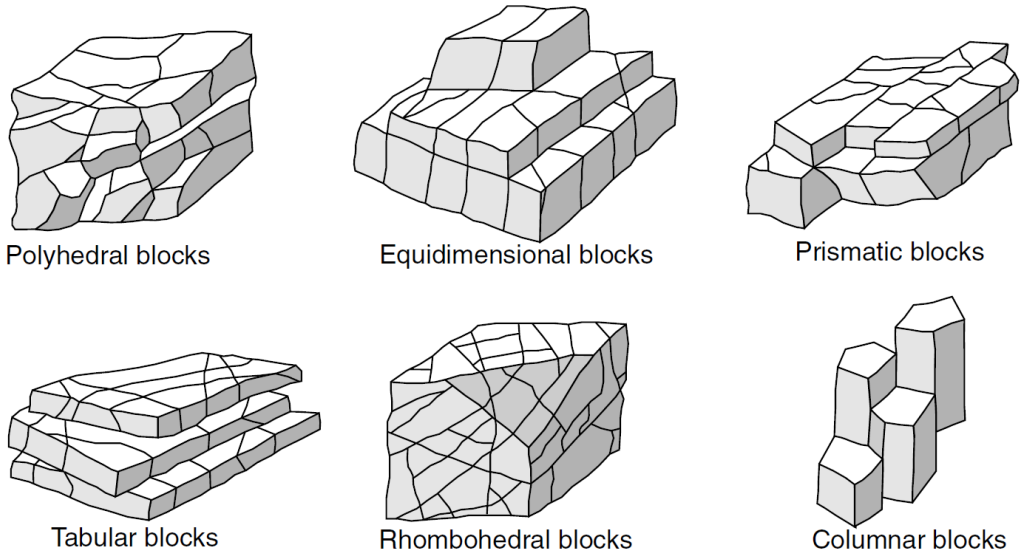

Figure 2.3: Block shape examples (Palmström, 2005).

A mathematical and easily applicable method to determine the shape and volumetric shape distribution of an investigated rock mass was developed by (Kalenchuk et al., 2006). In Figure 2.4, the classification system for block shapes is visualised. The parameters α and β are necessary to describe the flatness and the elongation of a block. In a subsequent approach, the methodology was applied and the characterisation of size and shape distribution of the blocks of a defined rock mass volume was evaluated (Kalenchuk et al., 2008).

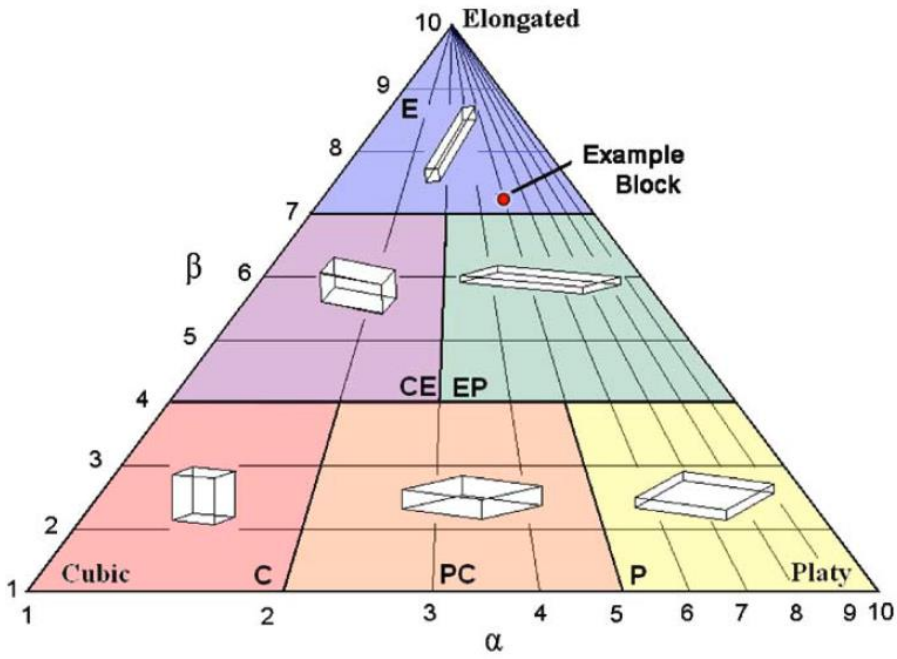

Figure 2.4: Block shape diagram showing zones that encompass basic shapes and simple sample blocks (Kalenchuk et al., 2006).

According to Kalenchuk et al. (2006), different representative values for the elongation shapes of blocks are calculated by equation (2.12). In this formula, β stands for the elongation of the blocks, expressed by the vertex to vertex proportions of an investigated block. The vectors $\vec{a}$ and $\vec{b}$ contain the three-dimensional Cartesian start and end coordinates of an investigated distance. For a perfect cube, the formula reveals 0.82. However, planar objects are returning a range of values which requires another descriptive parameter α to describe the flatness of a block. In addition, it has to be mentioned, that the approach cannot distinguish between convex and concave blocks, which has an influence on the determined BSD.

$$\beta = 10 \cdot \left[\frac{\sum \left(\vec{a} \cdot \vec{b} \right)^2}{\sum \|\vec{a}\|^2 \cdot \left\|\vec{b}\right\|^2} \right]^2 \tag{2.12}$$

Equation (2.13) describes the relationship between the surface area, the average chord length and the volume of any desired block.

$$\alpha = \frac{A_s \cdot l_{avg}}{7.7 \cdot V_B} \tag{2.13}$$

Both evaluated values are plotted in a triangular block shape diagram, whereby the corners are defined as the three extreme forms cubic, elongated and platy for block shapes.
This approach is used throughout this thesis and complemented by the determination of the dominant block orientation.

3 Methodology

The preliminary field investigation is based on the generation of a DSM using photogrammetry. Therefore, an outcrop of a quarry is captured with a series of high-resolution pictures which are further processed with the software ShapeMetrix^{3D} in order to get a meshed high-resolution point cloud. Applying the Discontinuity Set Extractor (DSE) allows the identification and characterisation of the discontinuity network in the rock mass (Riquelme et al., 2014). The discontinuity spacing and persistence can be determined by the application SMX Analyst using the results from DSE (Buyer & Schubert, 2017).
According to the data gathering, the study is continued with the simulation of a numeric discrete element model to obtain the block size distribution. This analysis is performed in 3DEC. The tool provides features for data export into text files, hence further processing of the block models needs no special applications.
In the last step, the block shape characterisation method after Kalenchuk et al. (2006) is applied to all identified blocks of the different models. The data processing was mostly performed in Matlab, version R2015a (The MathWorks Inc., 2008).

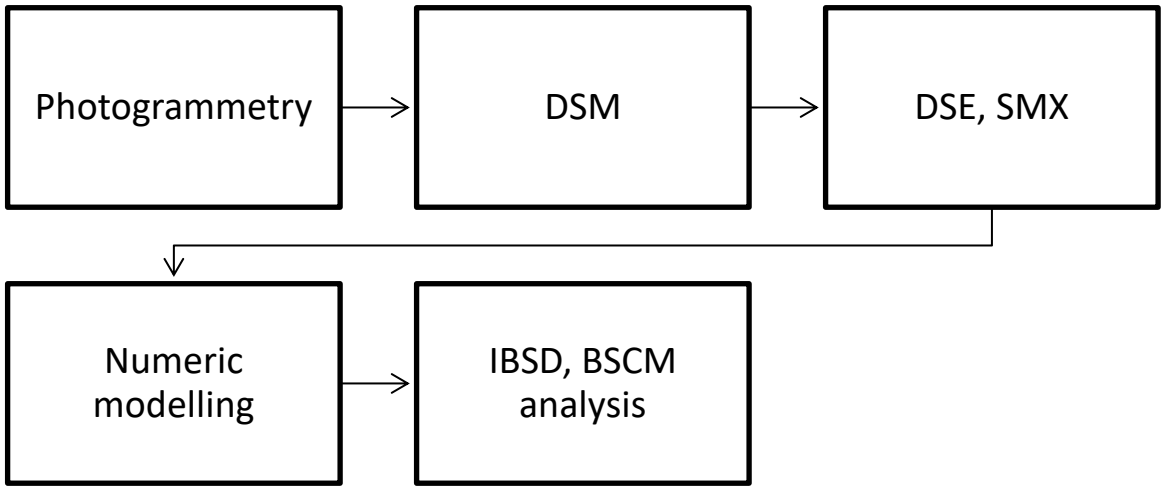

Figure 3.1: Flowchart for the data gathering and processing.

3.1 Data acquisition

For the photogrammetric investigation, a marble quarry in Gallmannsegg, which is located approximately 30 km to Graz (Styria, cf. Figure 3.2) was used. The investigated outcrop disposes three dominant joint sets with a main strike orientation of the foliation of 140/55.

The quarry is operated by the company ALPHA CALCIT Bergbau GmbH, which additionally provided a value for the current explosive consumption of 180 to 200 g/m³ (due to humidity, patronized emulsion explosives are used).

a b

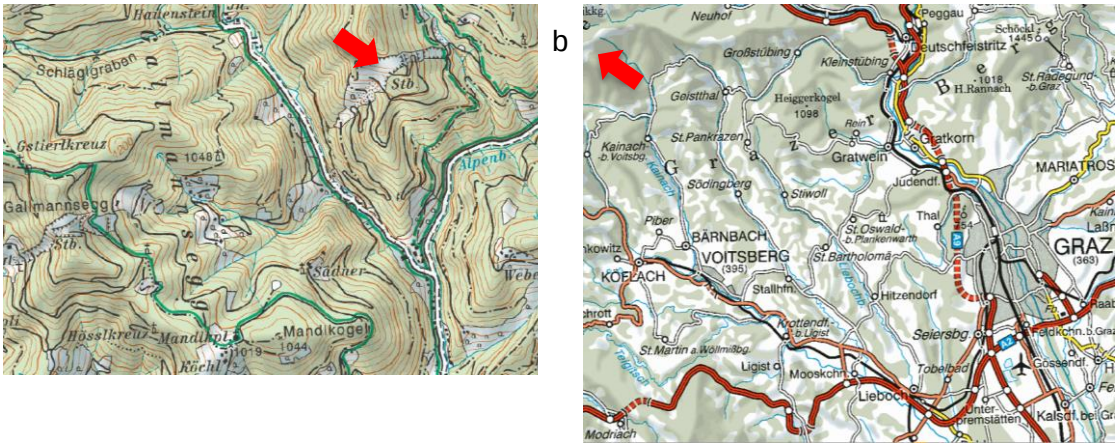

Figure 3.2: (a) Location of the marble quarry in Gallmannsegg, (b) location of Gallmannsegg on a map with Graz, marked with red arrows (Bundesamt für Eich- und Vermessungswesen (BEV), 2005).

3.2 Generation of the DSM

For the study, different DSM of separate outcrop walls of the quarry were generated by using the structure from motion approach implemented in ShapeMetrix^{3D}. It was necessary to create two 3D models (OC I and OC II, FIGURE 3.3) for the different demands of the subsequent processing steps of the DSE and ShapeMetriX^{3D}. The DSM contain both the whole quarry outcrop to get a potential wide range of captured discontinuities and a perpendicular oriented side wall. The pictures, to generate the DSM for the side wall, were taken with focal lengths of 17 and 50 mm within an attempted shooting distance of 10 to 20 m, resp. 70 mm at a shooting distance of 140 m for the whole outcrop. An overlap of approximately 80 % between the single pictures was maintained for all pictures taken.

The relatively high distance ensures the capture of the whole outcrop with a proper angle of the pictures, whereas the high overlap between two adjacent pictures ensures a good connectivity for the reconstruction algorithms.

Appendix A contains Table 6.1 which documents the model qualities to show. It should be mentioned, that the model for the semi-automatic DSE study requires a much higher coverage of 3D points.

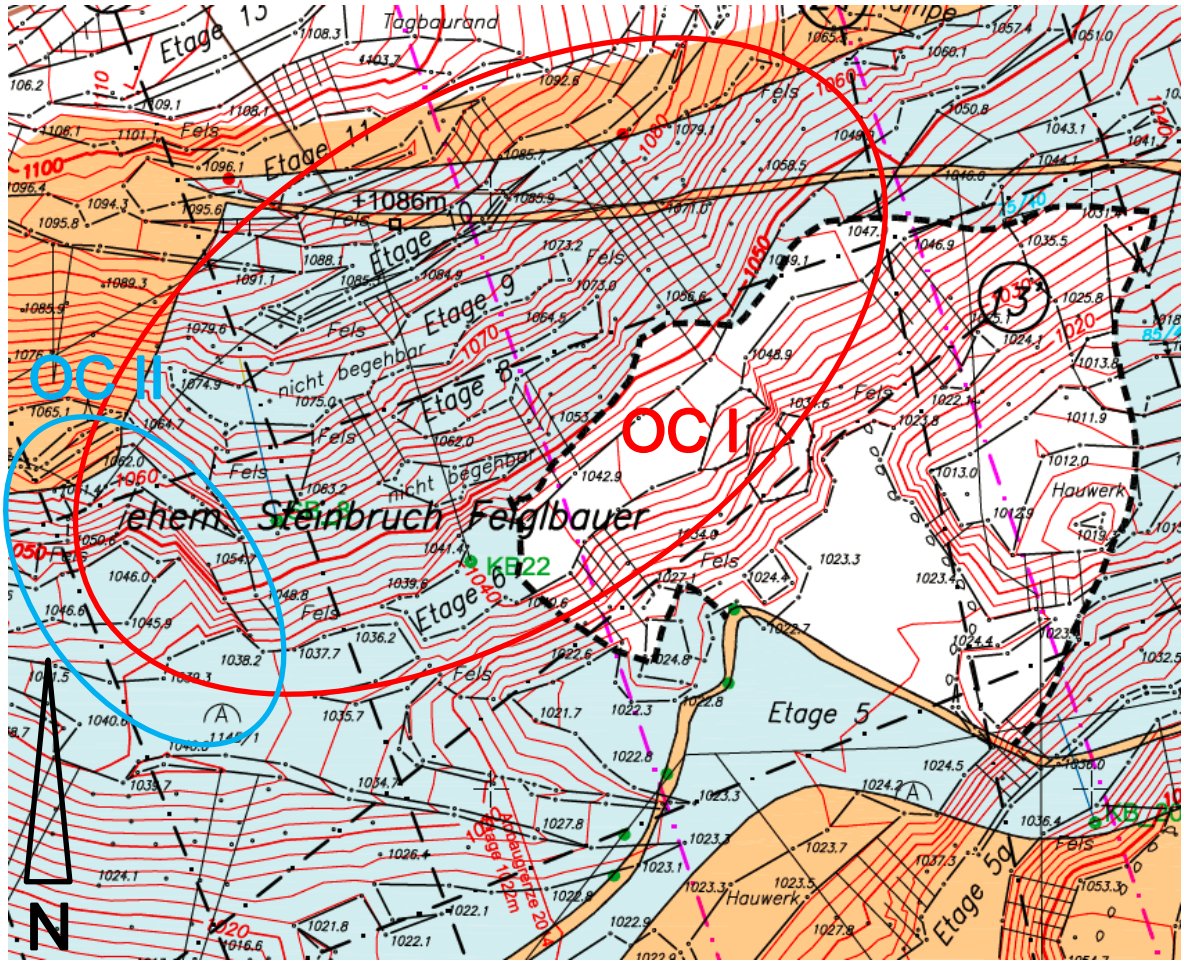

Figure 3.3: Section of the layout map of the quarry, including the investigated outcrops: The main outcrop wall, marked with a red ellipse and referred as Outcrop I (OC I) and the left edge of the main outcrop wall, marked with a blue ellipse and referred as Outcrop II (OC II) (Schuscha, 2016).

Within the CloudCompare version 2.8.1 (Girardeau-Montaut, 2017), the two DSM were trimmed to the relevant model areas to guarantee reasonable DSE analyses. The non-relevant sections include e.g. talus cones and the bottom of the quarry. Furthermore, small non-connected model sections and berms are eliminated. Figure 3.4 shows the unprocessed coloured point cloud, whereby the missing edge in the left section of the outcrop is considered in the second model for the DSE analysis.

a

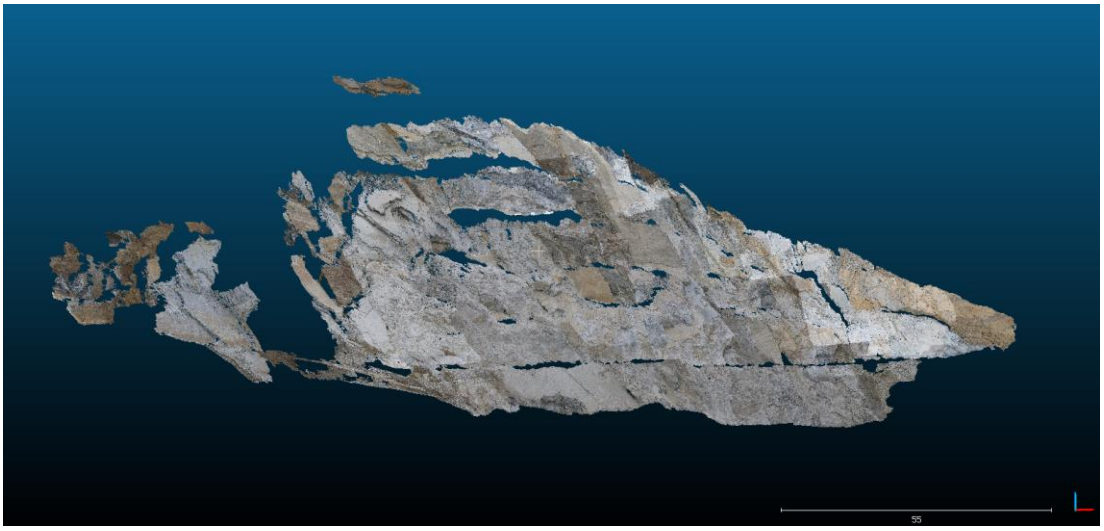

b

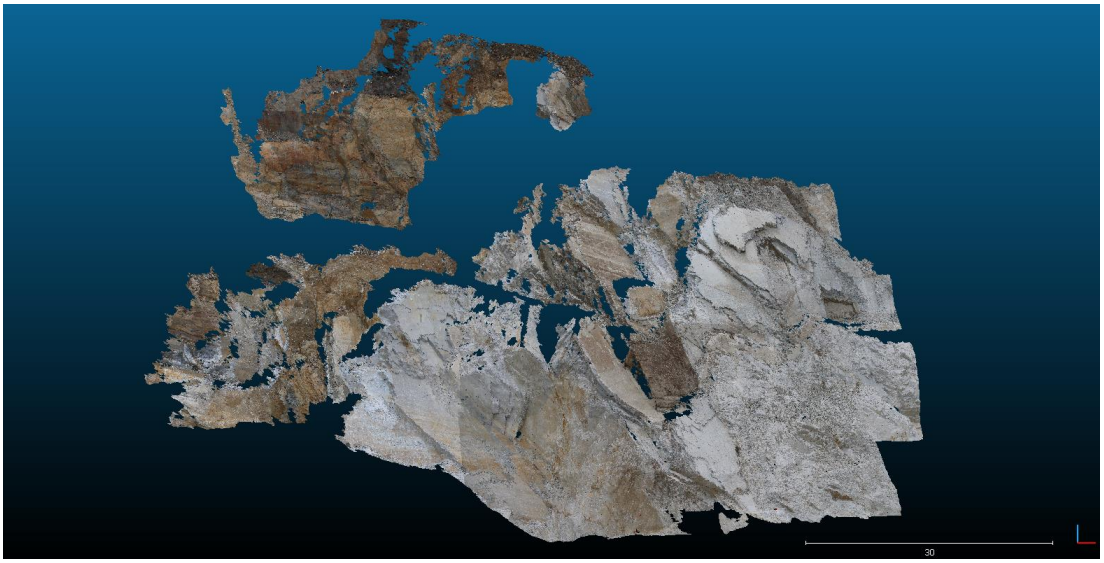

Figure 3.4: 3D point cloud model of the (a) outcrop I for the SMX analysis and of the (b) OC II for the DSE analysis, visualised in CloudCompare.

3.3 Discontinuity network characterisation

The geometrical characterisation of the discontinuity sets was performed by combining the two applications SMX Analyst and the DSE (Buyer & Schubert, 2017). The combination allows to use the strengths of both tools to obtain the most suitable measurements.

The semi-automatic joint set identification of the DSE allows a quick and highly detailed result compared to the manual discontinuity mapping with SMX Analyst, whereby it is still necessary to check the model for joints without exposed joint planes. It is not possible to identify such joints in the DSE. Therefore, they should be manually in SMX. The application of both methods is described in the following chapters.

The results for the discontinuity spacing of the manual approach were compared to the

automatically gained values of the DSE analysis by another SMX analysis of the structure map.

3.3.1 Discontinuity identification

3.3.1.1 Manual discontinuity mapping

A manual parameter study was performed previously in SMX Analyst to compare the density of the orientation poles and the total usage of the model's points with different input parameters. The manual mapping encompassed only OC I. Subsequently, it was checked how the evaluation of three or four discontinuity sets comply to the data gain from the following DSE analysis. The investigations pointed out that a fourth joint set lowers the density values and the total usage of the 3D points. Hence, a model with three discontinuity sets was chosen. However, in order to include also most joint planes of a fourth joint set identified by the clustering settings, the standard deviation was increased to take parts of the missed joints into account. The identification of three main joint sets is also congruent with the field observations during the data collection. Additionally, the definition of three joint sets simplifies the comparability to most of the analytical approaches (which are referring to three discontinuity sets).

3.3.1.2 Semi-automatic discontinuity identification

For the DSE analysis, OC II (Figure 3.5) which is exposing joint surfaces with various orientations, was selected to ensure the acquisition of all significant discontinuities. This section was used for the DSE analysis due to the stepped foliation planes and the good aperture of the main discontinuity sets at the outcrop edge. The aim of the semi-automated approach is the evaluation of the following values for all discontinuity sets:

- Spatial distribution of the joint planes
- Number of joints
- Dip directions and dip angles of the joint planes

The explanations of the parameters for the DSE analysis are listed in Table 3.1.

Table 3.1: Description of the input parameters of the DSE analysis (Riquelme et al., 2014; 2015).

Parameter	Description
k_{nn}	k nearest neighbours, calculated by using the nearest neighbour search function (The MathWorks Inc. 2008) and the Euclidean distance.
η_{max}	Tolerance for the co-planarity test is the maximum allowable deviation in a subset of points.
n	Size of the n by n grid for the KDE, must be a power of 2.
γ	Minimum angle between normal vectors of discontinuity planes.
N	User defined number of principal pole planes or for the sake of simplicity discontinuity sets.
γ_1	Minimum angle between the normal vector of a discontinuity plane and the normal vector of a point (cone for pole assignment).
k	Cluster distribution threshold for cluster alignment.

To compare the SMX evaluations to the DSE results, the SMX values were investigated with manually set clustering parameters. The investigation method allows the determination of suitable results, especially in accordance to the wide span of Outcrop I compared to Outcrop II. It must be noticed, that deviations of the dip directions of up to 20 degrees occur, which are still in the accepted range as they are considered through the spherical aperture of the manual investigations.

A minimum size of ten points per identified joint plane was selected in order to neglect too small, insignificant joint planes.

Again, various discontinuity set evaluations, listed in Table 3.2, were executed. The major interest of the parameter study was to identify the effects of a difference in the resolution of the Kernel Density Estimation (KDE) and the variation of the minimum angle between the normal vectors of the discontinuity sets to the density and the percentage of assigned points. According to the approach of Riquelme et al. (2014), k_{nn} was set to 30 and η_{max} to 20 % to optimise the deviation of the plane pole concentration to the principal pole. Evaluation No. 7 and No. 9 reveal the highest amount of used 3D points referred to the total amount of model points, assigned to the determined joint sets. The density results are in a comparable range for all evaluations and were neglected for the decision.

Figure 3.5: Overview of Outcrop II (compass direction: west-south-west), which was used for the DSE analysis.

Table 3.2: Input parameters for the DSE parameter study.

	Principal plane calculation						**Cluster analysis**
No	**k_{nn}**	**η**	**n**	**γ**	**N**	**γ_1**	**k**
1	30	0.2	512	30	3	30	1.5
2	30	0.2	1024	30	3	30	1.5
3	30	0.2	512	40	3	30	1.5
4	30	0.2	1024	40	3	30	1.5
5	30	0.2	512	30	4	30	1.5
6	30	0.2	1024	30	4	30	1.5
7	30	0.2	512	40	4	30	1.5
8	30	0.2	1024	40	4	30	1.5
9	30	0.2	512	35	3	30	1.5
10	30	0.2	512	35	4	30	1.5
11	30	0.2	1024	35	3	30	1.5

The parameters of evaluation No. 9 are used for following processing in this work (cf. Table 3.2) as their result includes the highest total amount of assigned points.

Through the individual colours red, green and blue, the assignment of the 3D points to the identified discontinuity sets in the point cloud model are clearly shown (cf. Figure 3.6 compared to the original DSM in Figure 3.4-b).

The model of the whole outcrop used for the 3D model in the SMX analysis is shown in Figure 3.7. As the main discontinuities are visible and therefore joint faces can be detected, this section is suitable for the manual discontinuity set evaluation.

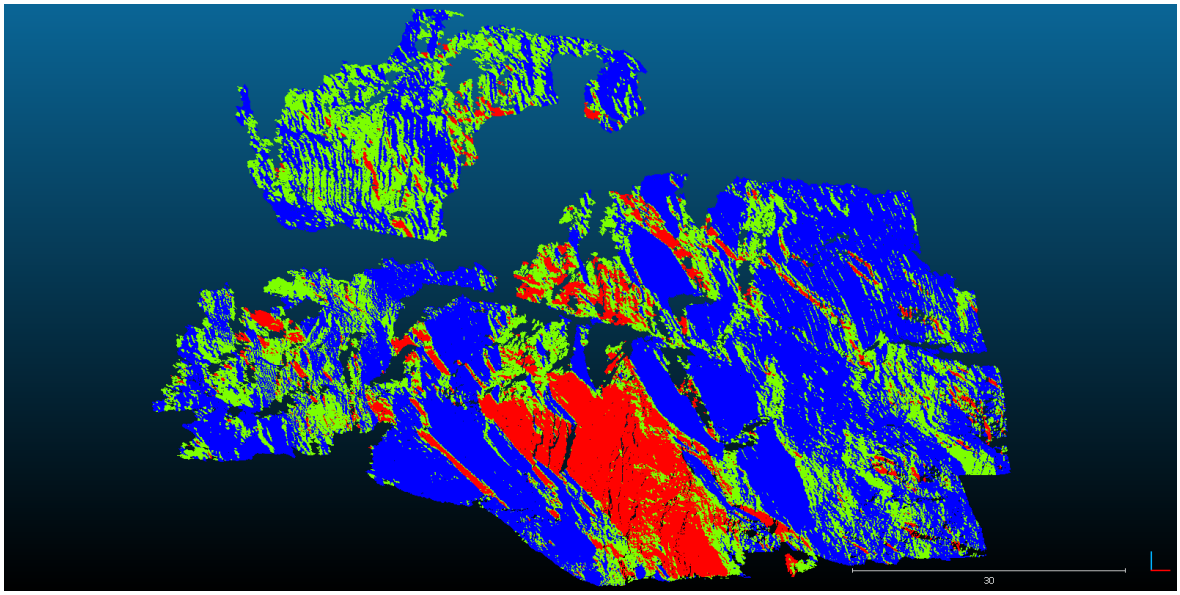

Figure 3.6: DSE evaluation No. 9 with three assigned discontinuity sets.

Figure 3.7: Quarry outcrop used for the manual SMX investigation.

3.3.2 Joint normal spacing

The multiple scan-line dialog of ShapeMetriX^{3D} allows the calculation of the joint normal spacing, based on the distances of the reference joint traces. However, it gives no values for the persistence of the DS. Further information regarding the determination is available in the user manual of the software (3GSM GmbH, 2015). Due to the missing information about the persistence, a comparison of the trace length to the size of the outcrop is required to get the input data for the 3D modelling. The following parameters are perceived for each structure set to define the input values for the numeric modelling:

- Set normal spacing
- Standard deviation of the discontinuity spacing
- Number of identified discontinuities

3.4 Modelling of the IBSD and BSD

Besides the mentioned input parameters, terms like a suitable model size and the elimination of the boundary blocks must be considered. As Cai et al. (2004) state, the effect of the intersection angle of the joint sets compared to the block sizes is relatively small, therefore a variation of the dip and the dip direction by considering the standard deviation was neglected in this test series to focus on the distribution of the spacing parameters.
Owing to low density values for the appearance of further discontinuity sets, the three major sets including the foliation were defined as input values (subchapter 3.3), the values are displayed in Table 3.3.

Table 3.3: 3DEC input parameters for the foliation and the two major discontinuity sets.

Joint set	DD [°]	D [°]	n [-]	s [m]	σ [m]
1	143.95	48.82	4109	0.58	1.87
2	31.07	87.01	6447	0.72	5.18
3	246.15	80.68	2514	0.79	7.59

Söllner (2014) proposes a replication factor of r = 100 for each numerical simulation to ensure statistical representativeness. This replication factor is applied to this study, as through the multiple simulations an acceptable variance of the mean value and the quantile values of the block volumes is achieved.

3.4.1 Determination of the model size and model composition

Three aspects influence the model size (Kluckner et al., 2015):

- Origin of discontinuities
- Definition of the boundary blocks
- Ratio of mean block area at the front face to the size of the mapping window

The origin of the joint sets is defined at the model centre, since Söllner (2014) did not recognise any significant differences in the results, compared to origins at the model face.
To fulfil the boundary block criterion, the edge lengths of the model must include the equivalent spacing at least twice. The largest spacing (including its standard deviation) in this test row would be the third discontinuity set with $s_3 + \sigma_3 = 8.38$ m. Thus, the minimal edge length of a cubic model would have to be approximated with 17 m. This would not fit for the smallest model with a = 10 m. However, for the estimation of the range of the model size and performance issues of the highly persistent models with substantial amounts of blocks, the criterion is not applied.
For the evaluation of the model size, the limitation ratio $A_{b,mean}/A_{out}$ must fit in a range of 0.01 to 0.07 to fulfil the criterion, when the boundary block criterion becomes effective. $A_{b,mean}$ describes the mean block area at the surface and A_{out} defines the face area of the outcrop. For simplification purposes (as the block surface area is provided by 3DEC) and to encounter the certain zone or the confidence interval of the ratio (cf. Figure 3.8), the block surface area was used for this parameter. Since it is desired to use cubic shaped models, the outcrop area A_{out} of the models is defined by $A_{out} = a^2$ with a as the edge length.

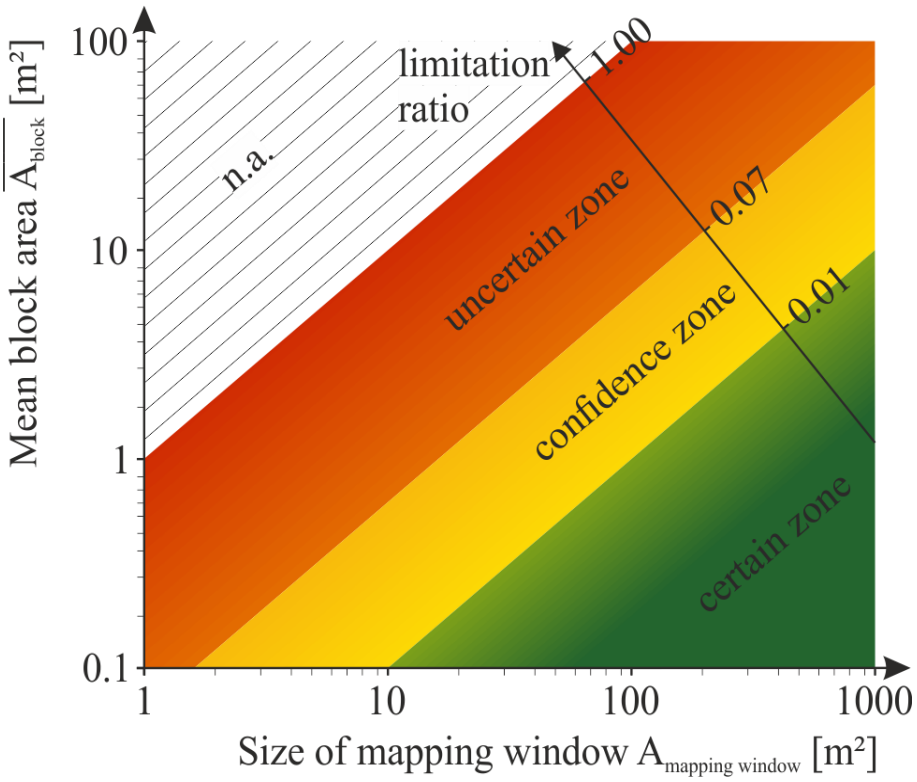

Figure 3.8: Diagram for the rating of the used outcrop area of the numeric model compared to its mean block surface area (Kluckner et al., 2015).

To find a range of model sizes, the worst-case situations for a possible disassembling of the rock mass are assumed. For defining these ranges, the persistence of the foliation was assumed to be less than 100 percent. The mean values of the block surface areas were calculated with a model replication of 100 to eliminate outliers. Table 3.4 contains the determination of the ranges for the cubic model sizes with edge lengths of a = 10 m, a = 20 m and a = 30 m. It shows that the ratios $A_{b,mean}/A_{out}$ fit into the given range of 0.01 to 0.07.

Table 3.4: Determination of the ratio of the block surface area to the model face.

Model ID	p_i [-]	$A_{b,mean}$ [m²]	A_{out} [m²]	$A_{b,mean}/A_{out}$ [-]
101	1.0	5.52	100	0.055
407	0.8	8.84	400	0.022
410	0.6	15.55	400	0.039
900	0.4	34.36	900	0.038

3.4.2 Persistence study

As no reliable persistence measurements are available and the measured trace lengths provide a disproportional range, the evaluated discontinuity set parameters are combined as four different test series with different combinations for the persistence values. The distributions of the determined trace lengths of the joint sets are visualised in Figure 3.9. In contrast to the persistence values of the model size evaluation, the values for discontinuity set 2 and 3 are combined in all possible variations within a range from 0.4 to 1.0 for joint set 2 and 0.4 to 0.8 for joint set 3. The values are decreased in steps of 20 percent within the determined range. An essential point is to assume the persistence of the foliation as 1.0 or 100 percent for all test models, which is for example indicated for bedding planes by Wittke (2014).

Table 3.5 shows the modifications and in addition the product of the persistence values, the worst-case scenario would be a persistence of 1.0 for all discontinuity sets. As shown in the table, the study assumes a rather fractured rock mass.

a

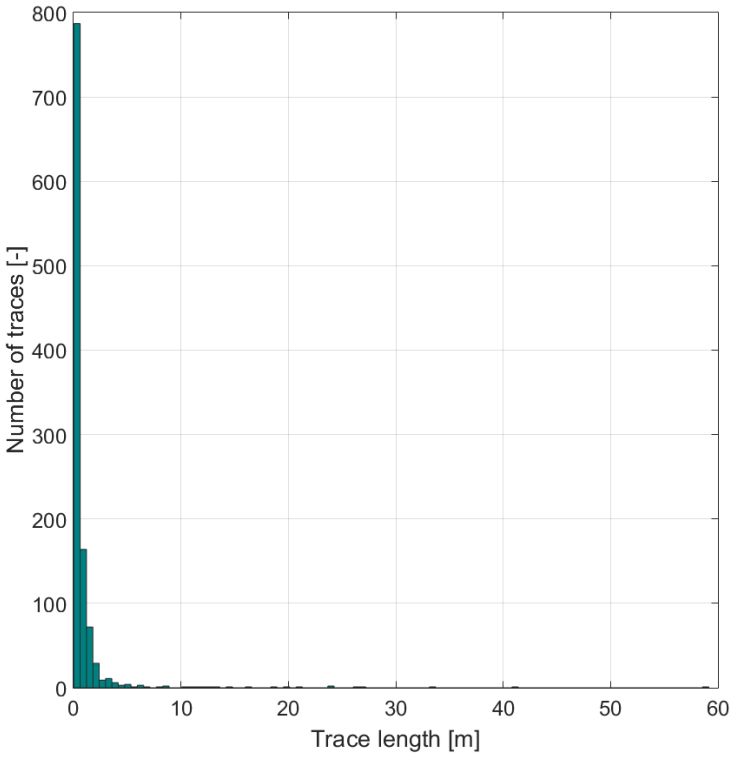
Number of traces [-]
Trace length [m]
0
100
200
300
400
500
600
700
800
0
10
20
30
40
50
60

b

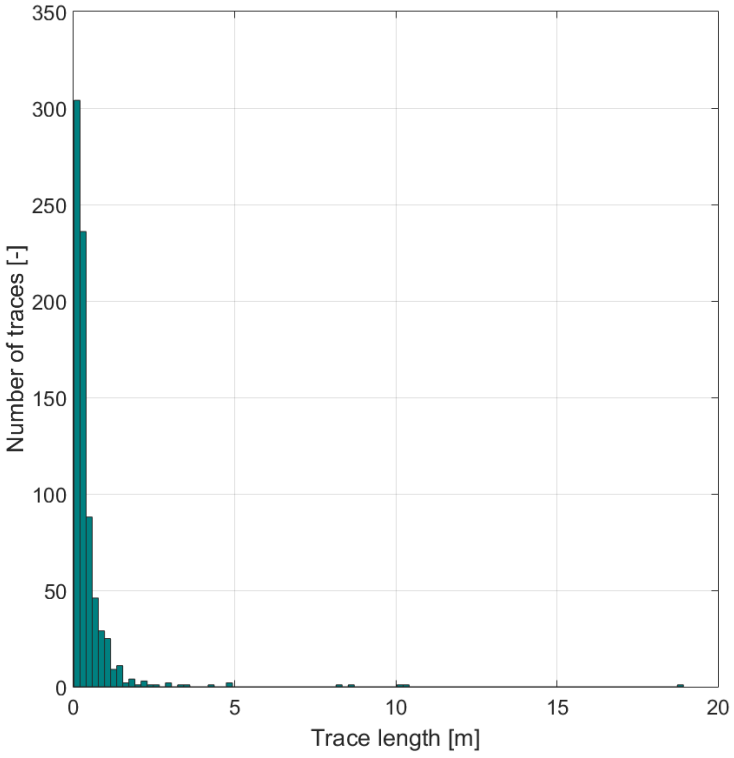
Number of traces [-]
Trace length [m]
0
50
100
150
200
250
300
350
0
5
10
15
20

c

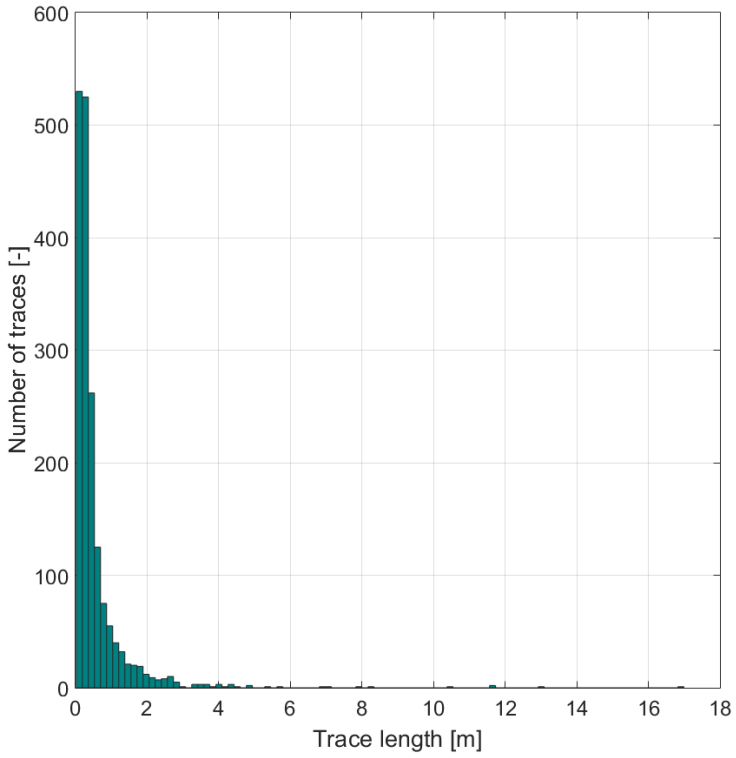

Figure 3.9: Trace lengths of (a) joint set 1, (b) joint set 2 and (c) joint set 3.

Table 3.5: Persistence values of test series, with three model simulations each.

Test series	Model ID	p_1	p_2	p_3	$\bar{p}$[1]
1	110	1.0	1.0	0.8	0.93
	102	1.0	1.0	0.6	0.87
	103	1.0	1.0	0.4	0.80
2	404	1.0	0.8	0.8	0.87
	405	1.0	0.8	0.6	0.80
	409	1.0	0.8	0.4	0.73
3	406	1.0	0.6	0.8	0.80
	414	1.0	0.6	0.6	0.73
	910	1.0	0.6	0.4	0.67
4	903	1.0	0.4	0.8	0.73
	902	1.0	0.4	0.6	0.67
	901	1.0	0.4	0.4	0.60

[1] $\bar{p} = \frac{\sum_{i=1}^{3} p_i}{3}$

3.4.3 Distribution of the block shapes and orientations

For the characterisation of the block shapes, it is necessary to describe the geometry of each single block. Therefore, the coordinates of the block corners must be provided, which is an implemented functionality of 3DEC. For the analysis, the formulations according to Kalenchuk et al. (2006) were scripted and the data processing semi-automatised by using Matlab.

The procedure after Kalenchuk et al. (2006) classifies a dimensionless α and β value for each block of the model. α is introduced to describe the relation between the surface area A_S, the block volume V and the average chord length l_{avg}. A normalization factor which is equal to 7.7 is defined to assure that for a cube α = 1. The range of α reaches from 1 to 10 and describes the flatness of a block and is calculated with equation (2.13).

The factor β is expressed by equation (2.12). It is calculated by a function of the sum of the dot products of the block coordinates, divided by the product of their vector lengths (defined by the Euclidean distance). For a weighting of the chord inter-relationships, the terms within the summations are squared. Only vertices with a span longer than their median value are considered for the subsequent parameter calculation of β. Furthermore, to create a more convenient scaling of β, the external squaring of the fraction term is applied.

The equations (2.12) and (2.13) express the relation of the mapping of α and β into a Cartesian coordinate system with a logarithmic abscissa. The base length ξ of the equilateral plot triangle for the applied processes is set to ξ = 1. In this equilateral case, the height η of the triangle is defined by $\eta = \xi \times \sin 60° = 0.866$. Further, β is defined within a range of 1 to 10, which leads to y values in a range from 0 to η as described in equation (3.1).

$$y = \left(\frac{\beta - 1}{10 - 1}\right)\eta \tag{3.1}$$

The values, which are plotted on the abscissa to take the triangular shape into account depend on y. x is plotted within a logarithmic scale from 1 to 10 and is settled between the triangle corners - ξ / 2 and ξ / 2 at the abscissa.

$$x = \left(\frac{\eta - y}{\eta}\right)\left(\log_{10}\alpha - \frac{\xi}{2}\right) \tag{3.2}$$

Due to the model replications, also the block shape distribution must be considered for each numerical simulation. This requires a collection of the result of each model in density plots

to achieve a representative visualisation. Figure 3.10 depicts two block shape distributions generated by equal model input parameters and shows why a density plot is necessary to create a distribution for all model replications. Therefore, the Kernel Density Method of Botev et al. (2010) is used to provide density values of the block shape distribution. For the KDE, a 64 times 64 kernel grid is used, as this size optimises the visualisation.

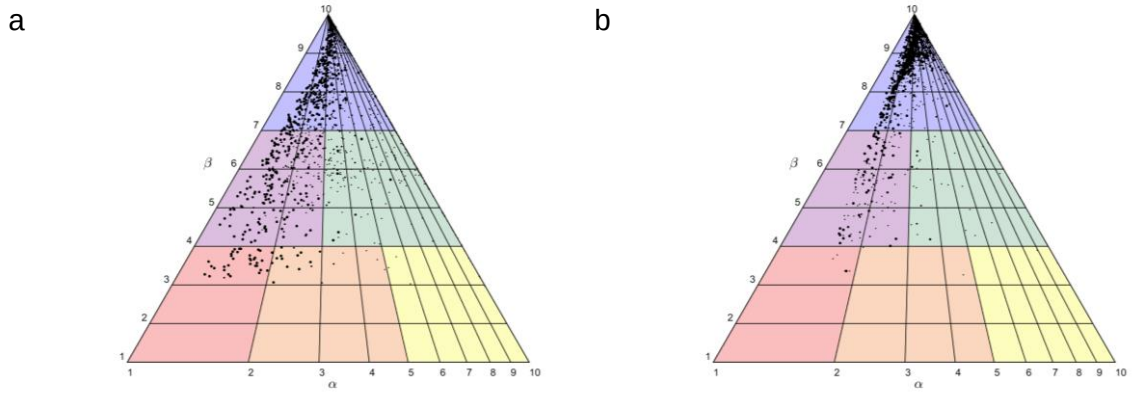

Figure 3.10: (a) Replication 14 and (b) replication 43 of the model 110 as exemplary block shape distributions.

As the block orientation is of importance to formulate a statement for the structure and the stiffness of a rock mass, the orientation of the main axis of the blocks is determined as the block vertices with the largest distances and plotted in an equal angular polar-grid of the lower hemisphere (Schmidt net). Again, the orientations are collected within a density distribution plot, determined by using the previously introduced Kernel Density Distribution method (Botev et al., 2010).The resolution of the KDE is also set to 64 times 64. The block orientation is expressed by the unit vector of the longest vertex to vertex distance of an investigated block (cf. equation (3.3)).

$$\overrightarrow{v_O} = \frac{\vec{b} - \vec{a}}{\left\|\overrightarrow{ab}\right\|} = \frac{\begin{bmatrix} b_1 \\ b_2 \\ b_3 \end{bmatrix} - \begin{bmatrix} a_1 \\ a_2 \\ a_3 \end{bmatrix}}{\sqrt{(b_1 - a_1)^2 + (b_2 - a_2)^2 + (b_3 - a_3)^2}} \tag{3.3}$$

4 Results

4.1 Discontinuity network characterisation

To combine the advantages of the DSE analysis and the SMX investigation, the results of both approaches were compared. Table 4.1 contains the combined input parameters for the numerical simulations, which are referring to the more detailed findings of the following sections 4.1.1 and 4.1.2.

Table 4.1: Combined input values for numeric modelling with three joint sets.

Joint set	DD [°]	D [°]	n	s [m]	σ_s [m]
1	143.95	48.82	4109	0.58	1.87
2	031.07	87.01	6447	0.72	5.18
3	246.15	80.68	2514	0.79	7.59

4.1.1 Discontinuity identification

In Table 6.2 (cf. Appendix A), the results of the DSE parameter study are shown. For further DSE investigations, the values of evaluation no 9 were used to ensure a maximum number of assigned 3D points. Table 4.2 contains the semi-automatically evaluated results of the DSE analysis.

Table 4.2: Results for the orientation of the joints in quarry face “Outcrop II” obtained from the DSE.

Joint set	DD [°]	D [°]	%[2]
1	143.95	48.82	63.53
2	031.07	87.01	12.97
3	246.15	80.68	5.52

Figure 4.1 shows the results of the DSE analysis, whereby the 3D points are assigned to three discontinuity sets. The assignment is visualised by the different colouration.
In Table 4.3 and Figure 4.2, the results of the manual SMX analyses are displayed. As the application gives no possibility to assign the structure set ID, it was necessary to assign the joint sets to the ID of this study’s definition.

[2] Number of assigned points over the total amount of points.

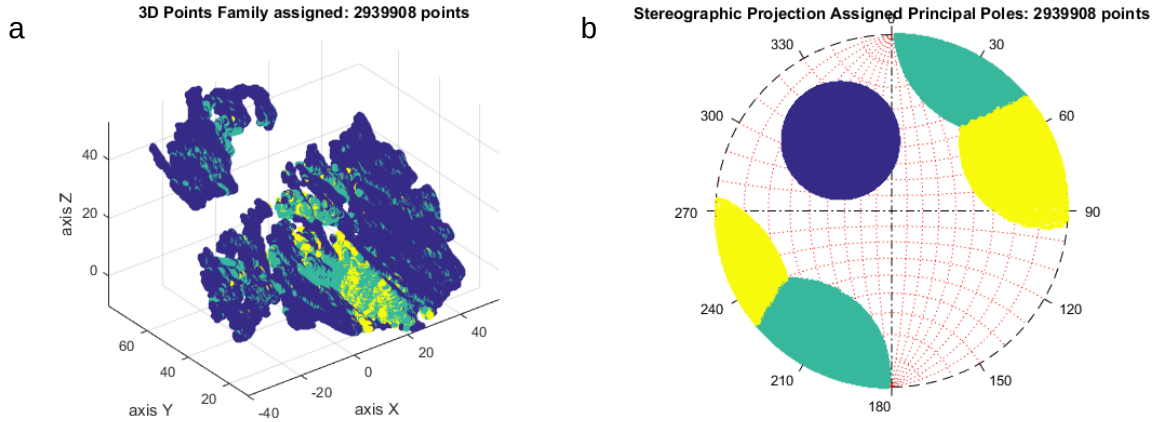

Figure 4.1: (a) Point cloud of the side wall of the outcrop and (b) the stereographic projection with the appropriate plane poles. Joint set 1 is marked in blue, joint set 2 in green and joint set 3 in yellow 3D points in (a) and principal poles in (b).

Table 4.3: Results, obtained from manual SMX analyses of the two DSM with various membership angles.

Outcrop	Membership angle [°]	Joint set	Joint set SMX	DD [°]	D [°]	Spherical aperture [°]	Cone of confidence [°]	Degree of orientation [%]
I	30	1	3	144.46	51.76	9.53	1.26	97.26
		2	1	9.13	76.80	16.39	3.98	92.04
		3	2	57.12	89.95	16.11	2.50	92.30
I	35	1	3	144.62	52.24	9.69	1.26	97.17
		2	2	13.04	77.26	20.27	4.80	88.00
		3	1	236.27	89.81	17.82	2.63	90.64
I	40	1	3	144.44	52.39	10.26	1.32	96.83
		2	2	12.63	77.21	20.62	4.80	87.60
		3	1	235.77	89.21	18.97	2.71	89.43
II	30	1	3	145.96	50.80	5.48	1.64	99.09
		2	1	20.41	82.45	13.99	3.61	94.15
		3	2	233.02	85.57	9.95	4.53	97.01

Figure 4.2 shows the stereographic projection of the discontinuity analysis, performed by the manual SMX Analyst mapping. The illustrated colours red, green and blue show the assignment to the identified discontinuity sets, whereby the black plane poles were not assigned.

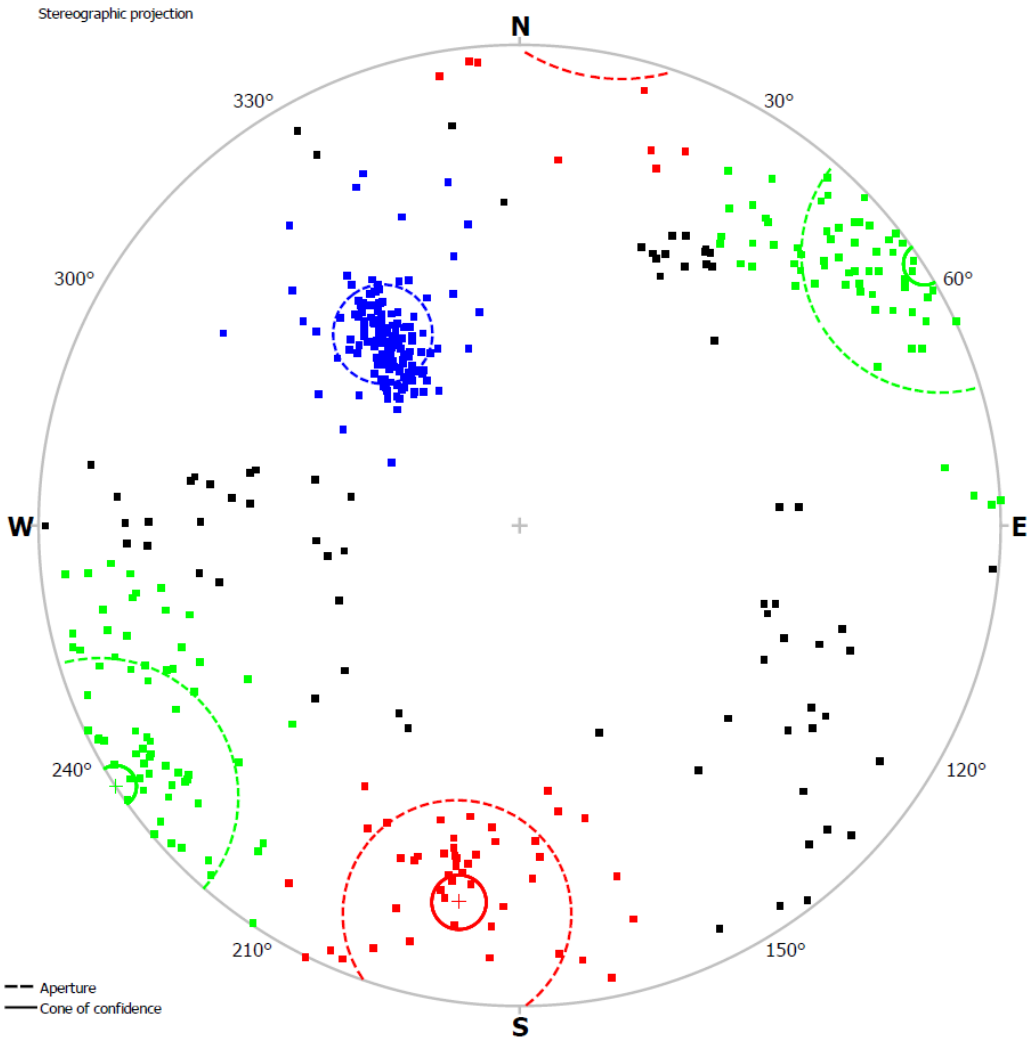

Figure 4.2: Stereographic projection of the through the SMX analysis evaluated and assigned plane poles. Joint set 1 is marked with blue, joint set 2 with red and joint set 3 with green plane poles. The black plane poles were not assigned.

4.1.2 Joint normal spacing

Table 4.4 contains the results for the spacing parameters of the SMX analysis. It includes an evaluation with three and one with four discontinuity sets.

In Table 4.5 the parameters for the joint normal spacings for the DSE analysis after the multiple scanline analyses are listed.

The semi-automatically identified trace maps which were determined during evaluation of the joint normal spacing are outlined in Appendix A, Figure 6.1.

Table 4.4: Spacing parameters for three joint sets, obtained through SMX.

Joint set	n [-]	$\bar{s}$ [m]	$\tilde{s}$ [m]	σ_s [m]	F [1/m]	F_{min} [m]	F_{max} [m]
1	156	13.78	6.87	16.12	0.07	0.00	83.78
2	729	2.41	1.09	3.27	0.41	0.00	29.04
3	562	6.70	1.36	13.21	0.15	0.00	77.24

Table 4.5: Spacing parameters evaluated from the DSE generated structure map.

Joint set	n [-]	$\bar{s}$ [m]	$\tilde{s}$ [m]	σ_s [m]	F [1/m]	F_{min} [m]	F_{max} [m]
1	4109	1.24	0.58	1.87	0.80	0.00	12.87
2	6447	2.99	0.72	5.18	0.33	0.00	48.51
3	2514	4.16	0.79	7.59	0.24	0.00	66.26

4.2 Modelling of the IBSD

4.2.1 Persistence study

4.2.1.1 Test series 1

In Table 4.6, the model ID and the respective persistence values are listed along with their corresponding results of the block size distribution. The results are consisting of the median values and the standard deviations of the mean block volumes and the quantiles of the volume distribution curve of the model runs. Figure 4.3 shows the development of the values, dependent on the decreasing persistence. Furthermore, Figure 4.4 plots the cumulative distribution functions of the simulations, with all replicated models each. In addition, the quantile values and the mean value are delineated.

Table 4.6: Results of test series 1 for block volumes with corresponding standard deviations.

Model ID	p_1	p_2	p_3	$\bar{p}$	V_{mean}	σ_{Vmean}	$V_{0.25}$	$\sigma_{V0.25}$	$V_{0.50}$	$\sigma_{V0.50}$	$V_{0.75}$	$\sigma_{V0.75}$
110	1.0	1.0	0.8	0.93	0.798	0.105	0.047	0.012	0.211	0.040	0.769	0.115
102	1.0	1.0	0.6	0.87	1.069	0.214	0.063	0.028	0.265	0.089	1.003	0.242
103	1.0	1.0	0.4	0.80	1.585	0.325	0.093	0.047	0.426	0.150	1.502	0.443

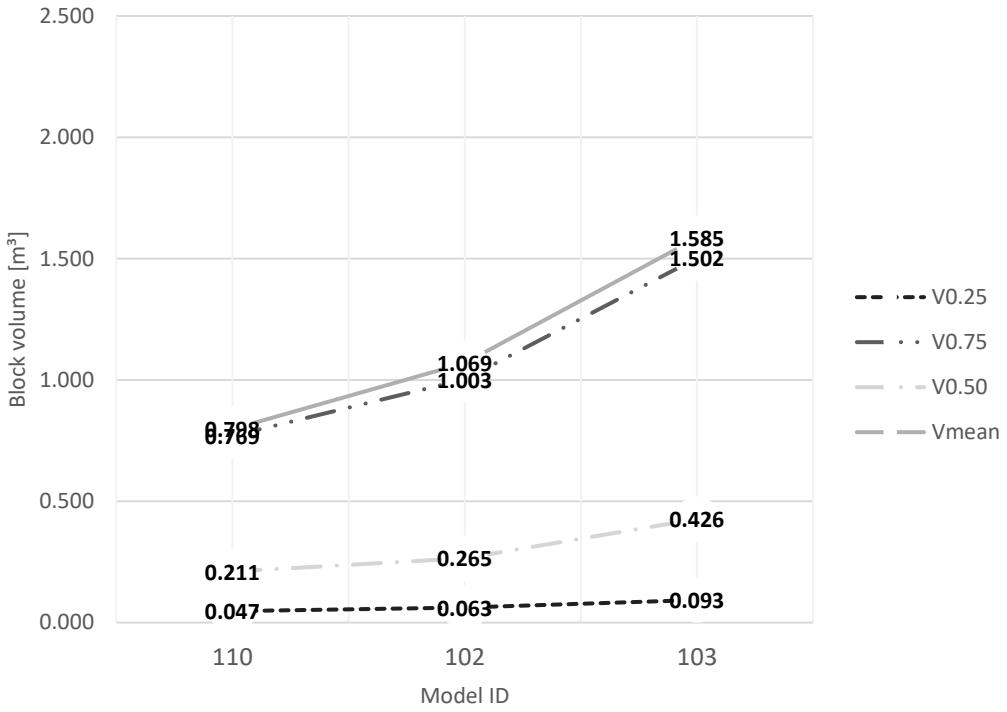

Figure 4.3: Result for block volumes of test series 1.

a

Model 110:

$V_{0.25}$ = 0.047 m³

$V_{0.50}$ = 0.211 m³

$V_{0.75}$ = 0.769 m³

V_{mean} = 0.798 m³

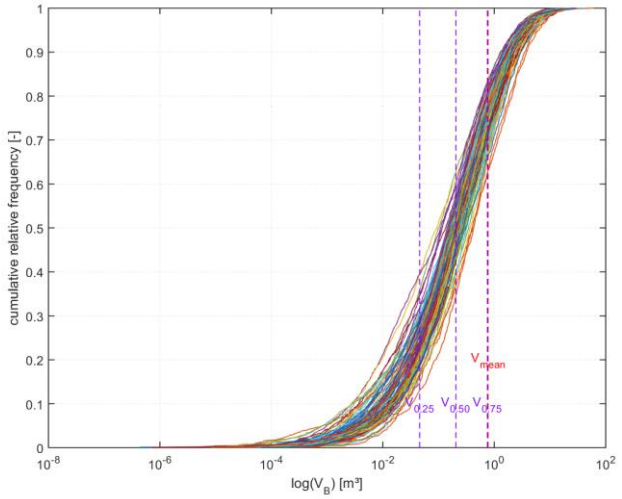

b

Model 102:

$V_{0.25}$ = 0.063 m³

$V_{0.50}$ = 0.265 m³

$V_{0.75}$ = 1.003 m³

V_{mean} = 1.069 m³

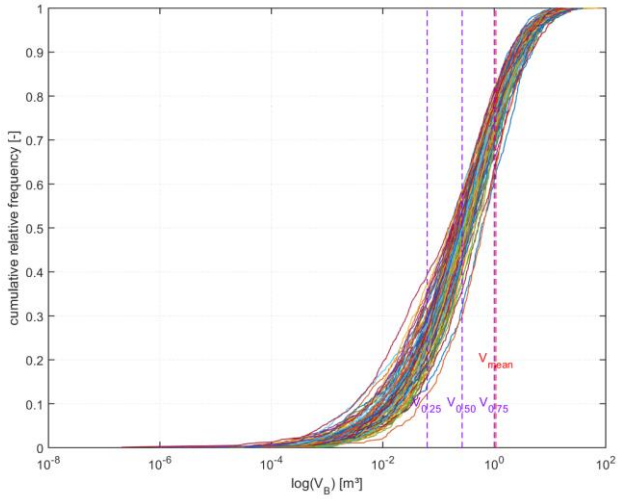

c

Model 103:

$V_{0.25}$ = 0.093 m³

$V_{0.50}$ = 0.426 m³

$V_{0.75}$ = 1.502 m³

V_{mean} = 1.585 m³

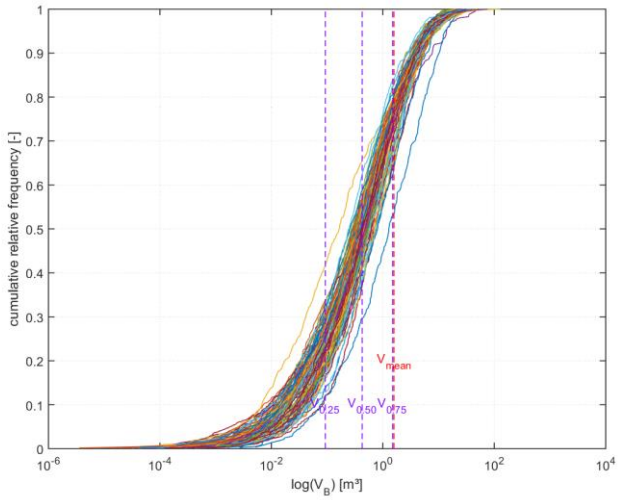

Figure 4.4: Results for cumulative distribution function of test series 1 including (a) model 110, (b) model 102 and (c) model 103.

4.2.1.2 Test series 2

Table 4.7 lists the model ID of the second test series and the applied persistence values are presented together with the resulting values of the block size distribution. The product p of the persistence values p_i is located in a range from 0.73 to 0.87. The listed results consist of the median values and the standard deviations of the mean block volumes and the quantiles of the volume distribution curve of the model replications. Figure 4.5 shows the development of the values, dependent on the decreasing persistence. Furthermore, Figure 4.6 is plotting the cumulative distribution functions of the simulations, with all replicated models each. Moreover, the quantile values and the mean value are delineated.

Table 4.7: Results of test series 2 for block volumes with corresponding standard deviations.

Model ID	p_1	p_2	p_3	$\bar{p}$	V_{mean}	σ_{Vmean}	$V_{0.25}$	$\sigma_{V0.25}$	$V_{0.50}$	$\sigma_{V0.50}$	$V_{0.75}$	$\sigma_{V0.75}$
404	1.0	0.8	0.8	0.87	1.006	0.128	0.059	0.014	0.262	0.048	0.943	0.137
405	1.0	0.8	0.6	0.80	1.308	0.148	0.076	0.017	0.339	0.057	1.238	0.165
409	1.0	0.8	0.4	0.73	2.006	0.248	0.117	0.026	0.525	0.088	1.908	0.264

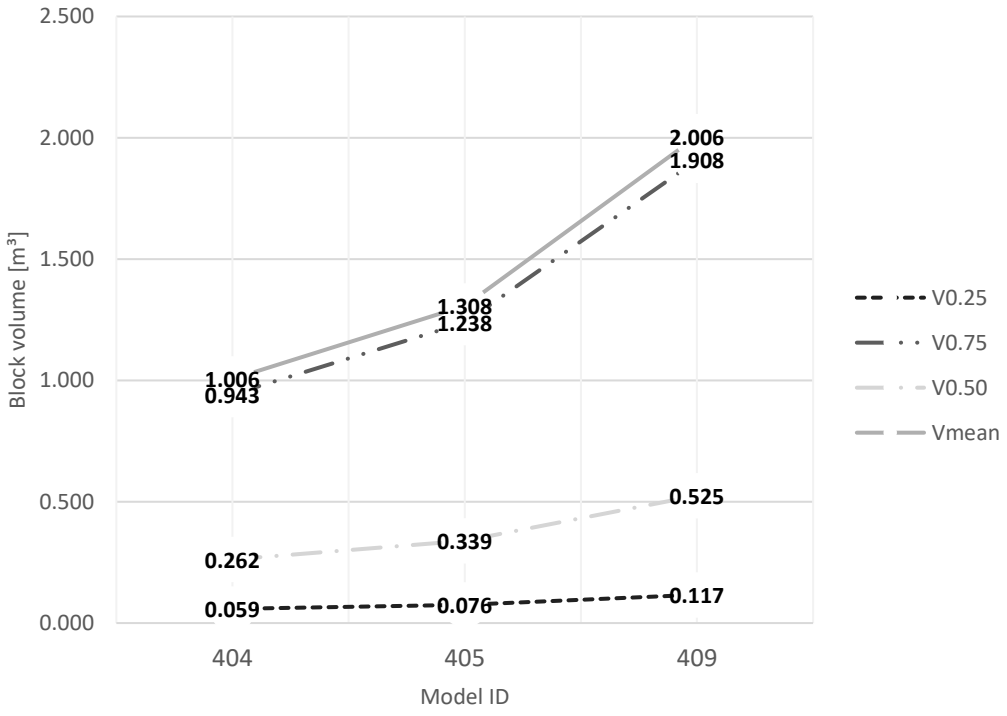

Figure 4.5: Result for block volumes of test series 2.

a

Model 404:

$V_{0.25}$ = 0.059 m³

$V_{0.50}$ = 0.262 m³

$V_{0.75}$ = 0.943 m³

V_{mean} = 1.006 m³

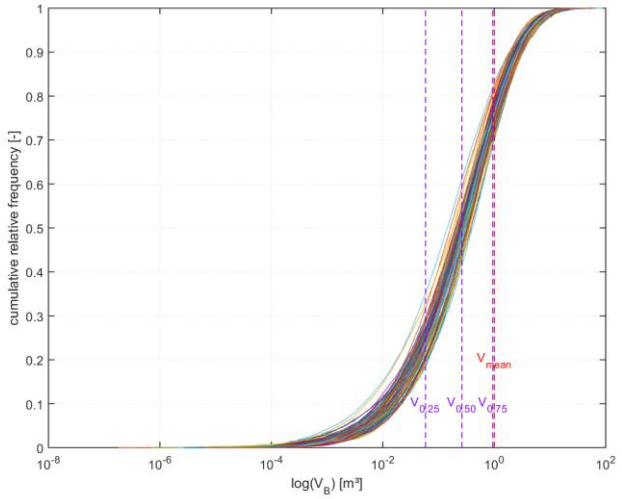

b

Model 405:

$V_{0.25}$ = 0.076 m³

$V_{0.50}$ = 0.339 m³

$V_{0.75}$ = 1.238 m³

V_{mean} = 1.308 m³

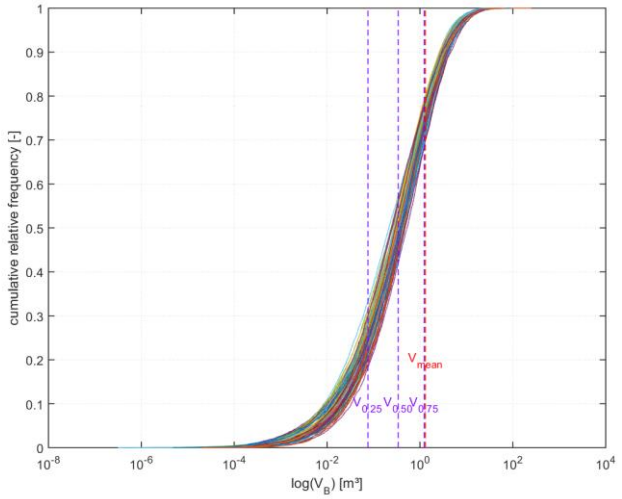

c

Model 409:

$V_{0.25}$ = 0.117 m³

$V_{0.50}$ = 0.525 m³

$V_{0.75}$ = 1.908 m³

V_{mean} = 2.006 m³

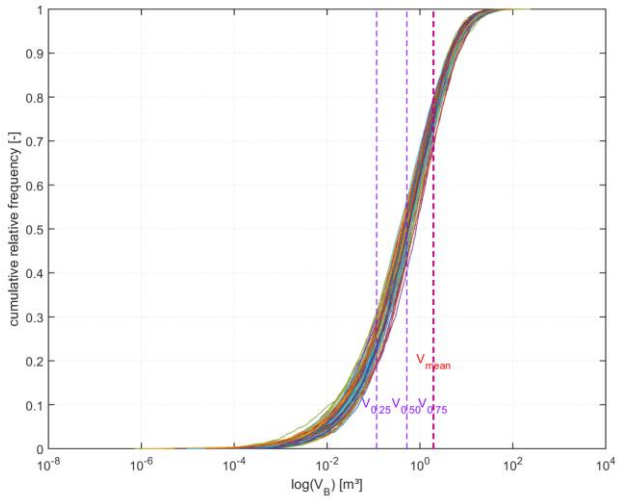

Figure 4.6: Results for cumulative distribution function of test series 2 including (a) model 404, (b) model 405 and (c) model 409.

4.2.1.3 Test series 3

For test row 3, Table 4.8 contains the model identification and the input values for the persistence. Simultaneous to the previous simulation series, the results of the block size distribution are presented. The range of the product p of the persistence values p_i reaches from 0.67 to 0.80. In addition, the results of the median values with their standard deviations are listed together with the quantiles of the curve for the block size distribution. Figure 4.7 shows the trend for the decreasing persistence which is defined in the individual model runs. Additionally, the cumulative distribution functions are visualised in Figure 4.8, including the associated mean and quantile values.

Table 4.8: Results of test series 3 for block volumes with corresponding standard deviations.

Model ID	p_1	p_2	p_3	$\bar{p}$	V_{mean}	σ_{Vmean}	$V_{0.25}$	$\sigma_{V0.25}$	$V_{0.50}$	$\sigma_{V0.50}$	$V_{0.75}$	$\sigma_{V0.75}$
406	1.0	0.6	0.8	0.80	1.292	0.198	0.078	0.021	0.345	0.072	1.230	0.211
414	1.0	0.6	0.6	0.73	1.757	0.245	0.103	0.027	0.463	0.094	1.658	0.281
910	1.0	0.6	0.4	0.67	2.612	0.313	0.149	0.033	0.676	0.112	2.425	0.338

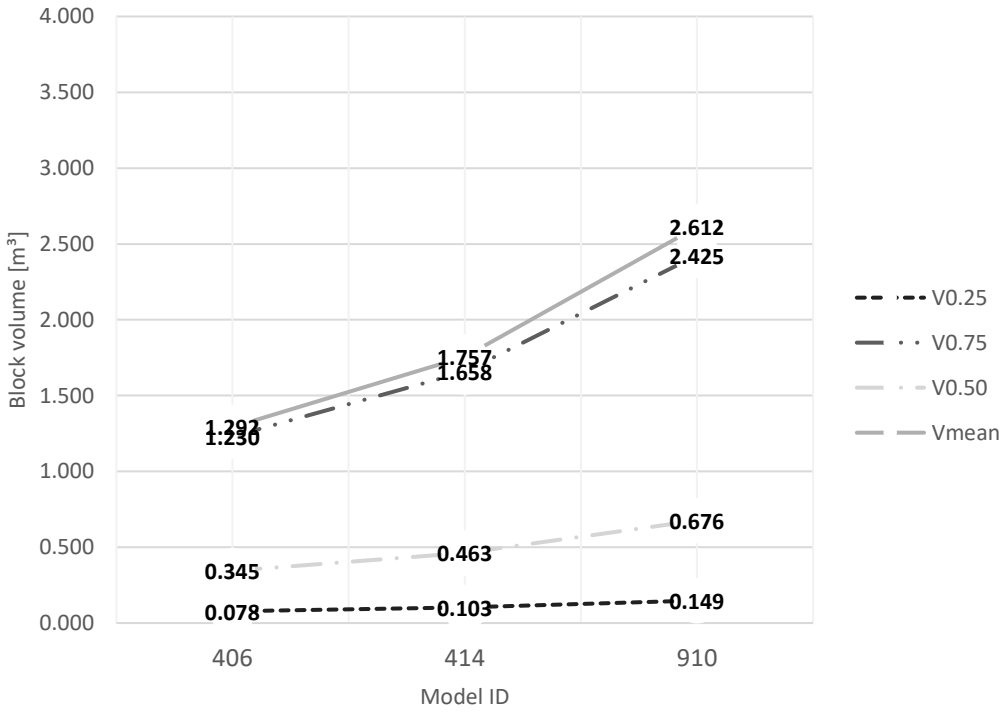

Figure 4.7: Result for block volumes of test series 3.

a

Model 406:

$V_{0.25}$ = 0.078 m³

$V_{0.50}$ = 0.345 m³

$V_{0.75}$ = 1.230 m³

V_{mean} = 1.292 m³

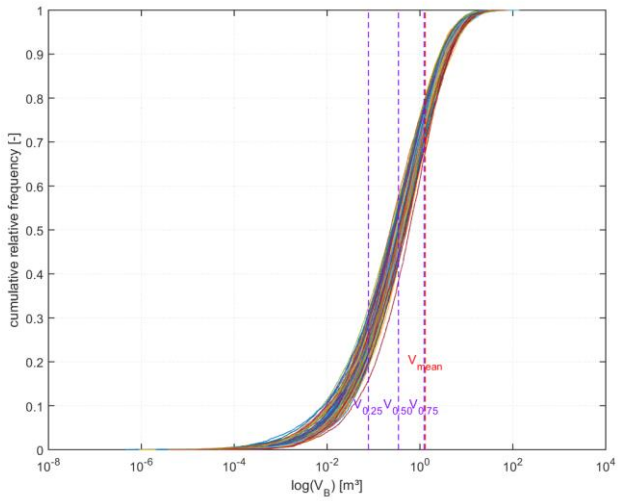

b

Model 414:

$V_{0.25}$ = 0.103 m³

$V_{0.50}$ = 0.463 m³

$V_{0.75}$ = 1.658 m³

V_{mean} = 1.757 m³

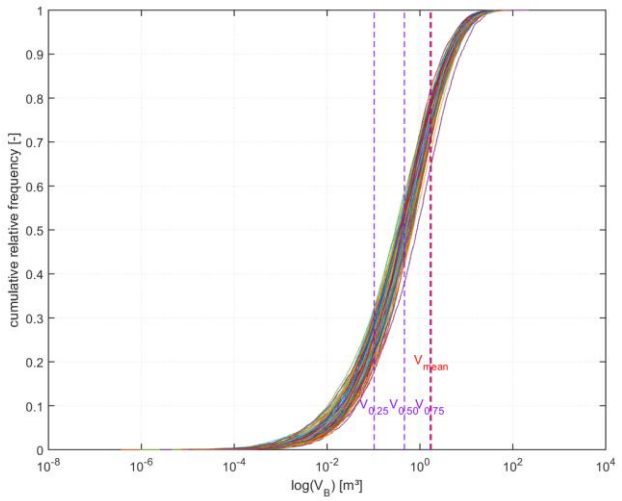

c

Model 910:

$V_{0.25}$ = 0.149 m³

$V_{0.50}$ = 0.676 m³

$V_{0.75}$ = 2.425 m³

V_{mean} = 2.612 m³

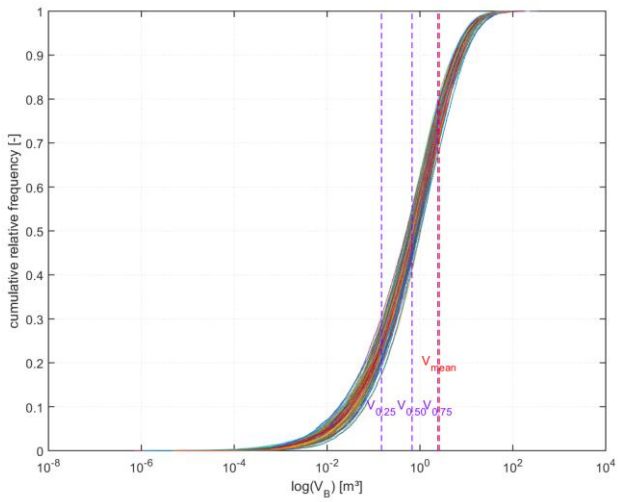

Figure 4.8: Results for cumulative distribution function of test series 3 including (a) model 406, (b) model 414 and (c) model 910.

4.2.1.4 Test series 4

In the last test series, the model ID with the assigned persistence values are listed in Table 4.9. The product p of the persistence values ranges from 0.60 to 0.73. The results of the block size distribution are presented along with their standard deviations. Figure 4.9 visualises the trend to bigger block sizes for decreasing persistence, assigned to the particular model simulations. In Figure 4.10, the cumulative distribution functions are shown together with the mean and quantile values of the block sizes.

Table 4.9: Results of test series 4 for block volumes with corresponding standard deviations.

Model ID	p_1	p_2	p_3	$\bar{p}$	V_{mean}	σ_{Vmean}	$V_{0.25}$	$\sigma_{V0.25}$	$V_{0.50}$	$\sigma_{V0.50}$	$V_{0.75}$	$\sigma_{V0.75}$
903	1.0	0.4	0.8	0.73	1.976	0.220	0.114	0.024	0.517	0.081	1.869	0.244
902	1.0	0.4	0.6	0.67	2.665	0.297	0.155	0.029	0.701	0.099	2.552	0.321
901	1.0	0.4	0.4	0.60	3.967	0.424	0.222	0.050	1.020	0.167	3.712	0.492

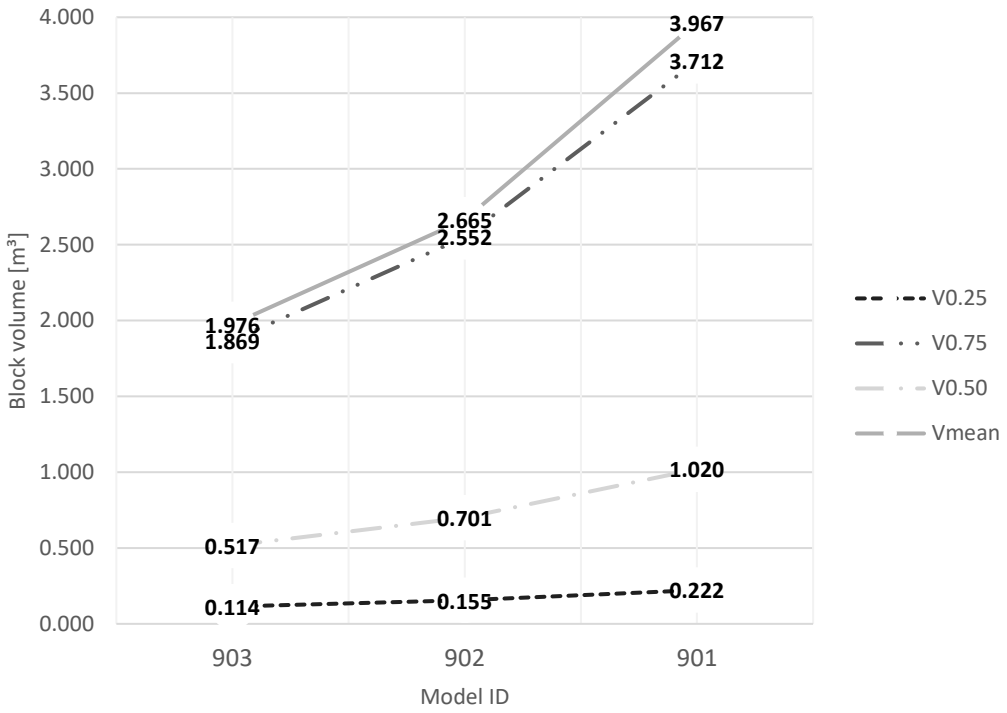

Figure 4.9: Result for block volumes of test series 4.

a

Model 903:

$V_{0.25}$ = 0.114 m³

$V_{0.50}$ = 0.517 m³

$V_{0.75}$ = 1.869 m³

V_{mean} = 1.976 m³

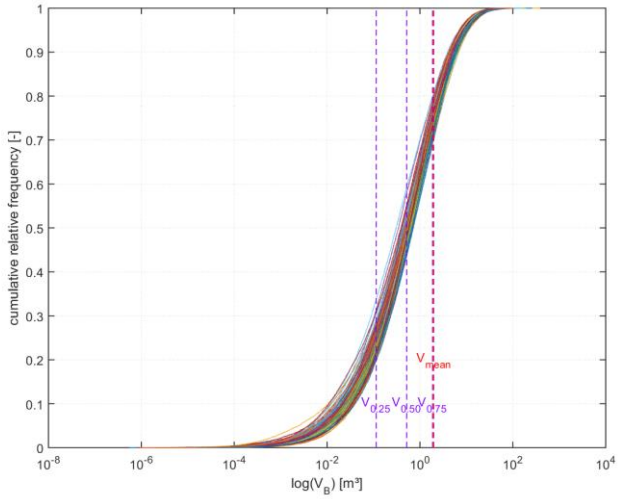

b

Model 902:

$V_{0.25}$ = 0.155 m³

$V_{0.50}$ = 0.701 m³

$V_{0.75}$ = 2.552 m³

V_{mean} = 2.665 m³

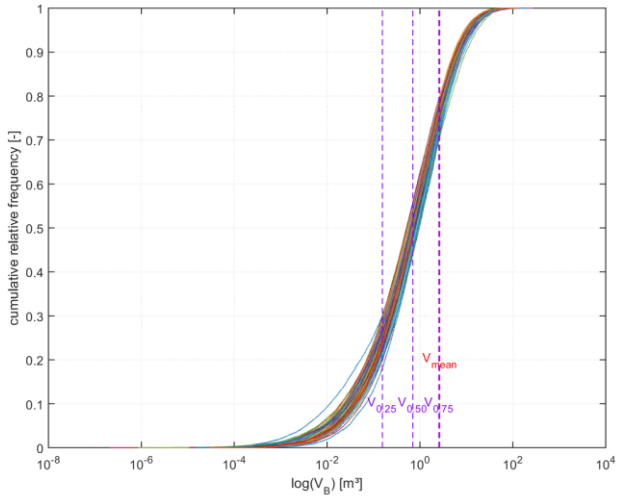

c

Model 901:

$V_{0.25}$ = 0.222 m³

$V_{0.50}$ = 1.020 m³

$V_{0.75}$ = 3.712 m³

V_{mean} = 3.967 m³

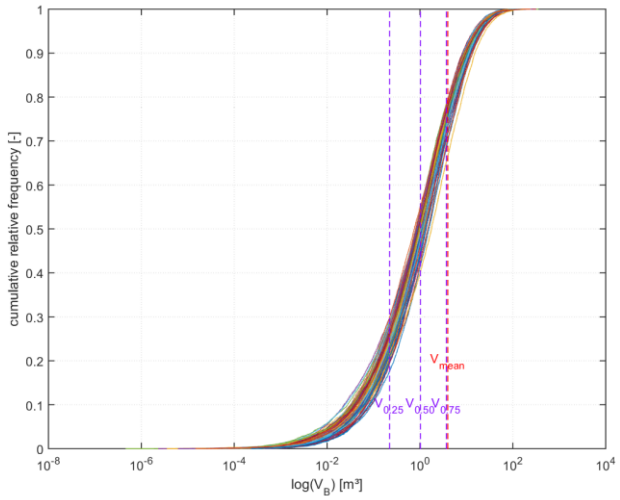

Figure 4.10: Results for cumulative distribution function of test series 4 including (a) model 903, (b) model 902 and (c) model 901.

4.2.2 Distribution of the block shapes and orientations

To consider the results for each of the 100 model replications, the visualisation by density distributions is necessary for each numeric model. The density distribution of the results of the block shape characterisation is shown in Figure 4.11-a for model 110, Figure 4.12-a for model 102 and Figure 4.13-a for model 103. All figures contain the corresponding density plots for the block orientations in their b section.
The dependency of the density distributions on the systematic decrease of the persistence values is correlating with the results from test row 2 to test row 4. Therefore, the results of the models belonging to test series 1 are representative for all four test rows shown.
In addition, the results for the residual test rows 2 to 3 are depicted in Appendix A:

- Test series 2, cf. Figure 6.2, Figure 6.3 and Figure 6.4.
- Test series 3, cf. Figure 6.5, Figure 6.6 and Figure 6.7.
- Test series 4, cf. Figure 6.8, Figure 6.9 and Figure 6.10.

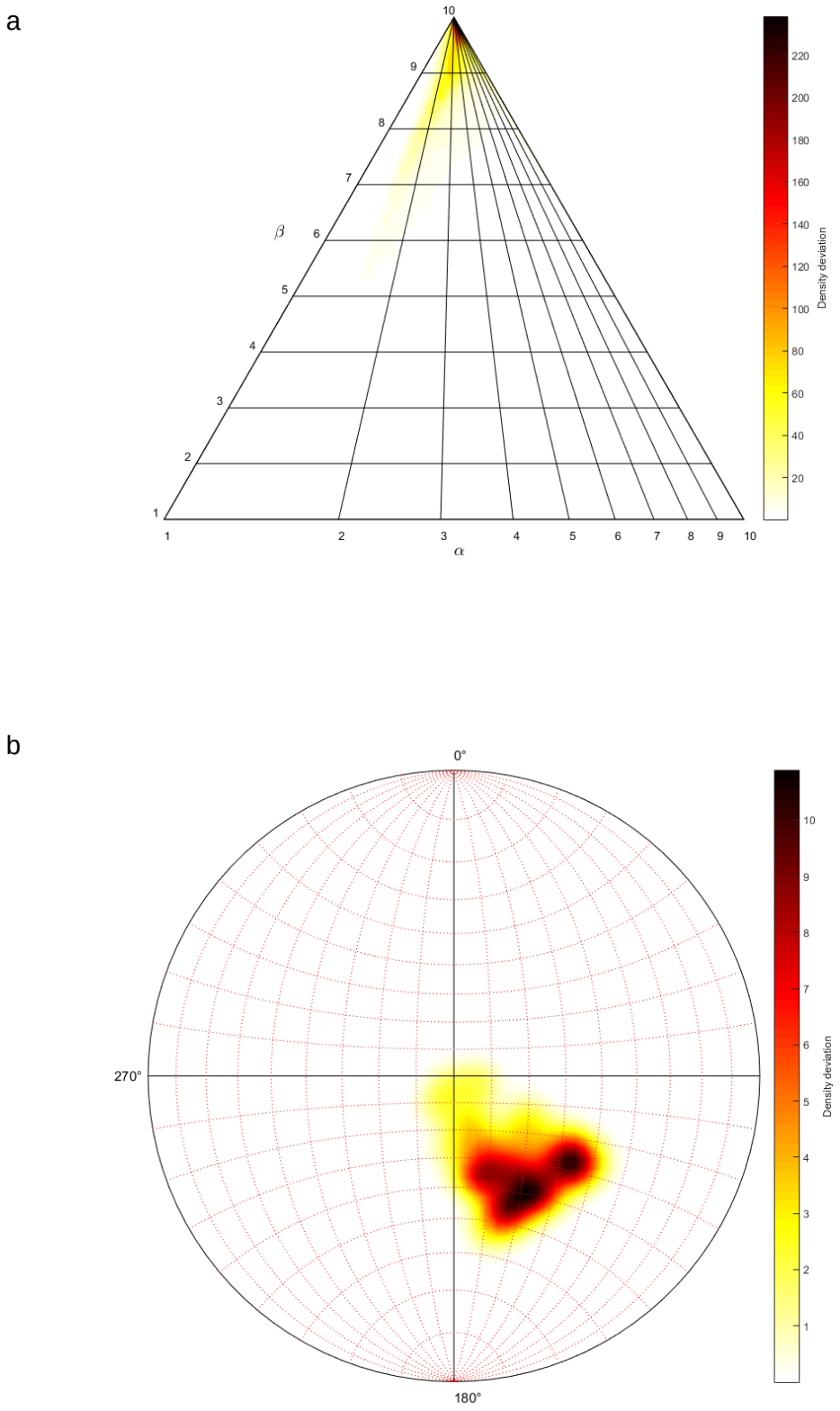

Figure 4.11: (a) Density plot of the block shape distribution and (b) density plot of the orientations of the main axes of the blocks of model 110, test series 1.

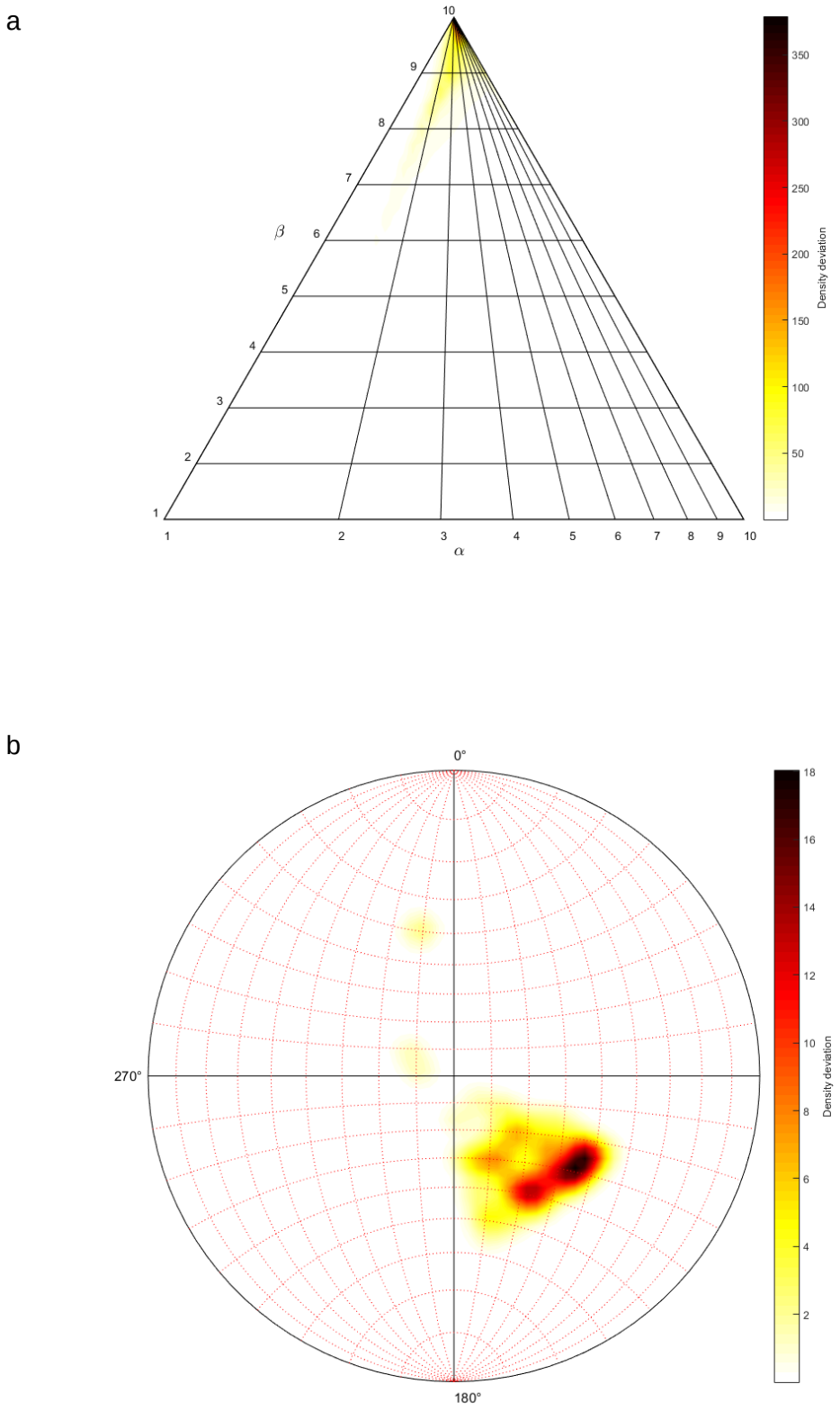

Figure 4.12: (a) Density plot of the block shape distribution and (b) density plot of the orientations of the main axes of the blocks of model 102, test series 1.

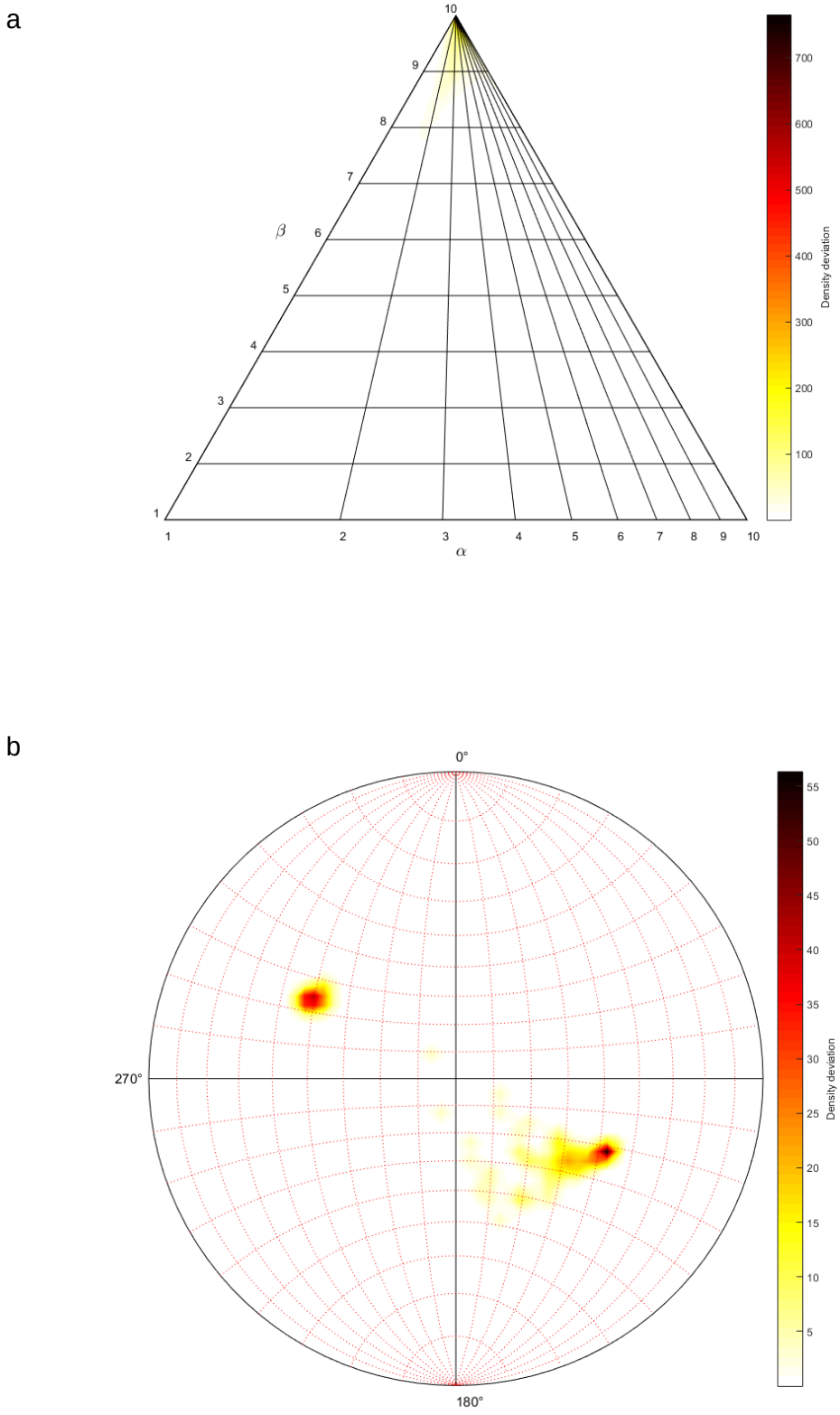

Figure 4.13: (a) Density plot of the block shape distribution and (b) density plot of the orientations of the main axes of the blocks of model 103, test series 1.

5 Interpretation and Discussion

5.1 Discontinuity network characterisation

The comparison of the manually with the semi-automatically determined dip direction and dip angle shows a plausible accordance of the evaluated values. Due to a better readability, the compared values are rounded in this paragraph. The dip direction of the foliation of 144° (DSE) versus 144 to 146° (SMX) matches, especially if the wide span of Outcrop I for the SMX analysis is considered. The same conclusion accounts for the dip angle of 49° (DSE) versus 51 to 52° evaluated through SMX. For joint set 2, the determined values of 031/87 (DSE) versus 009/77 to 020/83 (SMX) are accepted due to the high spherical aperture of the manual investigation (16 to 21°). The divergence of the manually evaluated values is caused by the wide outcrop span and the exclusion of a certain proportion of unidentified joint planes. This issue also applies for joint set 3, with dip and dip directions of 246/81 (DSE) versus 233/86 to 236/90 and 057/90 through SMX. The spherical apertures of these measurements are in a range of 10 to 19°, therefore the values are plausible as well. Furthermore, it must be considered that the manual analysis is governed with higher apertures due to the smaller amount of investigated 3D points.

Regarding the investigation method, the DSE allows the semi-automatic derivation of the discontinuity sets with a very high accuracy and it allows to assemble an arbitrary constellation of discontinuity sets. However, it is still necessary to understand the application, which needs an experienced user. Moreover, the performance for detailed DSM is time consuming and therefore, mistakes and inappropriate input parameters lead to significant delays. Furthermore, the DSE analysis needs a blocky rock mass, or at least clearly arranged joint planes to identify the block forming discontinuity sets. Cracks and normal to the outcrop wall occurring joints get not recorded, as they are not separately distinguished in a 3D point cloud. To overcome this shortcoming, a texture recognizing application would be necessary.

As DSE and SMX are using text files, the import of the DSE results into SMX is possible by the usage of scripts. Hence the SMX algorithm for the determination of the joint normal spacing was applied, but the method is rather complicated.

5.2 IBSD compared to analytical approaches

In the following chapters, the determined IBSD is compared to several analytical methods. The distribution considers the determined discontinuity sets with their corresponding joint

normal spacing (including the layer thickness of the foliation). It is necessary to compare the results to the analytical approaches, to verify the significance of the determination.
Table 5.1 lists the joint normal spacing and the angles between the discontinuity sets except the previously mentioned persistence values. The values are applied to the following analytical analyses.

Table 5.1: Joint normal spacing without standard deviation and angles between joint sets for the analytical approaches.

s_1 [m]	s_2 [m]	s_3 [m]	γ_1 [°]	γ_2 [°]	γ_3 [°]
0.58	0.72	0.79	74.92	87.00	36.89

In general, the quantile values of the block size distribution of all test series show a congruous trend. A decrease of the persistence p_i of one joint set by 20 % leads to an increase of all quantile values by roughly one third, while a further decrease of 20 %, approximately results in a duplication of the quantile values compared to the initial quantile values. For this observation, it must be noted that joint set 1 (foliation planes) was considered as persistent for all test rows. Moreover, in one test series, only the persistence of joint set 2 or 3 was decreased, while the other one was kept at a constant value as well. However, an increase of the block volumes is a logical consequence of a decreased persistence, but the correlation of the increase of the quantile values may be worth further examination. A potential investigation would be a further development of the approach of Söllner (2014), considering the introduced transformation factor T, which depends on the persistence as well.

5.2.1 Analytical approach after Palmström

As this approach provides an equation for the block volume (cf. equation (2.4)) which does not consider any persistence, the results for all tested models in this approach is the same (V_B = 0.570 m³). However, the result of the formula fits into the range determined in this study, as apparent in Figure 5.1. Without consideration of persistence and standard deviations for the joint normal spacings, the formula delivers values within the range of the 50 and the 75 percent quantile for test series 1 and 2 and in the range of the 50 percent quantile for test series 3 and 4. Thus, the results seem to be rather conservative and underestimates the IBSD. However, the results are plausible due to the lacking consideration of non-persistent joints and can still be an appropriate evaluation for the IBSD. The equation is still useful for quick volume estimations, especially if no persistence parameters are available.

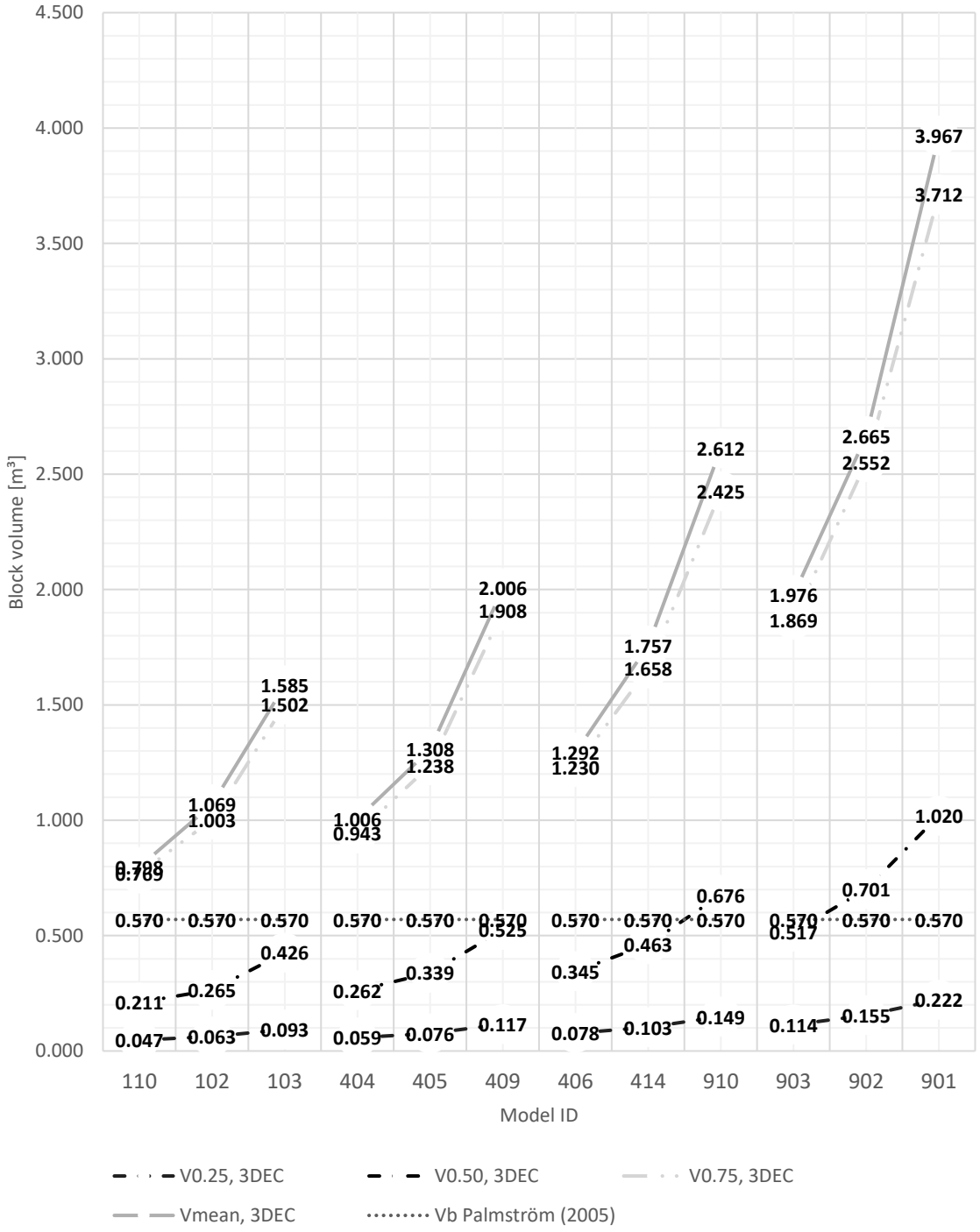

Figure 5.1: Mean values and quantile values of the IBSD of all test series including three model replications each, compared to the analytical approach of Palmström (2005).

5.2.1 Analytical approach after Cai et al.

According to equation (2.5), V_B is calculated from the joint normal spacing, the angles between the joint planes and the evaluated persistence parameters. Table 5.2 contains the results for this analytical approach.

Compared to the block size distribution, determined in this study, it is shown that the calculation follows the trend of increasing block size values for decreasing persistence parameters (cf. Figure 5.2). It is also shown, that the analytical formulation delivers values between the 50 percent and the 75 percent quantile of the block size distribution, which is a slight overestimation of the IBSD (referred to the median IBSD). However, the fact that the equation obtains accurate results within the determined range of block sizes by relatively low effort, entitles the application especially in time-critical situations. Regarding the interpretation of a determined block size of a rock mass, Kluckner et al. (2015) pointed out, that a range might give a better understanding than single values of the block volume. In particular, a statement about the range of expectable block sizes increases the reliability of designs of excavations and support measures.

Table 5.2: Block volumes resulting from the analytical approach of Cai et al. (2004).

Model ID	V_b [m³]
110	0.614
102	0.676
103	0.774
404	0.661
405	0.728
409	0.833
406	0.728
414	0.801
910	0.917
903	0.833
902	0.917
901	1.050

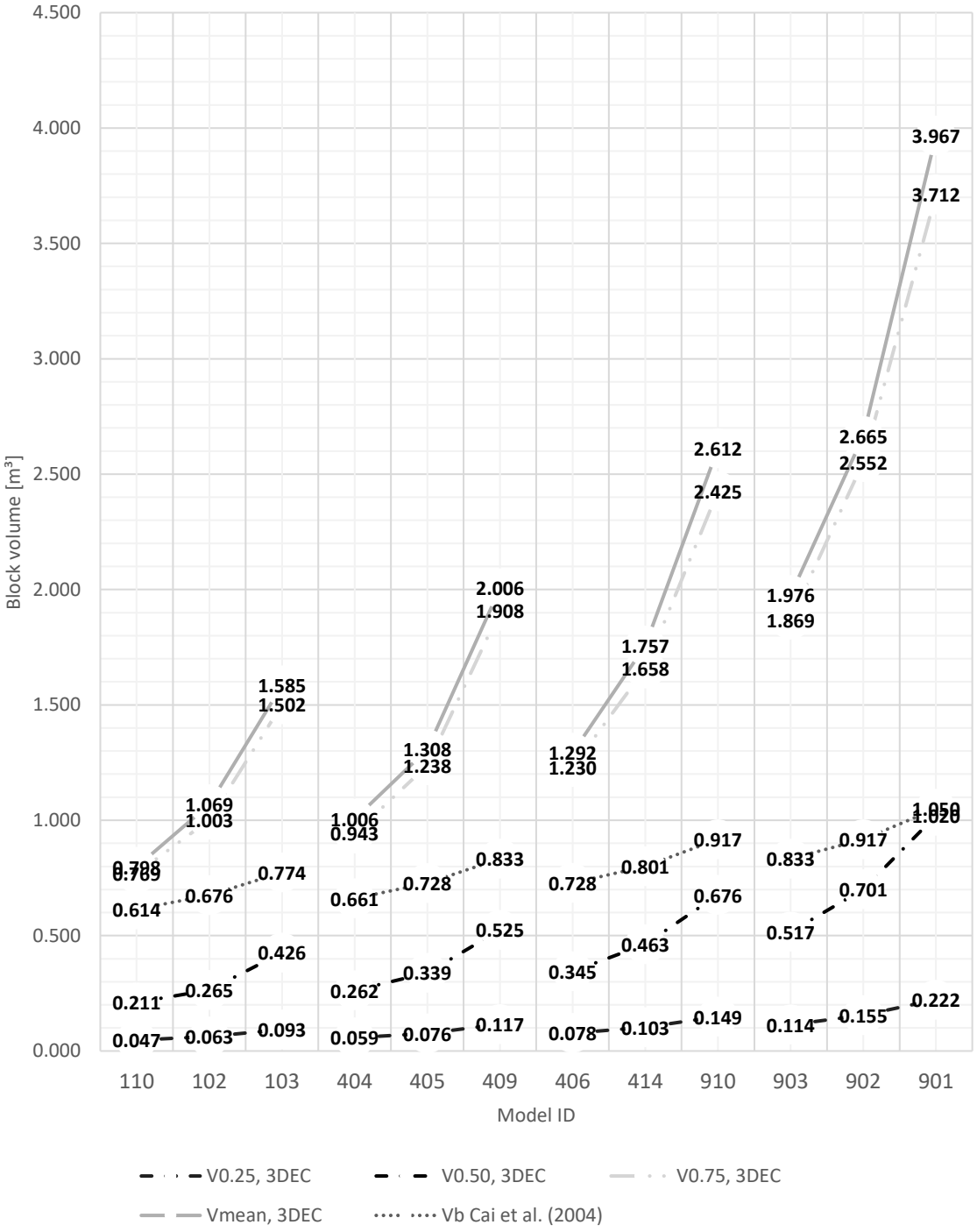

Figure 5.2: Mean values and quantile values of the IBSD of all test series including three model replications each, compared to the analytical approach of Cai et al. (2004).

5.2.2 Analytical approach after Kluckner et al.

Kluckner et al. (2015) developed analytical equations to describe a block size distribution. The results for the mean and the quantile values of the block size distribution, obtained by these equations are shown in Table 5.3. Figure 5.3 confirms the trend of the distribution, but also shows that the introduced standard deviations for the joint normal spacing increases the resulting range at both ends. Depending on a desired investigation, this can lead to questionable statements. For example, the dropout of the small block sizes in the determination is not relevant for stability investigations, but could be a serious aspect for occupational safety and excavation methods. Moreover, the missed evaluation of big block sizes affects the determination of the global rock mass strength.
However, the study initializes the analytical determination of a block size distribution. Moreover, the approach attests its high potential and should be considered for subsequent investigations and continuous improvements. And in addition, it was applied for the first time to a non-orthogonal aligned joint network and still presented reasonable results.

Table 5.3: Quantile values resulting from the analytical approach of Kluckner et al. (2015).

Model ID	$V_{b,25\%}$ [m³]	$V_{b,50\%}$ [m³]	$V_{b,75\%}$ [m³]	$V_{b,mean}$ [m³]
110	0.443	0.511	0.771	0.701
102	0.502	0.610	0.954	0.867
103	0.576	0.738	1.200	1.090
404	0.502	0.610	0.954	0.867
405	0.576	0.738	1.200	1.090
409	0.668	0.909	1.541	1.398
406	0.576	0.738	1.200	1.090
414	0.668	0.909	1.541	1.398
910	0.787	1.142	2.026	1.836
903	0.668	0.909	1.541	1.398
902	0.787	1.142	2.026	1.836
901	0.942	1.469	2.741	2.481

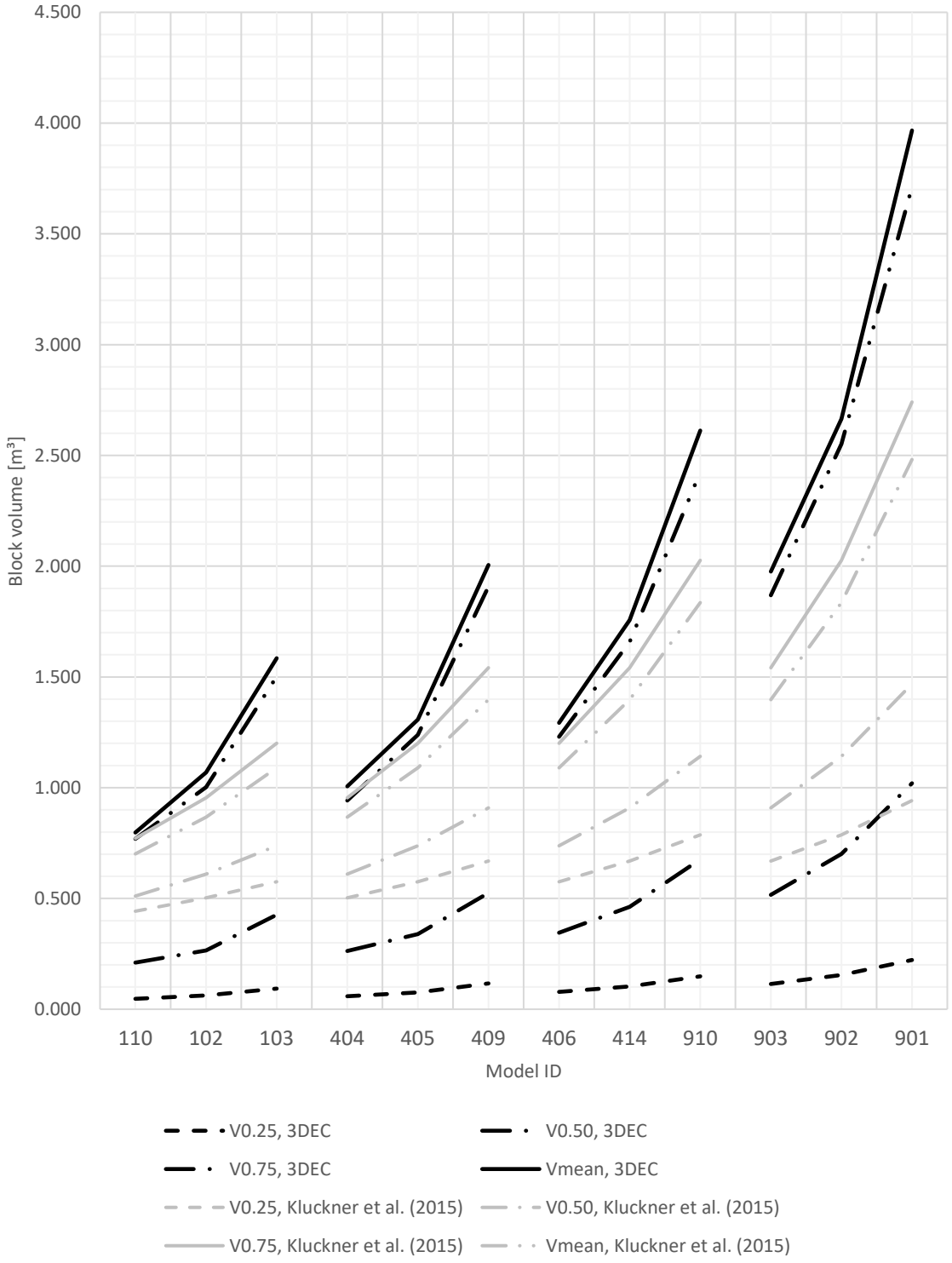

Figure 5.3: Mean values and quantile values of the IBSD of all test series including three model replications each, compared to the analytical approach of Kluckner et al. (2015)[3].

The consideration of the standard deviations of the measured input values in the model simulations resulted into a wider span of the ISBD. Moreover, a stronger increase of the

[3] The data labels in this chart were omitted for a better clarity.

block volumes for a certain decrease of the persistence can be observed. Through a precise (digital) characterisation of the investigated rock mass, a more accurate statement regarding the ISBD can be developed. Therefore, further research in the field of semi-automatic rock mass investigation is recommended to optimise the significance and the applicability of the results and the performance of the data processing methods. Furthermore, a continuous development of the existing empirical approaches is reasonable to provide a suitable method for engineering purposes.

5.3 Block shape distributions

The block shape characterisation method uses the information about the discontinuity network of an investigated rock face to provide information about its block geometry and allows conclusions on the expectable failure mechanisms. This knowledge can be used for example for the determination of optimised strength parameters or appropriate excavation methods.

The applied method provides objective results for the block shapes and orientations, based on the geometrical properties of the single blocks. It allows the mathematical description of the modelled blocks as well as a statement of probability for the BSD. Although the shapes are only classified into three primary shapes (elongated, cubic, platy) and three intermediate shapes, a significant improvement of the currently applied characterisation methods is achieved. The main improvements are the guaranteed objectiveness and the easy application in standardised processes. Furthermore, the block shape determination of a numeric model provides information on the whole investigated rock mass in opposition to a visual investigation of an outcrop. In addition, the evaluation of the block shapes compared to a field study is enhanced, since the gathered data set can be used for further implementations and interpretations.

The density plots for the BSD (cf. Appendix A) show a distribution for 100 model replications with a trend to elongated block shapes and a proportion of intermediate cubic elongated blocks. This trend is observed for all model simulations with various persistence parameters and therefore caused by the geometry of the discontinuity sets and the data for the joint spacing.

In this study, the block orientations of the investigated test series 1 to 4 are clearly concentrated at a certain area with a range between 10 to 40° of spherical aperture (cf. Appendix A). Considering consistent model sizes with decreasing persistence, the density deviation of blocks with similar orientated longest vertex to vertex axes increases. Coherently, the spherical deviation of the axis orientations decreases. Hence decreasing spherical distributed block orientations and a lower peak value for the density are observed

in relation to decreasing persistence values of the discontinuity sets.

Therefore, in Figure 5.4 and Figure 5.5 the peak values of the density distributions are selected to visualise the dependency on the persistence of the models. The peak values express the highest concentration of block orientations, but are not representative for the wide spread of the distributions. Compared to the density plots for the block orientations, it is shown that the block orientations are less scattered for the models with lower persistence values. Moreover, a densification of similar block forms for decreasing persistence is identified.

The resulting information can be applied for further studies regarding the determination of the rock mass stiffness, the excavation method or stability analyses. For the KDE, an input grid array with quadratic dimensions must be specified. The KDE saves the density results in certain cells, whose indices can be converted to arbitrary scales.

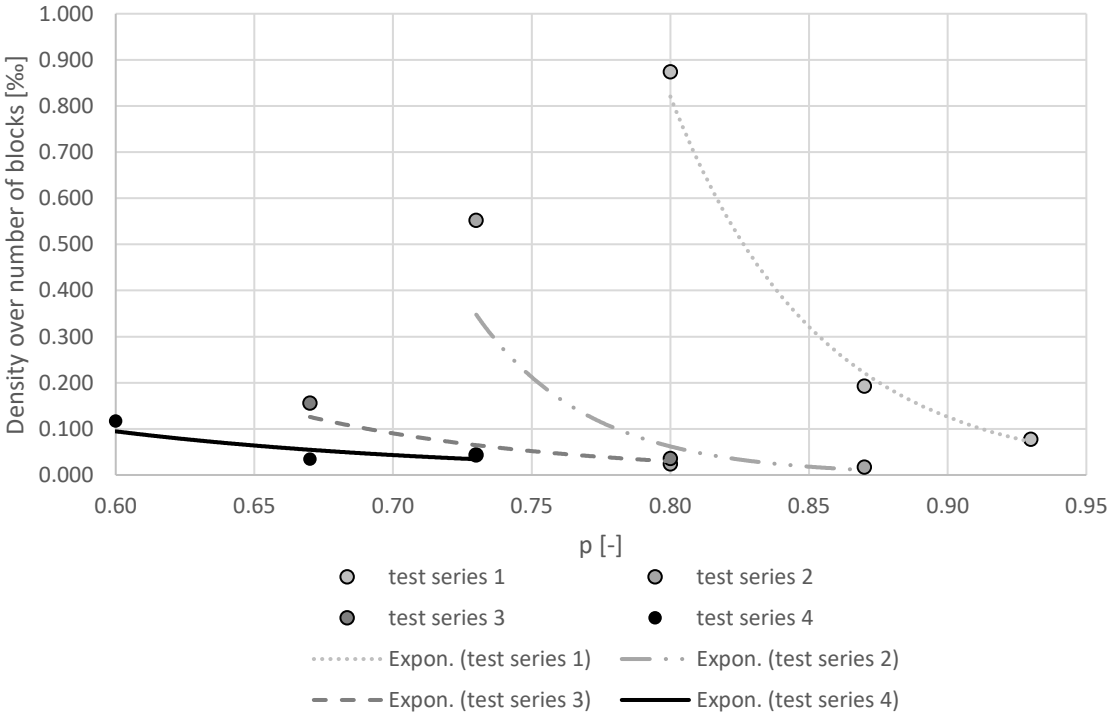

Figure 5.4: Peak values of the density distribution based on the total number of blocks in relation to the persistence of the investigated test series with exponential tend lines.

But one must keep in mind that a statement concerning the orientation of a block is only useful in combination with the block shape, since the resulting orientation must be interpreted differently for cubic, platy and elongated shapes. In the investigated quarry, the shapes were dominantly elongated and the orientation in general followed the orientation of the foliation. This statement is concluded from the determined results, since the orientated block axes dominantly exhibit a direction of 140 ± 25° and an axes dip angle of 50 ± 5°. These values are corresponding to the measured foliation of 144/49. The elongated

blocks are bounded with joint set 2 (031/87) and joint set 3 (246/81). The almost vertical dip angles and the related dip directions sustain the present block elongation. Blocks with the foliation thickness as the dominant block dimension are oriented with a nearly perpendicular main block axis and an axis direction with around 180° divergence to the dip direction of the bedding plane.

However, without a dominating elongated block axis or, like in this study a vertex to vertex span, the block orientation of a rock mass would be randomly distributed. This is caused by the fact that the extreme forms or limiting block shapes can have several vertex to vertex connections with equal length like delineated in Figure 5.5. The elongated shapes show a dominant orientation, but as shown, the orientation of the vertex connections can scatter for the idealised shapes and diverge from the main block axis. Anyway, the block orientation is of interest only for elongated and platy block shapes for the determination of the global rock mass stiffness. Regardless of this criterion, an investigation of a rock mass with equidimensional block shapes would not be able to identify a densification of block orientations.

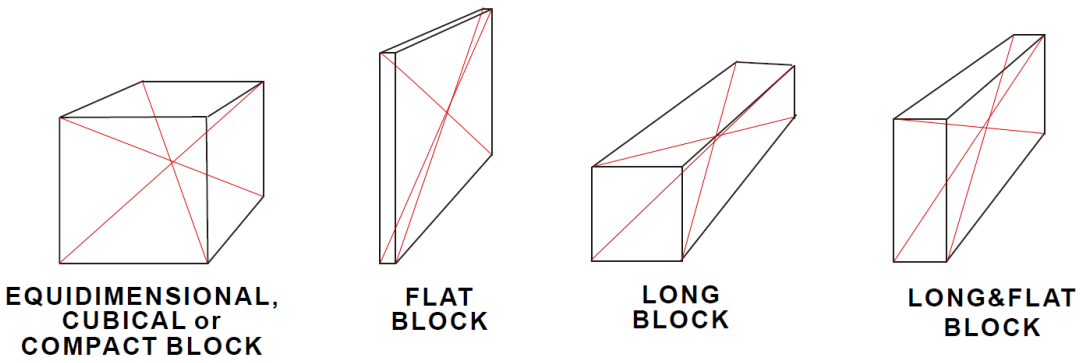

Figure 5.5: Main block shape types with various vertex to vertex distances of the same length and different orientations (red lines), modified from Palmström (1995).

6 Conclusion and Outlook

This study presents a consistent and semi-automatic process for rock mass characterisation, starting from photogrammetry and ending in numerical modelling. Intermediate results are collected and further processed through scripting techniques. The stepwise data processing ensures the possibility of readjustments and calibrations of the required input parameters.

The applied remote sensing technique enables, compared to manual geological mapping quick and precise data acquisition for the generation of a DSM. Through the combination of the applications DSE and ShapeMetriX^{3D}, the identification of existing discontinuity sets is executed by a point cloud analysis under the involvement of manual parameter adjustments and the manual mapping of unidentified joints. Hence, the obtained results are highly detailed, objective and reproducible. Subsequently, the obtained discontinuity set parameters are applied for the generation of a 3D numerical model considering statistical diversities. The 3D Distinct Element Code provides extensive data exportation features, which are used to receive the information for the determination of the in-situ block size distribution and the block shape distribution with corresponding block orientations. The median values of the block size distribution over four test series are situated in a range of 0.21 to 1.02 m³, dependent on the varied persistence parameters. Moreover, the 25 % quantile and the 75 % quantile are situated in ranges from 0.05 to 0.22 m³ and 0.77 to 3.71 m³. Furthermore, the acquired block size distribution was compared to several analytical approaches, which pointed out the compliances to these methods. In general, the distribution of the block orientation shows a densification within an orientation of 140 ± 25° with a corresponding dip of 50 ± 5°. However, the concentration of the block orientations is induced by the geometrical arrangement of the three major discontinuity sets. This geometrical situation also leads to higher proportion of elongated block shapes.

Through enhanced effort for the point cloud analysis and thoughtful preparations, an increase of the accuracy of the results was achieved. This study demonstrates an effective process flow for rock mass characterisation and provides promising findings for further block size and block shape investigations.

A modification of the export feature for identified discontinuity sets in the DSE would improve the work flow for the determination of the joint normal spacing. As the application is GNU licenced, the implementation of an export possibility of SMX compatible structure maps for further discontinuity set analyses would skip a further performance relevant process step. Furthermore, for prospective approaches, it might be of interest to extend the analytical approach of Kluckner et al. (2015) by considering determined standard deviations of its input parameters. Especially for engineering purposes without the requirement of a

numerical modelling, the accuracy of the resulting block size distribution of the proposed equations might be increased. In particular, the proposed determination for the block orientation demonstrates its potential for further investigations. The determination of the block orientations could be improved by considering an evaluation over multiple dominating vertex to vertex distances, instead of the presented length criterion. Furthermore, the resulting orientation deviation might be combined with a stiffness evaluating approach of Gottsbacher (2017), who studied the influence of miscellaneous block orientations onto the global stiffness of a jointed rock mass.

7 Bibliography

3GSM GmbH 2015. ShapeMetriX3D. 3D imaging for measuring and assessing rock and terrain surfaces. User Manual JMX Analyst for ShapeMetriX3D Version 3.5 with Addenda for Version 3.7 and 3.8. Available online at www.3gsm.at.

3GSM GmbH 2017. ShapeMetriX3D. Version 4.0.2. Requires a 64-Bit system and a NVidia graphics card in order to expand its full capabilities. Graz: 3GSM GmbH. Available online at http://www.3gsm.at/, checked on 5/16/2017.

Barton, N.; Lien, R.; Lunde, J. 1974. Engineering classification of rock masses for the design of tunnel support. In *Rock Mechanics* 6 (4), pp. 189–236. DOI: 10.1007/BF01239496.

Bieniawski, Z. T. (Ed.) 1989. Engineering rock mass classifications. A Complete Manual for Engineers and Geologists in Mining, Civil and Petroleum Engineering. New York: Wiley.

Botev, Z.I.; Grotowski, J.F.; Kroese, D.P. 2010. Kernel density estimation via diffusion. In *Ann. Statist.* 38 (5), pp. 2916–2957. DOI: 10.1214/10-AOS799.

Bundesamt für Eich- und Vermessungswesen (BEV) 2005. Austrian Map online. Vienna. Available online at www.austrianmap.at, updated on 5/6/2017, checked on 9/12/2017.

Buyer, A.; Schubert, W. 2017. Calculation the Spacing of Discontinuities from 3D Point Clouds. In *Procedia Engineering* 191, pp. 270–278. DOI: 10.1016/j.proeng.2017.05.181.

Cai, M.; Kaiser, P.K.; Tasaka, Y.; Minami, M. 2007. Determination of residual strength parameters of jointed rock masses using the GSI system. In *International Journal of Rock Mechanics and Mining Sciences* 44 (2), pp. 247–265. DOI: 10.1016/j.ijrmms.2006.07.005.

Cai, M.; Kaiser, P.K.; Uno, H.; Tasaka, Y.; Minami, M. 2004. Estimation of rock mass deformation modulus and strength of jointed hard rock masses using the GSI system. In *International Journal of Rock Mechanics and Mining Sciences* 41 (1), pp. 3–19. DOI: 10.1016/S1365-1609(03)00025-X.

Chen, N.; Kemeny, J.; Jiang, Q.; Pan, Z. 2017. Automatic extraction of blocks from 3D point clouds of fractured rock. In *Computers & Geosciences* 109, pp. 149–161. DOI: 10.1016/j.cageo.2017.08.013.

Gaich, A.; Pötsch, M.; Schubert, W. 2017. Digital rock mass characterization 2017 - Where are we now? What comes next? In *Geomechanik und Tunnelbau* 10 (5), pp. 561–

566. DOI: 10.1002/geot.201700036.

ÖNORM EN ISO 14689-1. 2004. Geotechnische Erkundung und Untersuchung – Benennung, Beschreibung und Klassifizierung von Fels Teil 1: Benennung und Beschreibung. Österreichisches Normungsinstitut: Wien.

Girardeau-Montaut, D. 2017. CloudCompare. 3D point cloud and mesh processing software. Version 2.8.1: Girardeau-Montaut, Daniel. Available online at http://www.danielgm.net/cc/, checked on 5/18/2017.

Gottsbacher, L.K.J. 2017. Calculation of the Young's Modulus for Rock Masses with 3DEC and comparing it with empirical methods. Master's Thesis. Graz University of Technology, Graz. Institute of Rock Mechanics and Tunnelling. Available online at https://online.tugraz.at/tug_online/wbAbs.showThesis?pThesisNr=62977&pOrgNr=37&pPersNr=102924#, checked on 12/23/2017.

Hoek, E.; Carter, T. G.; Diederichs, M. S. (Eds.) 2013. Quantification of the Geolocigal Strength Index Chart. 2013 16th International Multi Topic Conference (INMIC). Lahore, Pakistan, 19.12.2013 - 20.12.2013. American Rock Mechanics Association. Toronto: IEEE.

Hoek, E.; Kaiser, P. K.; Bawden, W. F. (Eds.) 1998a. Support of Underground Excavations in Hard Rock. Mining Research Directorate and Universities Research Incentive Fund. 3rd ed. Rotterdam: A.A. Balkema.

Hoek, E.; Marinos, P.; Benissi, M. 1998b. Applicability of the geological strength index (GSI) classification for very weak and sheared rock masses. The case of the Athens Schist Formation. In *Bull Eng Geol Environ* 57 (2), pp. 151–160. DOI: 10.1007/s100640050031.

International Society for Rock Mechanics 1978. Suggested Methods for the Quantitative Description of Discontinuities in Rock Masses. In *International Journal of Rock Mechanics and Mining Sciences & Geomechanics* (15), pp. 319–368.

Itasca Consulting Group, I. 2017. 3DEC. Distinct-Element Modeling of Jointed and Blocky Material in 3D. Version 5.20. Hard Disk: 500 MB, Processor: Dual core CPU (2 GHz), Memory (RAM): 1 Gbyte, Video Card: HD graphics card, 800 x 600 pixels, 32-bit color palette, OpenGL 1.3 or higher, Ports: 1 USB port is required for the security key: Itasca Consulting Group, Inc. Available online at http://www.itascacg.com/, checked on 5/16/2017.

Kalenchuk, K.S.; Diederichs, M.S.; McKinnon, S. 2006. Characterizing block geometry in jointed rockmasses. In *International Journal of Rock Mechanics and Mining Sciences* 43 (8), pp. 1212–1225. DOI: 10.1016/j.ijrmms.2006.04.004.

Kalenchuk, K.S.; McKinnon, S.; Diederichs, M.S. 2008. Block geometry and rockmass characterization for prediction of dilution potential into sub-level cave mine voids. In *International Journal of Rock Mechanics and Mining Sciences* 45 (6), pp. 929–940. DOI: 10.1016/j.ijrmms.2007.10.006.

Kern, J. 2017. Beispiel einer Ermittlung der in situ Blockgrößenverteilung auf Grundlage von Bohrlochdaten und Oberflächenmessungen. Master's Thesis. Graz University of Technology, Graz. Institute of Rock Mechanics and Tunnelling. Available online at https://online.tugraz.at/tug_online/wbAbs.showThesis?pThesisNr=62985&pOrgNr=37&pPersNr=102924.

Kim, B.H.; Cai, M.; Kaiser, P.K.; Yang, H.S. 2006. Estimation of Block Sizes for Rock Masses with Non-persistent Joints. In *Rock Mech. Rock Engng.* 40 (2), pp. 169–192. DOI: 10.1007/s00603-006-0093-8.

Kluckner, A.; Söllner, P.; Schubert, W.; Pötsch, M. 2015. Estimation of the in situ Block Size in Jointed Rock Masses using Three-Dimensional Block Simulations and Discontinuity Measurements.

Lambert, C.; Thoeni, K.; Giacomini, A.; Casagrande, D.; Sloan, S. 2012. Rockfall Hazard Analysis From Discrete Fracture Network Modelling with Finite Persistence Discontinuities. In *Rock Mech Rock Eng* 9 (4), p. 1095. DOI: 10.1007/s00603-012-0250-1.

Palmström, A. 1995. RMi - a system for characterizing rock mass strength for use in rock engineering. In *Journal of Rock Mechanics and Tunneling Techniques* 1 (2).

Palmström, A. 2000. Block Size and Block Size Distribution, 1-12. DOI: 10.1016/B978-1-85573-345-9.50005-4.

Palmström, A. 2005. Measurements of and correlations between block size and rock quality designation (RQD). In *Tunnelling and Underground Space Technology* 20 (4), pp. 362–377. DOI: 10.1016/j.tust.2005.01.005.

Pötsch, M. 2011. The analysis of rotational and sliding modes of failure for slopes, foundations, and underground structures in blocky, hard rock. Dissertation. Graz University of Technology, Graz. Faculty of Civil Engineering.

Riquelme, A.J.; Abellán, A.; Tomás, R. 2015. Discontinuity spacing analysis in rock masses using 3D point clouds. In *Engineering Geology* 195, pp. 185–195. DOI: 10.1016/j.enggeo.2015.06.009.

Riquelme, A.J.; Abellán, A.; Tomás, R.; Jaboyedoff, M. 2014. A new approach for semi-automatic rock mass joints recognition from 3D point clouds. In *Computers & Geosciences* 68, pp. 38–52. DOI: 10.1016/j.cageo.2014.03.014.

Schuscha, E. 2016. Kalksteinbergbau Feiglbauer. Geologische Karte Tagbaustand 23.8.2016. mit Darstellung von: Katastersituation, Schürfen, Schurfbohrungen, Berechtigungen, Höhenschichtlinien, Tagbausituation, Wegenetz, Gebäude und Schnittspuren. Leoben: Dipl.-Ing. E. Schuscha Ingenieurkonsulent für Markscheidewesen.

Söllner, P. 2014. Determination of the in situ Block Size Distribution as a Parameter for the Rock Mass Characterization based on Measurements and Statistical Methods. Master Thesis. Graz University of Technology, Graz. Institute for Rock Mechanics and Tunnelling.

Stavropoulou, M. 2013. Discontinuity frequency and block volume distribution in rock masses. In *International Journal of Rock Mechanics and Mining Sciences* 65, pp. 62–74. DOI: 10.1016/j.ijrmms.2013.11.003.

The MathWorks Inc. 2008. MATLAB. MATLAB and Statistics Toolbox. Version R2015a. Natick, Massachusetts.

Wang, L.G.; Yamashita, S.; Sugimoto, F.; Pan, C.; Tan, G. 2003. A Methodology for Predicting the In Situ Size and Shape Distribution of Rock Blocks. In *Rock Mechanics and Rock Engineering* 36 (2), pp. 121–142. DOI: 10.1007/s00603-002-0039-8.

Wittke, Walter (Ed.) 2014. Rock Mechanics Based on an Anisotropic Jointed Rock Model. (AJRM). WBI GmbH. Berlin, Germany: Wilhelm Ernst & Sohn, Verlag für Architektur und technische Wissenschaften GmbH & Co. KG.

Appendix A

This appendix collects all results, which are not referred in the approach:

- Quality of the Digital Surface Model
- Parameter study for the Discontinuity Set Extractor
- Evaluation of the joint normal spacing in ShapeMetriX^{3D}
- Density plots for block shape distribution
- Density plots for block orientation

Table 6.1: Quality of the generated DSM.

Outcrop	Sub images	Number of 3D points	Total surface area [m²]	Average geometric image resolution [m / px]	Average 3D point spacing [m / pt]	Image size [Mpx]
1	80	2,369,954	15,978.2	0.0048	0.08	689.42
2	43	4,092,829	7,315.0	0.0045	0.04	368.81

Table 6.2: DSE results of the parameter study to evaluate optimised input values to assign a maximum number of 3d points to the discontinuity sets.

Evaluation	Joint set	Dip	Dip direction	Density	%[4]
1	1	48.82	143.95	18.0104	47.24
	2	41.39	189.34	1.4458	14.44
	3	69.09	173.38	1.0549	19.16
2	1	48.74	143.69	18.1301	52.19
	2	47.29	185.92	1.561	23.17
	3	86.99	30.95	0.8914	14.78
3	1	48.74	143.69	18.1301	57.13
	2	86.99	30.95	0.8914	14.13
	3	49.39	197.58	0.8856	18.72
4	1	48.74	143.69	18.1301	57.13
	2	86.99	30.95	0.8914	14.13
	3	49.39	197.58	0.8856	18.72
5	1	48.82	143.95	18.0104	47.24
	2	41.39	189.34	1.4458	14.33
	3	69.09	173.38	1.0549	17.95
	4	87.01	31.07	0.9014	14.1
6	1	48.74	143.69	18.1301	47.7
	2	47.29	185.92	1.561	17.86
	3	86.99	30.95	0.8914	13.96
	4	75.51	170.51	0.5741	14.21
7	1	48.82	143.95	18.0104	53.66
	2	87.01	31.07	0.9014	13.19
	3	49.96	197.93	0.8872	15.8
	4	82.86	171	0.2382	11.73
8	1	48.74	143.69	18.1301	53.32
	2	86.99	30.95	0.8914	13.24
	3	49.39	197.58	0.8856	15.94
	4	82.73	170.89	0.2452	11.88
9	1	48.82	143.95	18.01	54.51
	2	58.96	187.42	0.99	22.85
	3	87.01	31.07	0.90	13.60
10	1	48.82	143.95	18.01	50.34
	2	58.96	187.42	0.99	20.01
	3	87.01	31.07	0.90	13.54
	4	81.86	157.52	0.28	9.87
11	1	48.7436	143.69	18.13	54.02
	2	67.65	179.85	1.07	22.41
	3	86.99	30.95	0.89	13.61

[4] Number of assigned points over the total amount of points.

a

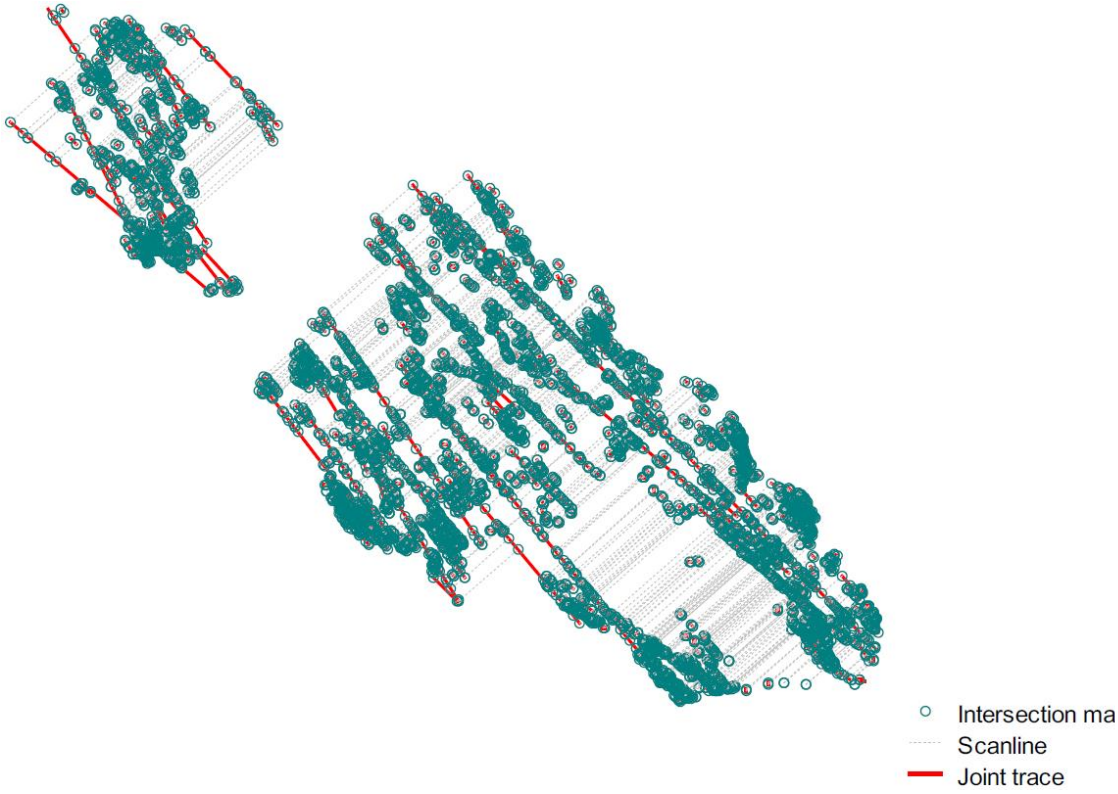
Intersection ma
Scanline
Joint trace

b

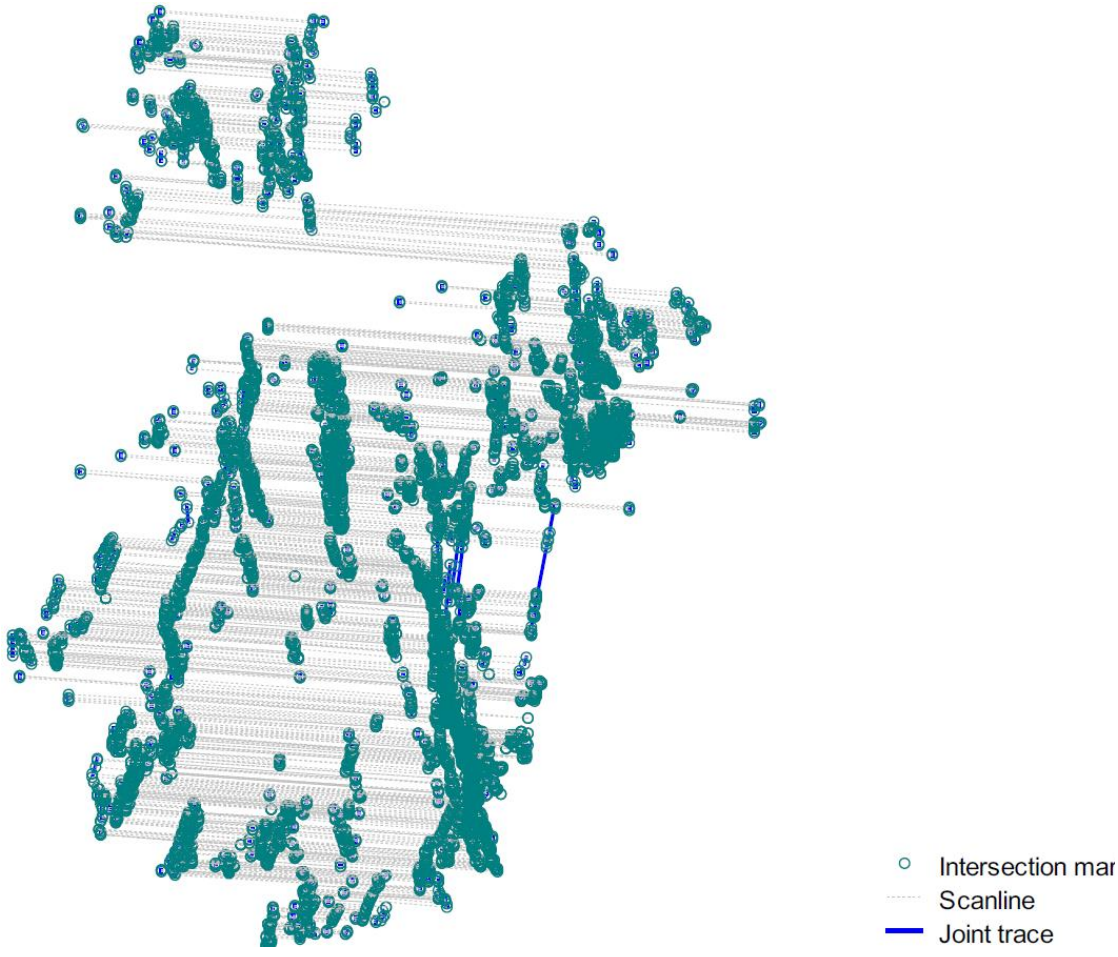
Intersection mar
Scanline
Joint trace

c

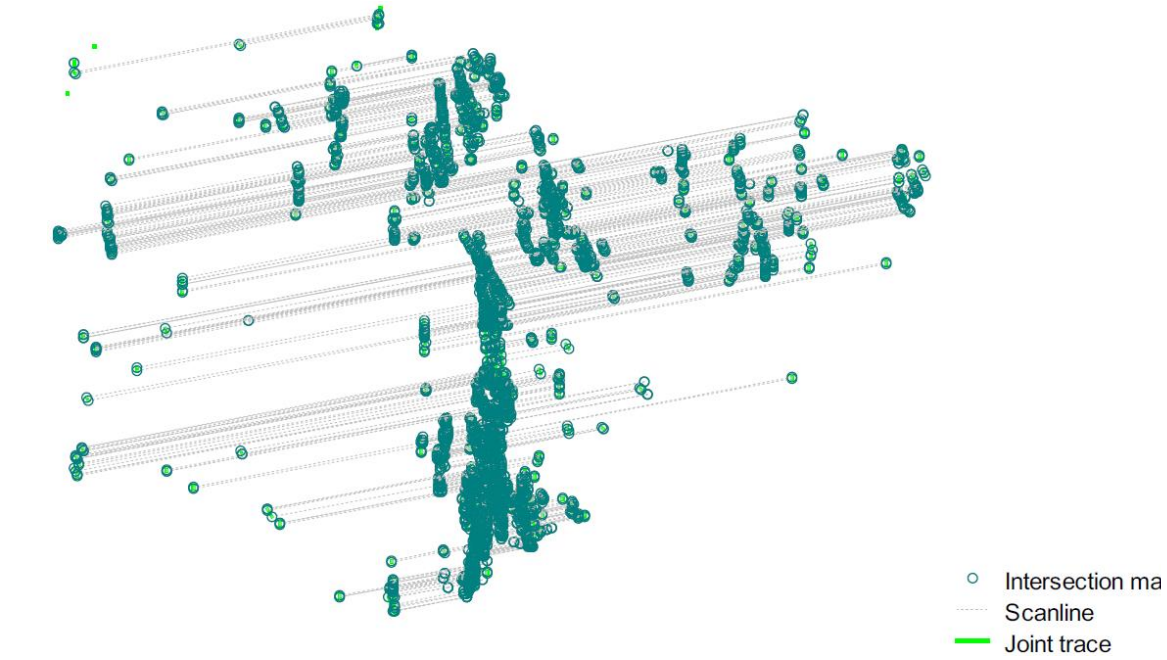

Figure 6.1: Trace map for the evaluation of the joint normal spacing for discontinuity set 1 (a), discontinuity set 2 (b) and discontinuity set 3 (c), obtained by ShapeMetrix^{3D}.

a

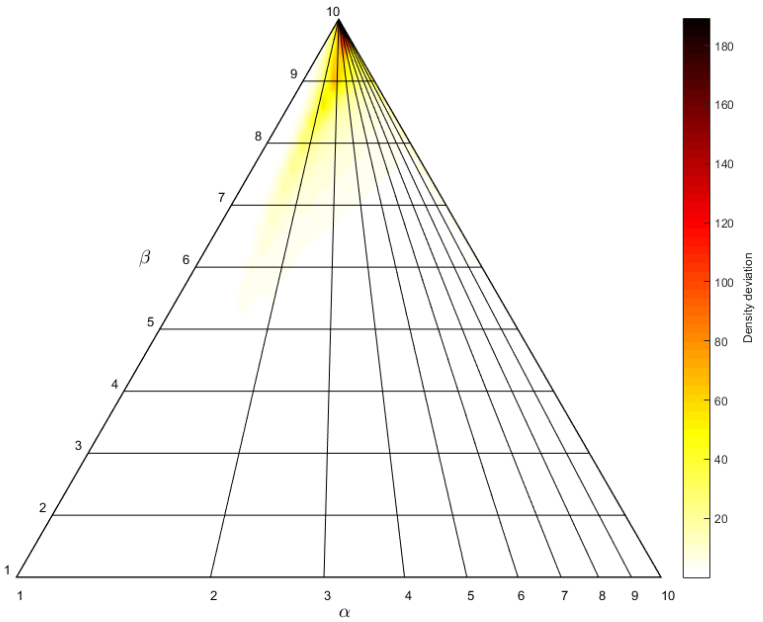

b

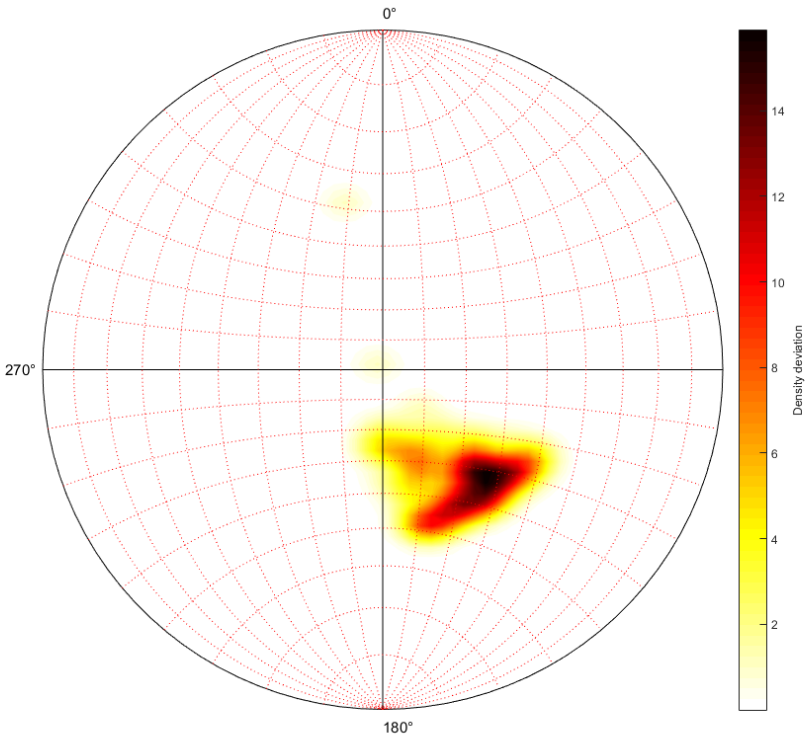

Figure 6.2: (a) Density plot of the block shape distribution and (b) density plot of the orientations of the main axes of the blocks of model 404, test series 2.

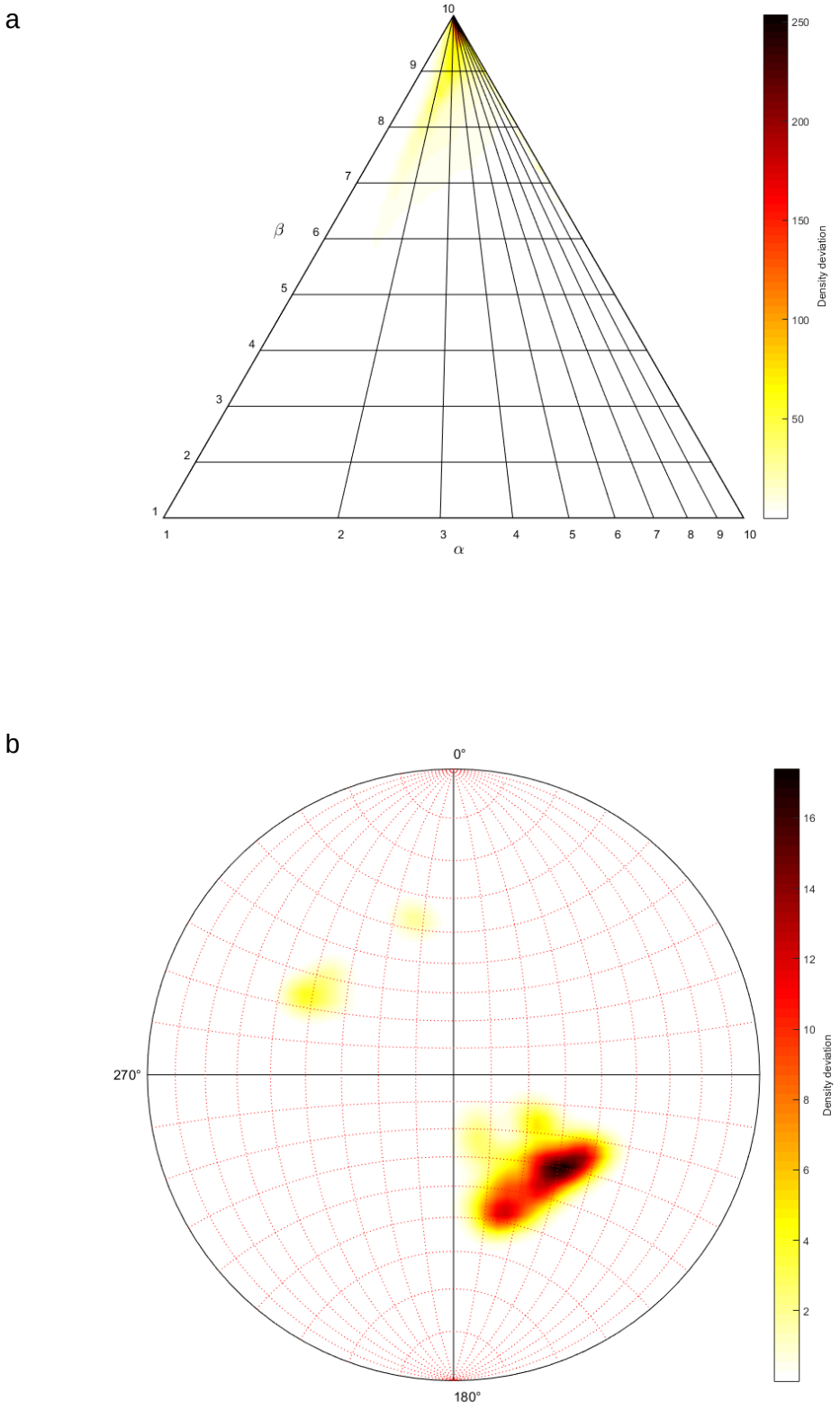

Figure 6.3: (a) Density plot of the block shape distribution and (b) density plot of the orientations of the main axes of the blocks of model 405, test series 2.

a

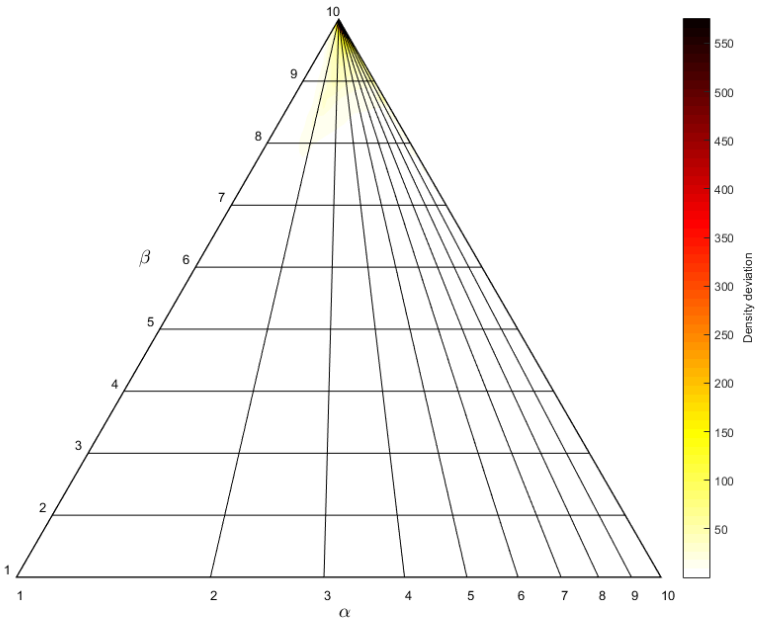

b

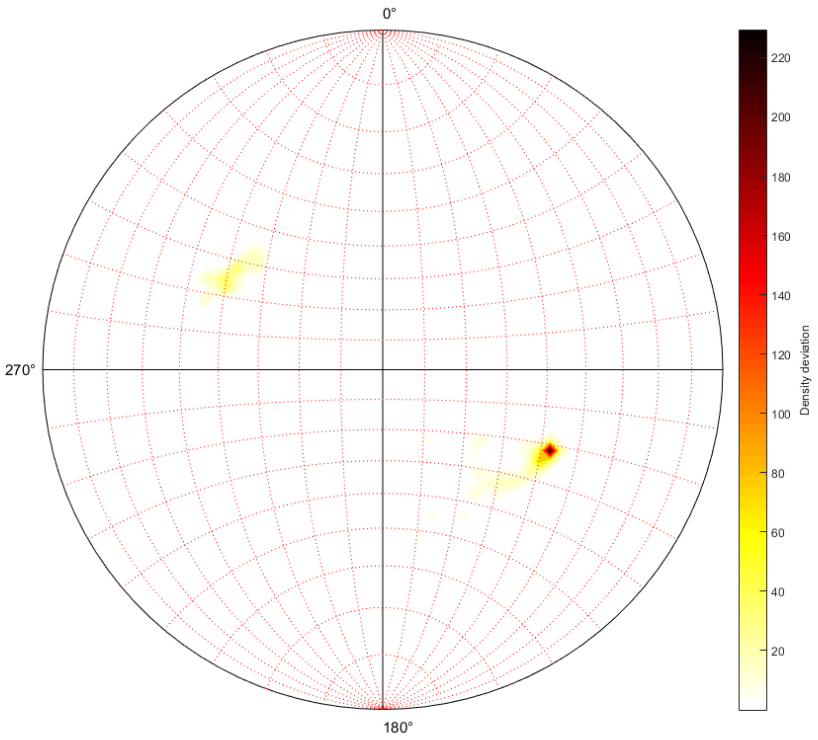

Figure 6.4: (a) Density plot of the block shape distribution and (b) density plot of the orientations of the main axes of the blocks of model 409, test series 2.

a

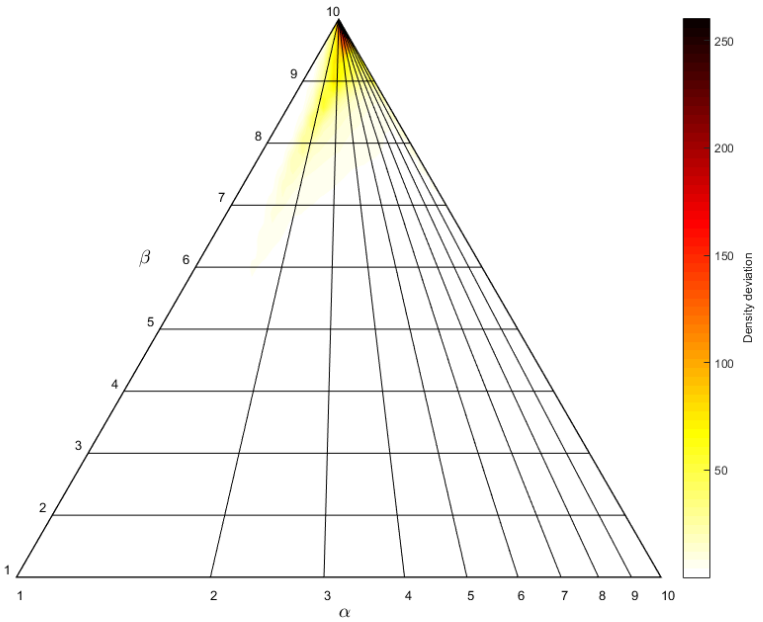

b

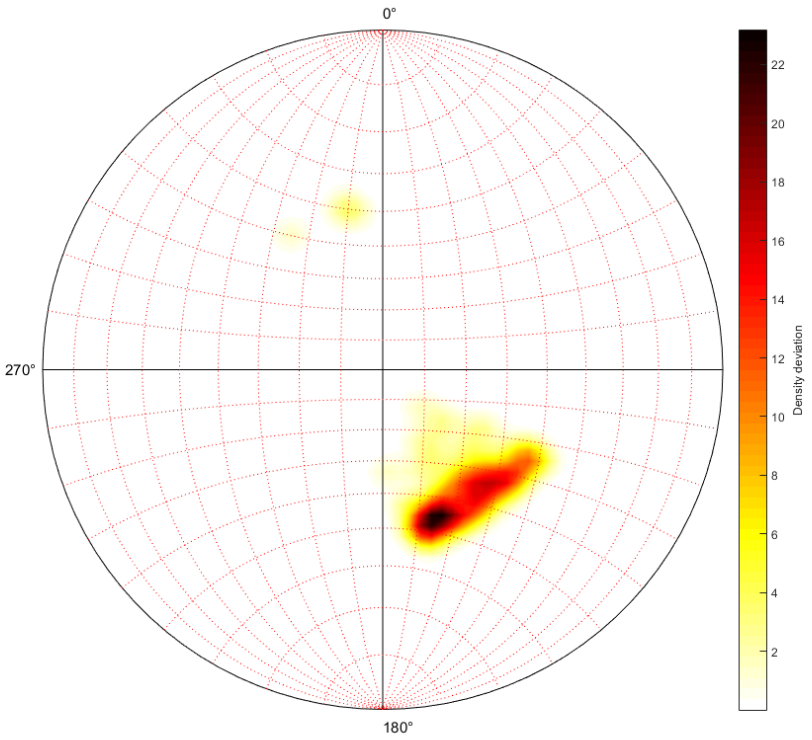

Figure 6.5: (a) Density plot of the block shape distribution and (b) density plot of the orientations of the main axes of the blocks of model 406, test series 3.

a

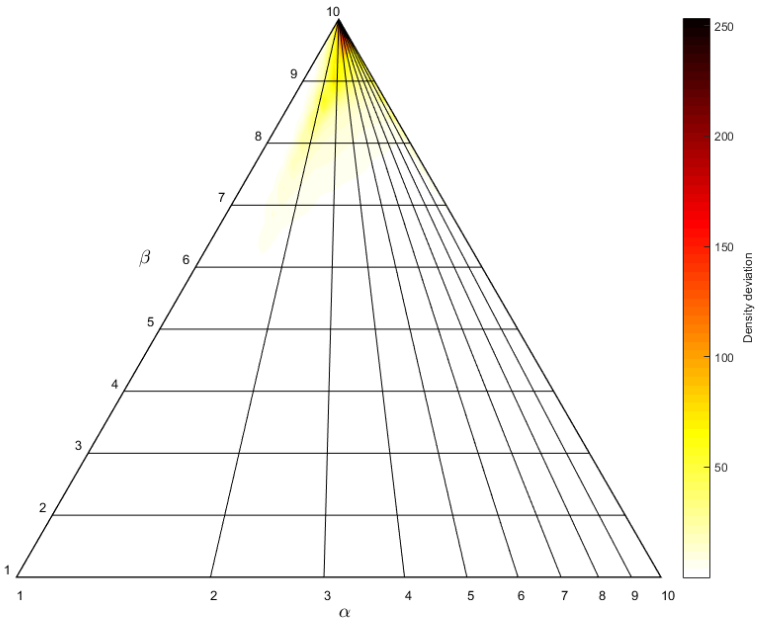

b

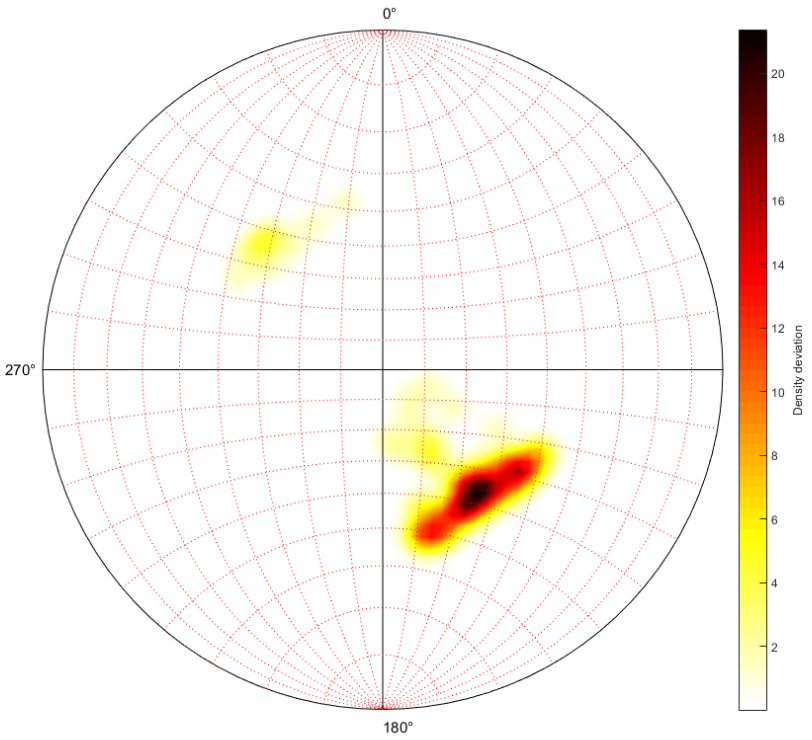

Figure 6.6: (a) Density plot of the block shape distribution and (b) density plot of the orientations of the main axes of the blocks of model 414, test series 3.

a

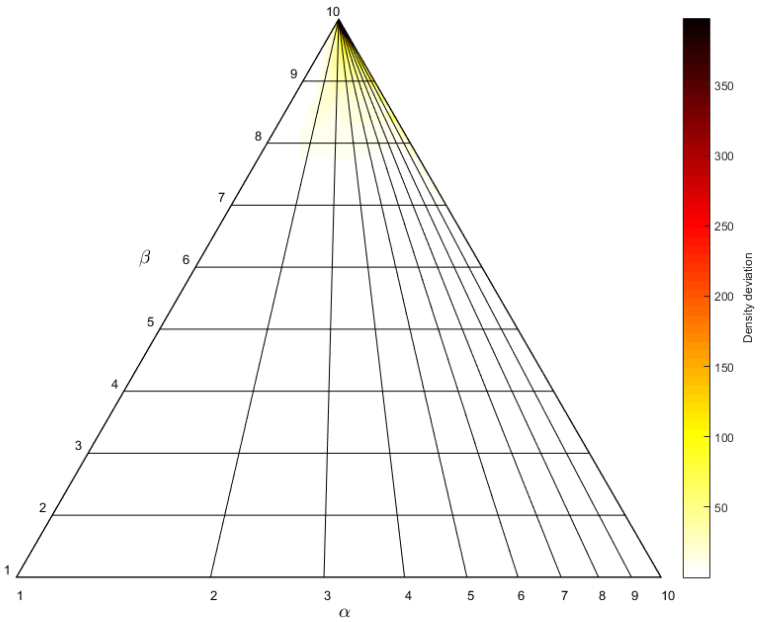

b

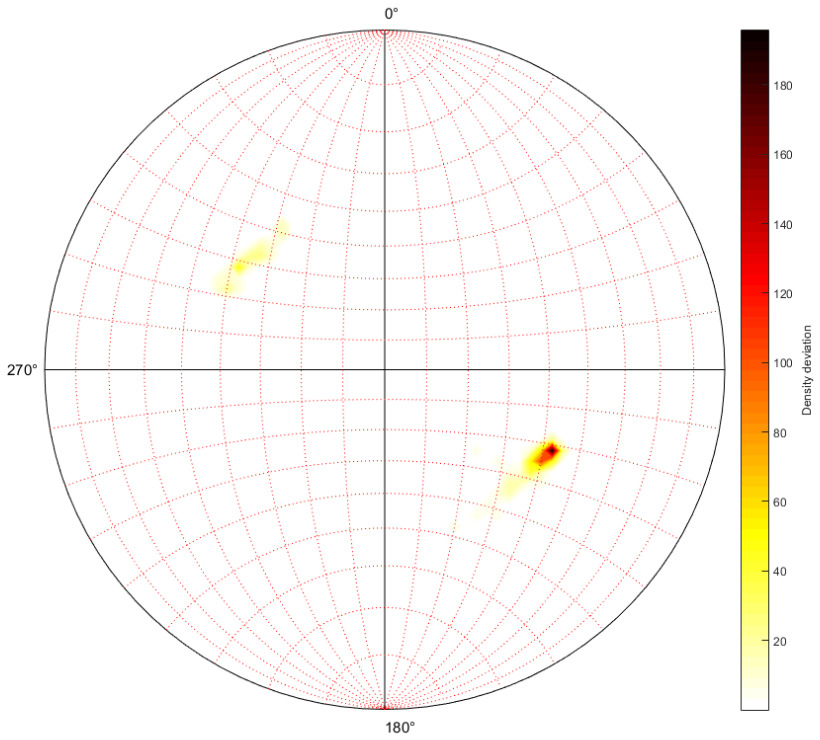

Figure 6.7: (a) Density plot of the block shape distribution and (b) density plot of the orientations of the main axes of the blocks of model 910, test series 3.

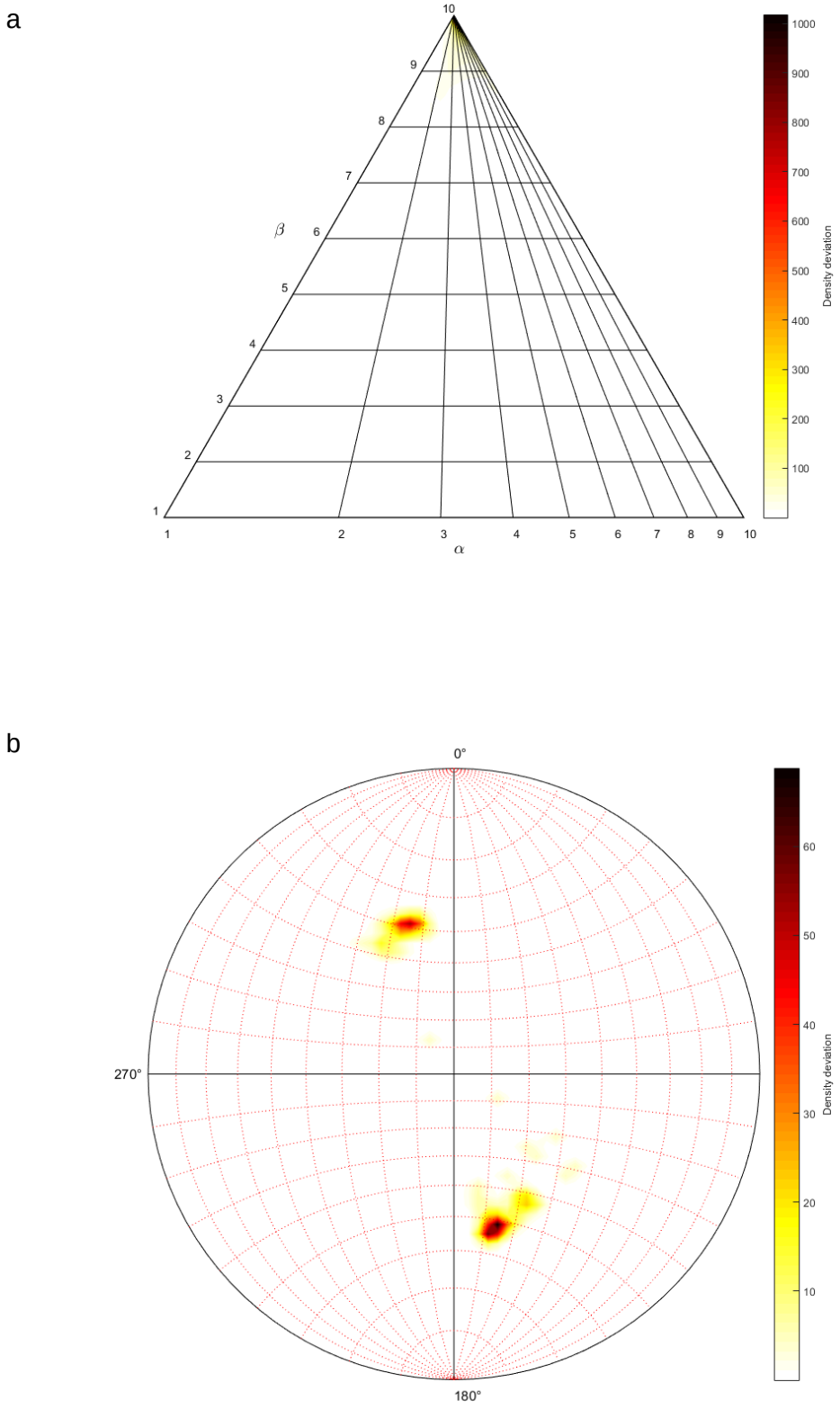

Figure 6.8: (a) Density plot of the block shape distribution and (b) density plot of the orientations of the main axes of the blocks of model 903, test series 4.

a

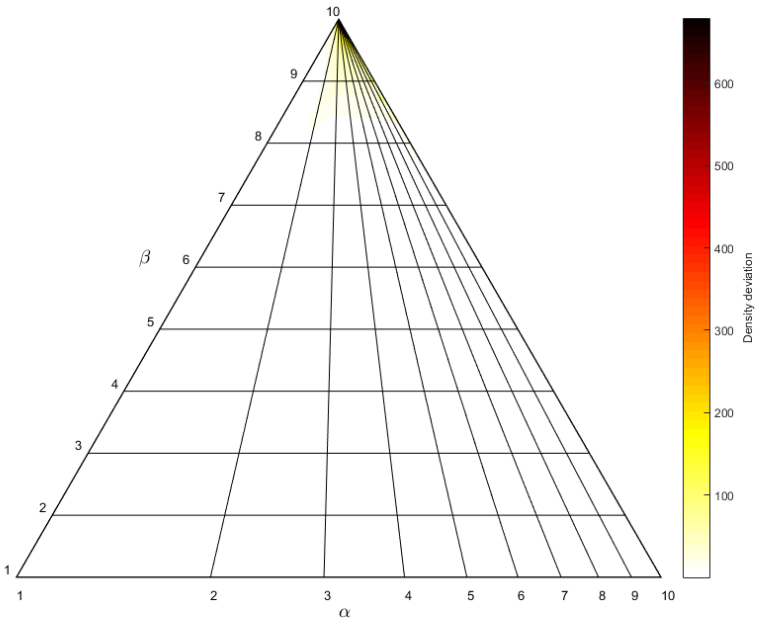

b

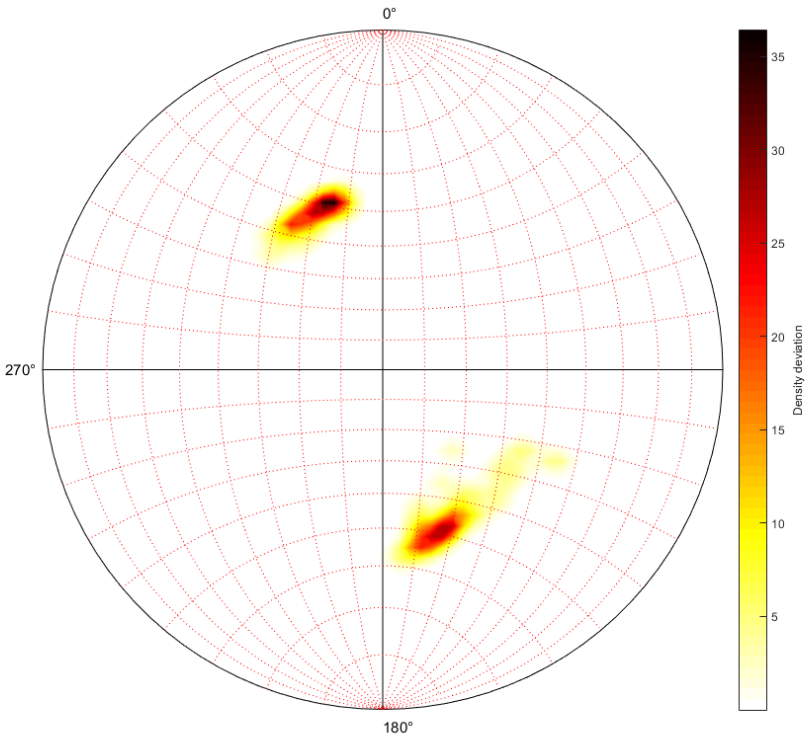

Figure 6.9: (a) Density plot of the block shape distribution and (b) density plot of the orientations of the main axes of the blocks of model 902, test series 4.

a

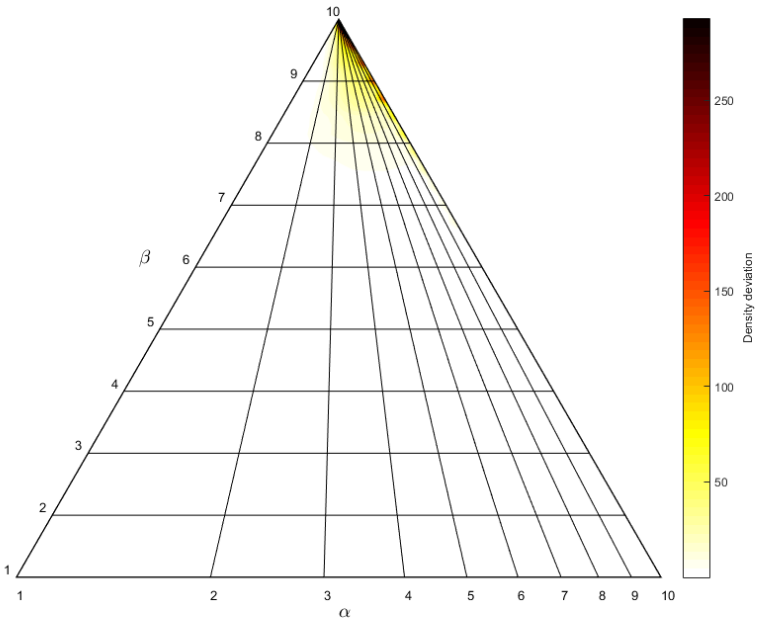

b

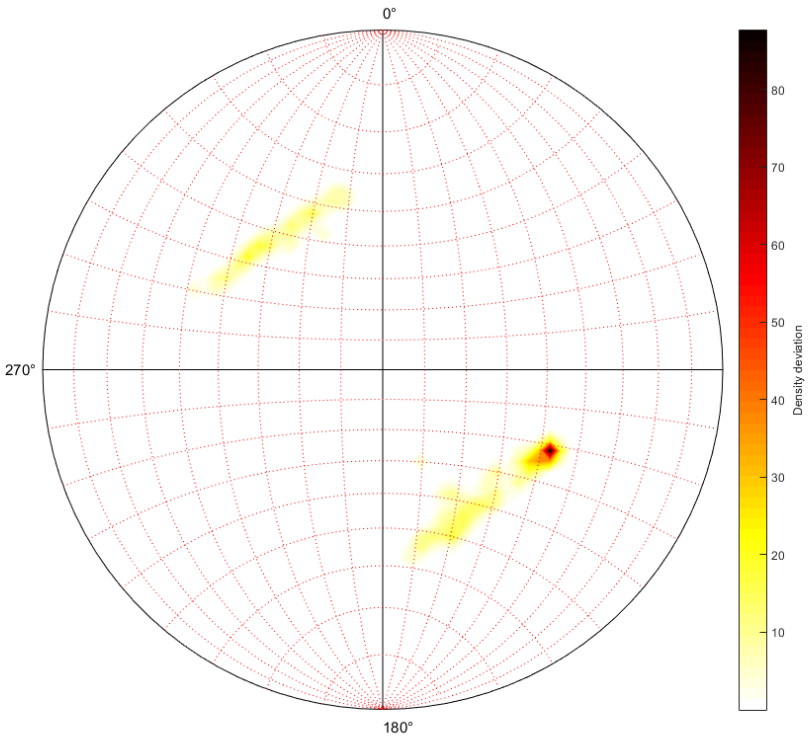

Figure 6.10: (a) Density plot of the block shape distribution and (b) density plot of the orientations of the main axes of the blocks of model 901, test series 4.